# Numerical and Experimental study of flow through swelling porous media

Shivam Manohar Salokhe

PhD

2022

# Numerical and Experimental study of flow through swelling porous media

Shivam Manohar Salokhe

A thesis submitted in partial fulfilment of
the requirements of the University of
Northumbria at Newcastle for the degree of
Doctor of Philosophy

Research undertaken in the Faculty of
Engineering and Environment

2022

# Abstract

In Engineering studies, the flow through porous media is an active subject of research due to its practical applications. The applications include liquid composite moulding techniques, industrial wicks, hygiene products, industrial filtration etc. The computational modelling of flow through porous media is often based on a single-phase or multiphase continuum using Darcy's law under rigid or swelling conditions. The computational models of fluid flow through porous media help to design and optimise for different engineering applications such as industrial wicks, baby diapers, paper towels, liquid composite moulding processes and heat pipes. The swelling of porous media as a result of liquid absorption by solid particles considerably affects the fluid flow through porous media. As a result, the resistance to fluid flow through porous media increases due to a reduction in the porosity and permeability of porous media.

Hence, the assumption of rigid porous media while developing the computational models is not always correct. The exclusion of swelling effects could lead to a serious error in the predictions from the developed computational model in terms of liquid front positions. Hence the inclusion of swelling effects in computational modelling is crucial and very few works are attempted to model such a flow condition. Further, for the computational modelling of capillary pressure effects, the available multiphase approaches are based on multiple fitting parameters. These parameters need to be measured experimentally or estimated analytically which makes it challenging to implement. The resulting computational model would not predict the liquid front accurately if the correct values of these fitting parameters are not known.

In this study, a novel methodological approach is proposed which allows us to account for the swelling and capillary pressure effects within the porous media. The novel combination of the Finite Volume Method and Volume of Fluid method (FVM-VOF) is used for the first-time to model the liquid absorption and swelling effects within porous media. The proposed methodological framework allows us to model the swelling and capillary pressure effects within porous media precisely with lesser fitting parameters. The use of the volume of fluid method helped to track the liquid-air interface accurately under different working conditions.

The computational models are developed for the different flow scenarios. For the case of flow-through non-absorbing swelling porous media, the modelling approach is first validated against the experimental data obtained from the literature. Further, 2D computational models for the liquid composite moulding process (LCM) are developed and studied. The results demonstrated the effects of permeability and the number of inlet gates on the mould fill times. The proposed methodology is further extended to model the flow through rigid porous media under absorbing conditions. A new analytical model predicting the liquid front locations under draining conditions is proposed. A novel boundary condition allowing us to model the liquid holdup within porous media is proposed. The effect of gravity and the size of the porous domain have a significant effect on the liquid front locations under different values of capillary pressures. The swelling behaviour of the cotton fabric is studied experimentally. A novel method of measurement of porosity changes as a result of swelling is proposed. The experimental results for the porosity changes highlighted the limitations of analytical models which are used to predict the porosity changes. The new correction factors for the existing analytical model are proposed and validated. These factors account for the inter-fibre interactions within the woven fabrics The results related to liquid absorption performance tests revealed that gravitational effects along with the swelling effects considerably affect the liquid absorption performance of fabrics. Finally, the computational models are developed for the case of flow-through swelling porous media under absorbing conditions. The model is developed using the data obtained from experiments. The model is further extended for the case of the flow-through single-layered and multi-layered diapers. It was observed that the changes in the permeability of layers considerably affect the liquid front shapes within the porous media. The outcomes from this study would help researchers to model the swelling and capillary pressure effects accurately with few basic input parameters. The proposed approach has demonstrated its ability to model the applications of forced imbibition in swelling conditions such as Liquid Composite moulding processes used to manufacture composites. The proposed approach can be used to model the applications such as industrial wicks, tissue papers, paper napkins, and hygiene products where flow is dominated by capillary forces and swelling effects in some cases.

# Declaration

I declare that the work contained in this thesis has not been submitted for any other award and that it is all my work. I also confirm that this work fully acknowledges opinions, ideas and contributions from the work of others.

Any ethical clearance for the research presented in this thesis has been approved. Approval has been sought and granted by the Faculty Ethics Committee on 16 December 2019.

**I declare that the Word Count of this Thesis is 39631**

**Name: Shivam Manohar Salokhe**

**Signature**

**Date: 6th April 2022**

# Publications

1. Salokhe, S., Rahmati, M. and Masoodi, R., 2021. Numerical modelling of the flow in a swelling preform during LCM mould filling. Journal of Reinforced Plastics and Composites, 40(13-14), pp.490-504
2. Salokhe, S., Rahmati, M. and Masoodi, R. Numerical simulation of flow through absorbing porous media; Part 1: Rigid porous media. Journal of Porous Media 25(5):53–75 (2022)
3. Salokhe, S., Rahmati, M. and Masoodi, R. Experimental investigation of cotton fibre swelling" (under review - Journal of Fluids Engineering)
4. Salokhe, S., Rahmati, M. and Masoodi, R. Numerical simulation of flow through absorbing porous media; Part 2: Swelling porous media (Ready to submit to Journal of Porous media)

# Acknowledgements

I would like to express my deepest gratitude to my parents Mr and Mrs Manohar Pandurang Salokhe for their extensive support throughout my journey. I am extremely grateful to my principal supervisor Dr Mohammad Rahmati and my external supervisor Dr Ryan Masoodi for their invaluable advice, continuous support, and patience during my PhD journey. Their immense knowledge and plentiful experience have encouraged me in all the time of my academic research and daily life. Without their support and mentoring, this research would not have been possible. I would like to thank my second supervisor, Prof Jane Entwistle, for her regular support and valuable feedback on the work.

I would like to thank all other members of staff in the Faculty of Engineering and Environment who have supported this work. I would like to thank Mr Philip Donnelly, Mr Simon Neville, and Mr Garry Martin from the Department of Arts Design for helping out on many occasions throughout the project. I would like to thank my colleagues Dr Faheem Malik, Dr John Nkor, Dr Abba Mustfa and Mr Shivdarshan Sherugar for their valuable support during my PhD.

I would like to thank my sister Mrs Sharadha Pratik Shinde, and my brothers Bhau, Dada, and Shambhu for supporting me and encouraging me with their best wishes. I would like to thank my fiancé Miss. Manasi Kiran Chavan for her valuable support during the final year. Finally, I would like to thank all my dearest friends who helped me through the ups and downs and helped me spend a memorable time in the UK

*This thesis is dedicated to my parents*

# Table of Contents

# List of Figures

# List of tables

# List of Abbreviations

| Abbreviation | | Unit |
|---|---|---|
| $A$ | Cross-section area of the porous sample | $m^2$ |
| $A_f$ | Cross-section area of the preform | $m^2$ |
| $a$ | Cross-section area of the pipe | $m^2$ |
| $b$ | Absorption coefficient | |
| $c$ | a constant that depends on the structure of porous media | |
| $C_2$ | Inertial resistance | 1/m |
| $D$ | Diameter pf fibre/sphere bead | m |
| $D_o$ | Initial Diameter of fibre. | m |
| $f$ | External source term | |
| $g$ | Gravitational acceleration | $kg/m^2$. s |
| $h_o$ | Initial liquid height in pipe | m |
| $h_1$ | Final liquid height in pipe | m |
| $h_f$ | Wicking height | m |
| $K$ | Permeability | $m^2$ |
| $K_o$ | Initial permeability | $m^2$ |
| $K_{ra}$ | Relative permeability | - |
| $L$ | Length of the porous sample | M |
| $P$ | Modified pressure | Pa |
| $P_c$ | Capillary pressure | Pa |
| $P_{in}$ | Inlet pressure | Pa |
| $p_w$ | Pressure within the wetting phase | Pa |
| $p_{nw}$ | Pressure within the non-wetting phase | Pa |
| $p_s$ | Suction pressure at the interface | Pa |
| $p_{pore}$ | Pore averaged pressure | Pa |
| $p_{atm}$ | Atmospheric pressure | Pa |
| $R_c$ | Capillary radius | m |
| $r_f$ | Radial flow front location | m |
| $r_{fb}$ | Radius of fibres | m |
| $r_o$ | Initial radial flow front | m |

| | | |
|---|---|---|
| $r_{sp}$ | Radius of a spherical bead | m |
| $S$ | Sink terms | |
| $S_i$ | Source terms | |
| $S_w$ | Saturation of the wetting phase | |
| $S_n$ | Saturation of the non-wetting phase | |
| $t$ | time | sec |
| $t_o$ | Time-related to initial liquid height | sec |
| $t_1$ | Time-related to final liquid height | sec |
| $t_w$ | Wetting time | sec |
| $u$ | Physical velocity | m/sec |
| $u_r$ | Superficial velocity | m/sec |
| $V_{sample}$ | Volume of sample | $m^3$ |
| $W_s$ | Weight of sample in a saturated state | kg |
| $W_d$ | Weight of sample in a dry state | kg |
| $x_f$ | Liquid front location for the case of forced imbibition case | m |

*Greek symbols*

| | | |
|---|---|---|
| $\alpha_w$ | Volume fraction of the wetting phase | |
| $\varepsilon$ | Porosity | |
| $\varepsilon_o$ | Initial porosity | |
| $\mu$ | Dynamic Viscosity of fluids | $N.s/m^2$. |
| $\rho$ | Density of fluids | $Kg/m^3$ |
| $\gamma$ | Surface tension | N/m |
| $\Theta$ | Contact angle | Degrees |
| $\varphi$ | Effective physical properties | |

# Chapter 1 Introduction

## 1.1 Introduction to Project

Porous media is a broad term that refers to a wide variety of substances; the most common are fibrous aggregates such as cloth, catalytic supports and filter paper with micro-pores, Industrial wicks and filtration beds formed of granular porous media and porous rocks such as dolomite and limestone (Bijeljic, 2000). Porous materials are used in a wide range of engineering and science applications including textile, automotive, civil, geophysics, hydraulics, petroleum, and chemical engineering. They are also used in a variety of hygiene products such as diapers and wipes. The applications mentioned above are heavily dependent on the properties of porous materials such as porosity and permeability (Dullien and Brenner, 2012) (Liu and Chen, 2014).

The spontaneous movement of liquids through porous materials is called *"imbibition"*. For nearly a century, the imbibition in porous media has been a topic of great interest for engineers and scientists due to its practical importance and inherent complexity (Bell and Cameron, 2002). The imbibition is also known as wicking, and this can also be aided by externally applied pressure as in the case of the liquid composite moulding (LCM) processes (Advani, 2018) (Bickerton et al., 2013). The best examples of wicking flow applications are tissue paper, industrial wicks, napkins and paper-based devices etc.(Patari and Mahapatra, 2020) (Beyhaghi et al., 2014). Natural fibres are now being used in a variety of engineering applications ranging from automotive industries to hygiene industries due to their cost-effective and environmentally friendly properties (Dhaliwal, 2019). The natural fibres undergo swelling upon absorption of the wetting liquid. Fibre swelling is an important parameter that effects on the imbibition through porous materials. As a result of swelling the porosity and permeability of porous materials reduces causing the increased resistance to flow (Melciu and Pascovici, 2016) . The swelling effect has opened a new dimension of research aiming at analytical and computational fluid dynamic (CFD) modelling of imbibition process.

The CFD modelling of flow through porous media is an effective tool to analyse, optimise and verify the performance of different industrial applications. A variety of methodological frameworks are used to model the flow through porous media under

different conditions. Various deserialization methods for flow governing equations such as Finite element Method (FEM), Finite Volume Methods (FVM) Finite element Control Volume (FE-CV) etc. have been used to model single and multiphase flow through porous media. For example, for modelling the swelling effects the Finite Element Control Volume method (FE-CV) has been used with in-house-built codes (such as PORE-FLOW by the University of Wisconsin -Milwaukee (Raoof et al., 2013), LIMS© by the University of Delaware (Simacek et al., 2004), PAM-RTM© by ESI group etc) with limited availability (Masoodi et al., 2012a). Further, Finite Volume Based solvers are widely used to model the flow at the pore-scale to understand the interaction between liquid and porous structures (Pinilla et al., 2021) (Liu and Wu, 2016) (Jeong et al., 2017) (Molins et al., 2012). Numerous other examples of CFD modelling of flow through porous media can be found in the literature such as Li et al. (2016a) simulated the flow of heat pipe using, Pooyoo et al. (2014) modelled the interaction between waves and perforated plates using Finite Volume based methods. The CFD can be used as a tool to design and optimise engineering applications that use porous media. For example, the CFD modelling of liquid composite mould filling is used to design the moulds, and the modelling of wicking flow through industrial wicks would help engineers to analyse the delivery of a specified amount of liquid to the top of the wick (Tan and Pillai, 2010) (F. Zarandi and Pillai, 2021). The flow of liquid through absorbing porous media can be viewed as a system of multiphase flow where non-wetting fluid gets displaced by wetting fluid. This flow scenario is mostly modelled by the two well-known multiphase approaches based on the Richards Equation and Eulerian-Eulerian method. The models based on these two approaches are popular in the computational modelling of capillary-driven flow in porous media (Pachepsky et al., 2003) (Zarandi et al., 2018) (Azhar and Sanyal, 2019). These two models are based on several fitting parameters which make them challenging to implement to model even a simple flow scenario.

The present study focused on the development of a new methodological framework to model the flow through a porous medium under the following different flow scenarios; a) the flow through non-absorbing swelling porous media b) the flow through absorbing porous media under rigid conditions c) flow through absorbing porous media under swelling conditions. The Volume of the fluid method along with the Finite volume method (FVM-VOF) is used for the first time to model the above cases. Firstly,

to model the flow through a swelling porous medium under non-absorbing conditions, the work conducted by Masoodi et al. (2012a) is extended. Chapter 6 includes computational models for a 1D flow scenario where the liquid front moves in only a single direction (rectilinear flow case). The developed models are validated against the experimental data from the literature. In real-world LCM applications where the liquid injection takes place from a point source within the mould results in the circular liquid front pattern. This case of mould filling is treated as a 2D flow scenario. Further, the validated models are extended to simulate the mould-filling process. The combination of FVM-VOF is further extended to model the flow through absorbing porous media under rigid conditions. The computational models for 1D,2D and 3D flow cases are developed and validated. A new boundary condition to mimic the liquid holdup within porous media is proposed as presented in Chapter 7. The experimental investigation of the swelling performance of the cotton fabric is conducted as presented in Chapter 4. Finally, to extend the method for the case of flow-through absorbing porous media under swelling conditions, the computational models are developed using the experimental data and extended for the case of flow-through diaper-like geometries presented in Chapter 8.

## 1.2 Motivation for the study

The swelling effect is one of the major key parameters that affect liquid imbibition in porous media. As a result of swelling, the pore size reduces which results in increased resistance to flow. In other words, the capillary pore radius, porosity, and permeability are the function of location and time. The exclusion of this effect leads to serious errors in the prediction of liquid front locations. Only a few researchers have studied this effect by analytical and experimental approaches. Masoodi et al (2011) (2012a) (2012b) in their efforts modelled the flow through a swelling porous medium under absorbing and non-absorbing conditions. The overall study included the modelling of the 1D flow (rectilinear flow) cases only. The assumption of 1D flow simplifies the mathematical models governing the process However in practice, the flow scenarios are not limited to a 1D scenario which makes it limited to use. The liquid mould filling process is more complex than just 1D flow scenario. The mould sometimes consists of multiple injection ports which results in circular flow front patterns (2D flow case) at beginning. Moreover, the series of experiments need to conduct to design and optimise moulds which is time consuming and costly. For the case of flow-through

non-absorbing swelling porous media, the literature review highlighted the need for computational modelling by considering the 2D flow scenario which resembles the actual mould-filling process in LCM applications. Besides, the assumption of single-phase flow limits its application where heat transfer between two fluids needs to be included in the model. Single-phase assumption limits the extension of the model for the cases of multifluid systems.

Further, for the case of flow-through absorbing porous media under rigid conditions, several researchers modelled the liquid absorption process in porous media using either a single-phase or multiphase approach. As mentioned in the reviewed literature, to model the flow using the multiphase approach using existing frameworks based on Richard's equation and the Eulerian-Eulerian method, the resulting computational model requires a lot of fitting parameters such as relative permeability, relative viscosity, entry pressure for wetting phase. Hence, one cannot model the liquid absorption process accurately if one of these parameters is missing. To get these parameters one needs to conduct a series of complicated experiments (Diersch et al., 2011). Also, there is still a gap in knowledge when the liquid is being absorbed in porous media for the following conditions: 1) Where capillary forces act in the direction of gravity 2) Where capillary forces are acting in both directions (the combination of wicking and drainage flow). The study of these flow scenarios would help to understand the details of flow within real-world applications such as diapers, napkins, sanitary products etc which is hard to study experimentally. Also, limited data is available for the case of flow-through absorbing porous media under swelling conditions. The data includes changes in fibre diameter, porosity and permeability as a result of swelling. The literature showed that to model all these different flow scenarios, mostly the Finite Element Method based modelling approaches are adopted. However, the majority of researchers used inhouse built code with limited features, and the flow is assumed as single-phase flow only which limits the applicability of their method. For the case of liquid absorption modelling, the available multiphase-based approaches are hard to implement due to their complexity. There is still a gap in knowledge about the applicability of other multiphase modelling approaches such as the Finite volume and Volume of Fluid methods to model the above-mentioned flow scenarios.

The major advantage of modelling these scenarios would help engineers to design and optimise real-world applications such as composite moulding processes, industrial wicks, tissue papers and hygiene products such as diapers, and sanitary napkins whose computational modelling is rarely done, in the reviewed literature. The development of computational models helps to minimise the reliance on on-field experiments to test the products under different working conditions. The computational modelling would save both time and costs associated with product design Hence, the present work will focus on the modelling of the flow in liquid absorbing and non-absorbing swelling porous media using the combination of Finite Volume and Volume of fluid method. The use of the volume of fluid method will allow us to model and track the liquid-air interface efficiently. The modelling of these scenarios would help us to understand and study the factors which are experimentally hard to determine such as pressure and velocity distribution throughout the domain. This is the first time when the Volume of Fluid method is used to model the different flow scenarios through swelling porous media. The assumption of multiphase flow would help to understand the interactions between phases in isothermal conditions and it can be easily extended to model non-isothermal conditions as well. Another important advantage of the proposed approach is that any commercial software based on the Finite Volume Method can be used to model swelling and capillary pressure effects.

## 1.3 Aims and Objectives

The swelling of fibrous porous media opened a new dimension in the modelling of liquid transport in porous media. The swelling mechanisms occur during the interaction of water or bio-resin with environmentally friendly fibres such as bamboo etc. During the liquid absorption process, the porous materials may undergo some morphological changes due to fibre swelling. The exclusion of this effect from numerical simulations could lead to serious errors. Hence, gaining a possible clear picture of fluid motion through a swelling porous medium is a prerequisite for different applications such as the development of Liquid Composite Processes, hygiene products and the paper industries to determine the liquid hold-up capacity.

The first aim of this research is to develop computational models to accurately capture the liquid-air interface in different flow conditions such as flow-through non-absorbing and absorbing porous media under a) rigid and b) swelling conditions. The second aim is to investigate the performance of the porous material experimentally for different working

conditions that are not evident in the literature. The obtained data then will be used to validate the numerical models wherever required. Finally, the validated models will be used to investigate the performance of porous media under different conditions that are similar to real-world applications such as paper towels or diapers.

The following are the objectives to reach the aims:

1. To identify the current gaps of different methods used to model the flow through porous media under swelling conditions.
2. To develop the computational models for the different flow scenarios and validate them using the analytical approaches and experimental data obtained from the literature.
3. Experimentally investigate the performance of liquid-absorbing materials according to a set of experiments. The main aim of this part is to obtain the experimental data to validate the computational models.
4. Extending the validated modelling framework to model the different case studies which deal with real-life applications such as flow inside a mould, diapers etc.

## 1.4 Statement of the Distinctiveness and Contribution to the Area of the Study

This research, for the first time, uses the combination of Finite Volume and Volume of Fluid method to model the flow-through liquid absorbing swelling porous media. The research proposed a novel methodological framework to model the flow through swelling porous media under non-absorbing and absorbing conditions. The proposed methodology is employed to model real-world applications such as Liquid composite moulding, Industrial wicks and diapers. Unlike other available simulation tools, the proposed methodology can be applied to any commercial software based on finite volume methods. In this research, a new experimental method to measure porosity reduction is proposed. The proposed method allows us to track real-time changes in porosity as a result of swelling. This is followed by image processing that includes tracking the changes in the pore area of the unit cell at different time values This is the first time when real-time changes in porosity as a result of swelling are recorded and analysed.

This research will present extensive numerical simulations, experimental work, and an in-depth analysis of the results. The work proposes a novel approach which can be used to model the flow in swelling porous media under absorbing and non-absorbing conditions. The application of the proposed approach would allow us to track the liquid-air interface, pressure, and velocity distribution throughout the entire domain. Experimentally, these details are sometimes difficult or impossible to obtain. The comparison between numerical and experimental data will provide reliable and verified results which would help computational fluid dynamics to predict the performance of porous media accurately under different flow scenarios.

The outcomes of this research have applications in several areas. Firstly, in the industries such as pulp and paper industries where the understanding of the wicking performance of porous materials leads to a cost-effective way to increase the performance of the products. The different aspects of the wicking are important depending upon the applications such as mass/volume of liquid absorbed within the wicks, rate of wicking, wicking height and so forth. Hence computational modelling of such processes is an effective tool to study wicking performance. Secondly, the modelling of the swelling effect would help engineers design and optimise the liquid

Composite Moulding (LCM) processes. In LCM processes, the number of inlet and outlet ports needs to be decided based on the flow front location of impregnating fluid and designing the liquid injection system based on the changes in working pressure within the system and similar aspects. Further, for the case of hygiene products such as diapers, paper towels, and sanitary pads the modelling of the swelling effect would be helpful to investigate liquid absorption performance which would help engineers to optimise the existing design of these products.

## 1.5 Overview of thesis

The thesis starts with an introduction in Chapter 1 and a current-state-of-the-art literature review in Chapter 2. The review is mainly focused on present models and approaches used to model the flow through swelling porous media. The conclusion of chapter 2 identifies the current research gaps in the modelling and simulation of flow through swelling porous media.

Chapter 3 describes the analytical models of forced and natural imbibition. In this chapter the analytical models of wicking flow for 1D,2D and 3D are studied and corrected wherever needed.

The performance of the cotton fabric is experimentally investigated in Chapter 4. The measurement of changes in fibre diameter, porosity and permeability are described in detail. This is followed by a detailed analysis of liquid absorption within the cotton sample under a constant liquid head whose computational models are developed in Chapter 8.

Chapter 5 outlines the proposed novel numerical framework used in this study. The governing equations of fluid flow through porous media are described in detail. The methodology for modelling swelling effects and capillary pressure effects is described in detail.

Chapter 6 presents the computational results obtained for the case of non-absorbing swelling porous media. The boundary conditions along with the physical domain for validation and case studies. The chapter compares the effect of swelling on the liquid front in isotropic and orthotropic conditions. Additionally, it analyses the effects of inlet position on the total mould fill time. Chapter 7 presents the computational results for the case of rigid absorbing porous media. The chapter describes the results for the 1D, 2D and 3D wicking flow. Finally, the chapter describes the details of the newly proposed boundary condition.

Chapter 8 presents the computational results from a developed model for the case of absorbing swelling porous media. The developed model is based on the combination of methodologies used for chapters 6 and chapter 7. Interesting case studies are presented in this chapter that focuses on the flow-through hygiene products.

Finally, the thesis is concluded in chapter 9 using the results from the proposed numerical framework, and limitations. The suggestions for future studies are provided lastly.

# Chapter 2 Literature Review

## 2.1 Fundamentals of flow through porous media

A porous material is a structure containing pores (voids). These pores are filled with single or multiple fluid phases (gas or liquid). The porous media are most characterised by their porosity *(ε)*. The porosity is the fraction of the bulk volume within porous media that is occupied by void space or pores. The other properties of the porous media (e.g., permeability, capillary pressure) are usually derived using the media porosity and pore structure and its respective constitutes (fluid and solid matrix) (Aboukhedr, 2019). Some practical applications where flow through porous media is important are listed below in Table 2.1.

Table 2.1 Practical applications where imbibition plays an important role

| Application | Description |
|---|---|
| Textiles | Interaction of liquids and garments |
| Absorption | Removing liquids from a surface |
| Oil recovery | Displacement of oil by another immiscible liquid |
| Polymer composites | Invasion of voids in a preform by a resin |
| Hydrology | Moving groundwater from wet to dry areas of the soil |
| Printing process | Ink penetration into paper or coating a paper |
| Surface chemistry | Contact angle measurement |

The flow-through porous media is described by the well-known Darcy's law which relates the flow rate to the pressure drop ($\Delta p$) for the one-dimensional single-phase flow through a porous medium with a length of ($\Delta x$). Darcy learned that the flow rate through the porous medium is proportional to the pressure gradient along the length. Darcy's equation to calculate the flow rate q for horizontal, linear, single-phase flow is,

$$Q = -\frac{K\,A}{\mu}\,\frac{\Delta p}{\Delta x} \qquad 2.1$$

Where $K$ is permeability, $A$ is the cross-sectional area of the porous sample, $\mu$ is the viscosity of a fluid, $p$ is pressure, $\Delta x$ is the length of the porous sample and $Q$ is the volumetric flow rate. The flow of the fluid through a porous medium depends on the cross-sectional area $A$ that is normal to the flow direction, the pressure difference $\Delta p$

across the length of the flow path. Darcy's velocity is defined as $v = Q/A$. Darcy's law later generalised for three-dimensional flow as:

$$v = \frac{K}{\mu} . (\nabla p - \rho g) \qquad 2.2$$

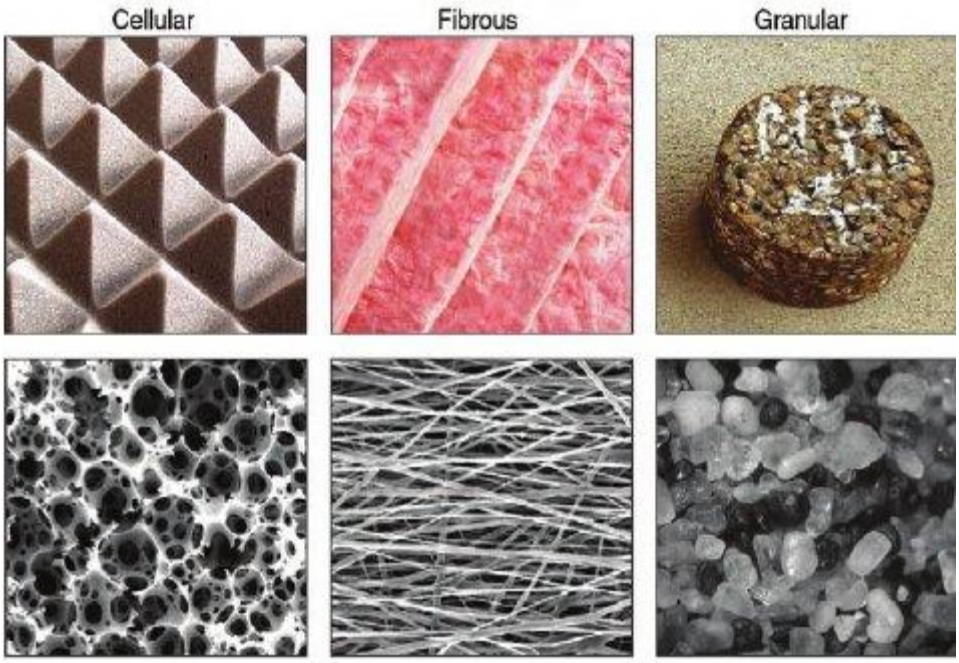


Figure 2-1 The different types of porous materials

The proportionality constant *K* in above Eq. 2.2 is called permeability. If the above equation is rearranged and dimensional analysis is performed, we see that unit of the permeability has the dimensions of area ($L^2$), where *L* is the unit of length. The area-related unit ($L^2$) is related to the cross-sectional area of the pore throat that connects two pores within porous media. Hence, a relatively larger pore throat relates to the larger values of permeability (Aboukhedr, 2019). The permeability of the porous media is a function of the geometry and porosity *(ε)*. of the porous media. An extensive set of works can be found in the literature to predict the permeability of the porous media theoretically. Table 2.2 shows the empirical formulas available to estimate the permeability. These formulas are generally in the following form,

$$K = D^2 \varphi(\varepsilon) \qquad 2.3$$

where $\varphi(\varepsilon)$ is the function of the porosity of porous media.

Table 2.2 The relations for φ(ε) for porous media made up of packed fibres, where c is a constant that depends on the structure of porous media cited in Masoodi and Pillai (2010)

| Author and Year | Proposed relation for $\varphi(\varepsilon)$ |
|---|---|
| Davies (1952) | $c\frac{1}{(1-\varepsilon)^{1.5}[1+56(1-\varepsilon)^3]}$ |
| Chen (1955) | $c\frac{\varepsilon}{(1-\varepsilon)}\ln\frac{0.64}{(1-\varepsilon)^2}$ |
| Bruschke and Advani (1993) | $c\frac{(1-\eta)^2}{\eta^3}\left(\frac{3\eta\cdot\tan^{-1}\sqrt{\frac{1+\eta}{1-\eta}}}{\sqrt{1-\eta^2}}+\frac{\eta^2}{2}+1\right)^{-1}$ where $\eta=\frac{4}{\pi}(1-\varepsilon)$ |
| Gebart (1992) | $c\left(\sqrt{\frac{1-\varepsilon_{min}}{1-\varepsilon}}-1\right)^{5/2}$ where $\varepsilon_{\min}=1-\frac{\pi}{2\sqrt{3}}$ |

## 2.2 Imbibition in porous media

Imbibition through heterogeneous porous media has gained importance due to its practical importance and inherent complexity in engineering applications. Imbibition is defined as the displacement of one fluid by another fluid within porous media. It is observed in a variety of everyday processes ranging from textile and paper treatment to groundwater and oil recovery (Melciu and Pascovici, 2016). If the imbibition happens as a result of the capillary effect, then it is called absorption or wicking. Wicking is considered a major factor contributing to the performance of industrial absorbing materials, such as diapers, wipes, and commercial wicks (Masoodi et al., 2010) (Chatterjee and Gupta, 2002). Figure 2.2 below shows an example of the wicking in the fibrous wicks.

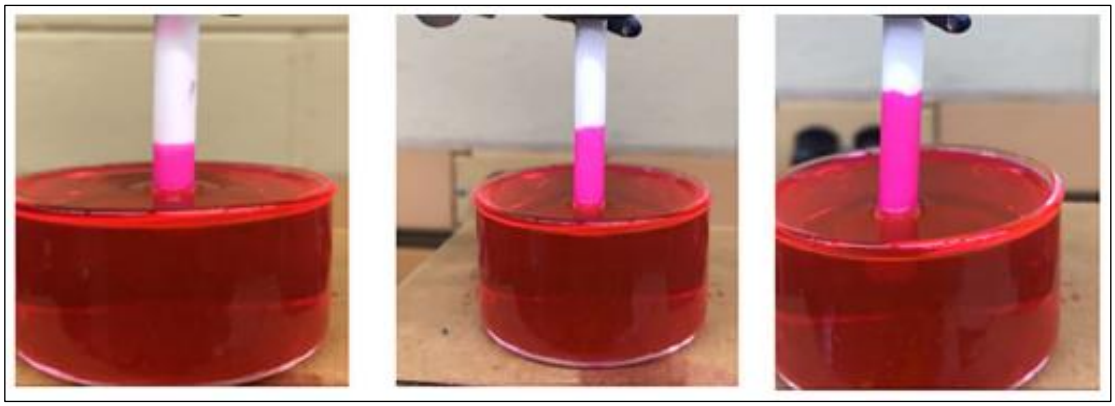

Figure 2-2 Wicking in industrial wick (Zarandi and Pillai, 2021)

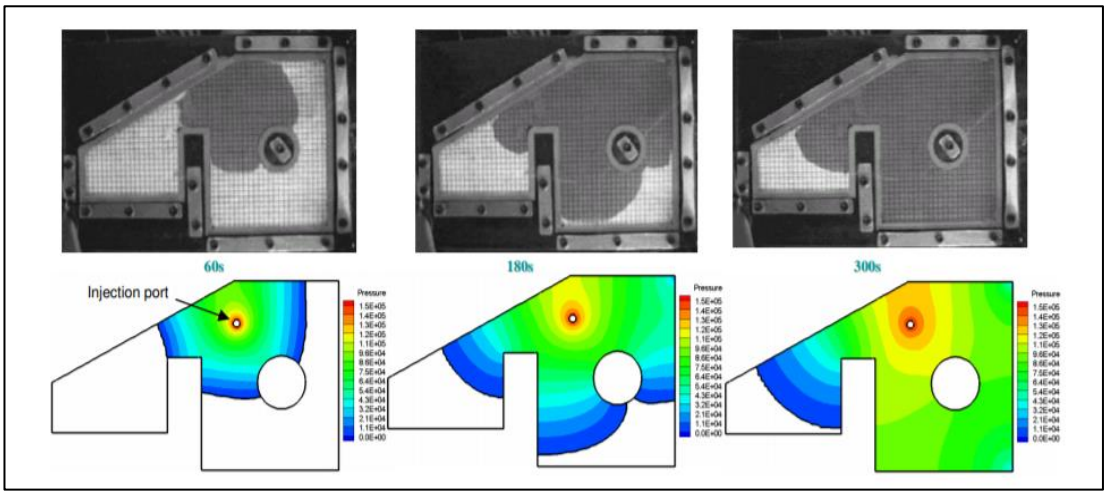


Figure 2-3 Injection of resin in a mould filled with fibres

The imbibition may also be the result of the application of the externally applied pressure. As shown in Figure 2.3, an example of liquid imbibition due to the application of external pressure is the liquid composite moulding process (LCM) used for manufacturing the polymer composites in which the resin at a prescribed pressure is forced into a fibrous preform. In this case, sometimes, the effect of the capillary pressure is neglected as the range of working pressures is higher than the resulting capillary pressure (Pillai, 2002) (Pillai, 2004) (Roy and Pillai, 2005).

### 2.2.1 **Capillary pressure**

The capillary pressure is a result of the partial negative pressure created at the liquid flow front as a result of the wicking phenomena. The difference in the surface energies of wet and dry solid matrices results in the generation of the capillary force at a solid-liquid interface. As a result, the liquid is pumped/pulled within the porous materials. The capillary forces arise due to the mutual attraction of liquid molecules and the

adhesion of these molecules to the solid medium. The wicking happens when the adhesion of dominates over the mutual attraction (Kissa, 1996) (Roy and Pillai, 2005).

When the wetting fluid comes in the contact with non-wetting fluid, the capillary pressure at the interface is taken as the difference between the pressures across the interface between two immiscible phases, it is given by (Masoodi et al., 2007),

$$p_c = p_{nw} - p_w \tag{2.4}$$

Where $p_c$ is capillary pressure, $p_{nw}$ is the pressure within a non-wetting fluid, $p_w$ is the pressure within a wetting fluid. The forces arising due to pressures within both phases are balanced as,

$$\pi R_c^2 p_{nw} = \pi R_c^2 p_w + \gamma \cos\theta (2\pi R_c) \tag{2.5}$$

Where $\gamma$ is the surface tension, $R_c$ is the radius of the capillary tube. Combing equations 2.3 and 2.4 leads to the well-known Young-Laplace expression to calculate the capillary pressure in a tube,

$$p_c = \frac{2\gamma \cos\theta}{R_c} \tag{2.6}$$

The estimation of the capillary radius is one of the biggest challenges when applying the Young-Laplace equation to calculate the capillary pressure within porous media (Masoodi and Pillai, 2010). This equation assumes that the porous media is a bundle of identical aligned capillary tubes of radius $R_c$. However, real porous materials with interconnected tortuous paths are not like bundles of identical capillary tubes. Hence, some assumptions must be made to calculate the equivalent capillary radius for the real porous media. The accurate method to calculate the equivalent capillary radius is the capillary rise experiment, in which the capillary forces are balanced by the hydrostatic forces acting in opposite directions. Once the value of the capillary pressure is known, the equivalent radius can be calculated using Equation 2.5 (Masoodi and Pillai, 2012a).

The equivalent capillary radius can also be estimated by analysis of the microstructure of the porous materials. Some researchers used the approach that is based on fitting the circles in the pore spaces and suggested taking corresponding radii to equivalent capillary radius. Masoodi and Pillai (2012a) used the energy balance approach to propose the generalised form to estimate the capillary pressure as a function of the

microstructure of porous media. The proposed expressions to estimate the capillary pressure are given by, (Masoodi and Pillai, 2012a)

i. Flow across a Bank of the same Radius Fibres

$$p_c = \frac{1-\varepsilon}{\varepsilon}\frac{\gamma \cos\ \theta}{r_{fb}} \tag{2.7}$$

where $r_{fb}$ is the radius of fibres.

ii. Flow across a Porous Medium made of spherical particles

$$p_c = 3\frac{1-\varepsilon}{\varepsilon}\frac{\gamma \cos\ \theta}{r_{sp}} \tag{2.8}$$

where $r_{sp}$ is the radius of particles.

### 2.2.2 **Swelling porous media**

In the past few decades, industries have started to use natural fibres because of their environmentally friendly advantages such as biodegradability, enhanced energy recovery, and reduced tool wear in machining operations. The application of natural fibres ranges from hygiene industries to composite manufacturing industries (Rowell et al., 1997) (O'Dell, 1997).

The fibre swelling phenomenon is an important factor that affects the wicking/imbibition rate in many industrial applications such as diapers, papers, wipes, and napkins. The swelling happens due to the absorption of the liquid by constituent particles of fibrous porous media when they come in contact with water or organic liquids. The swelling changes the wickability and wettability of the porous media. The swelling behaviour is an important factor and useful property in pulp and paper industries since it leads to liquid absorption within porous media. The amount of absorbed water by fibres varies from 6% to 100% of weight in dry conditions (Chatterjee and Gupta, 2002). This absorbed water changes the porosity, capillary radius, and permeability of the porous media. Swelling initiates when fibre starts to get wet and ends when the equilibrium state is reached. Hence, this is a transient process that causes the above-mentioned properties to change with location once the liquid front passes through it. In other words, the capillary pore radius, porosity, and permeability are the function of location and time. As a result, the governing equations (Darcy's law, continuity, or momentum equation) should be modified to include the

swelling effects. In the thesis, modifications are made to the momentum equations to include the swelling effects.

## 2.3 Multiphase flow through porous media

The term multiphase flow covers a broad set of flow regimes and patterns, Such as the flow of two or more immiscible fluids through porous media. The fluid-solid tortuosity interaction within porous media can affect the flow behaviour of immiscible fluids. The co-existence of the immiscible fluid within porous media is differentiated by the terms wetting and non-wetting phase (Aboukhedr, 2019). The multiphase flow in porous media is driven by gravitational, viscous, and capillary forces. The gravitational force due to gravity causes the movement of the phases along the direction of the gravitational field. An example of the influence of gravity is the thermosolutal convection flow in the gaseous phase as a result of the density variations due to concentration and temperature gradients within the multiphase system. The capillary forces play a significant role in phase distribution within heterogeneous porous media. Finally, the viscous forces affect the relative motion of phase within porous media; the fluids with lower viscosity tend to move faster through porous media due to less viscous resistance to flow. Problems involving multiphase flow, mass and heat transfer in porous media occur in several engineering and scientific disciplines. Important technological applications include fluid separation in fuel cells, flow through textiles, heat pipes, enhanced oil recovery and carbon dioxide storage within porous media (Shams, 2018).

The multiphase flow through macroscopic porous media is described by using the extended version of Darcy's law introducing the saturation dependant parameter called *Relative permeability*. For the multiphase flow, the situation is complicated due to presence of the more than one phase. The secondary phase, depending on the structure of the porous medium, hinders the flow of the primary phase. Due to the co-existence of multiple phases within porous media, the interactions between phases and pore surfaces impose the restrictions on the amount of pore space a given phase can occupy (Baker et al., 2015). These interactions affect the flow behaviour within porous media see Figure 2-4

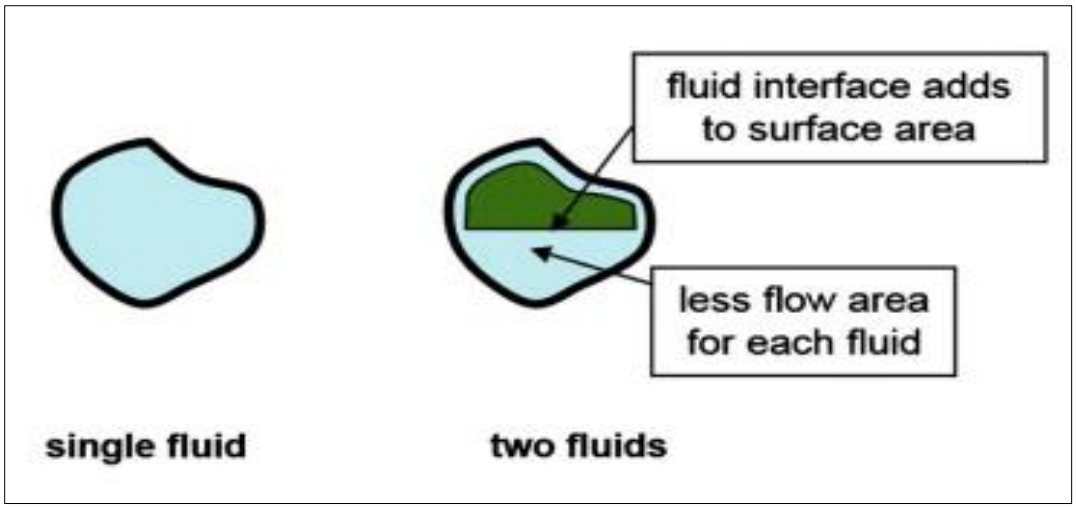


Figure 2-4 Cross-section of pore highlighting the effect of the presence of two phases on the surface area and cross-sectional area for flow through a pore (Ahmed, 2019)

The extended version of Darcy's law for two-phase flow is given by, ($\alpha=n_w$ for the non-wetting phase and $\alpha=n$ for the wetting phase)

$$v_\alpha = \frac{K_\alpha}{\mu_\alpha}.(\nabla p_\alpha - \rho_\alpha g) \qquad 2.9$$

where $K_a$ is the saturation dependant effective permeability of the αth phase. This extension of Darcy's law is established as the standard approach to calculating the specific fluxes in porous media. The effective permeabilities are measured directly with a set of experiments using small core plugs.

To account for the effect of the presence of multiple phases within porous media, the term relative permeability is introduced. Relative permeability is the ratio of effective permeability to absolute permeability,

$$K_{r\alpha} = \frac{K_\alpha}{K} \qquad 2.10$$

where $k_{r\alpha}$ is the saturation dependant permeability of $\alpha^{th}$ phase for given saturation of phase $S_\alpha$ and $K$ is the absolute permeability. The phase saturations of wetting and non-wetting phase are given by, $S_w$ and $S_n$. The phase saturations are related as,

$$S_w + S_n = 1 \qquad 2.11$$

The relative permeability of the fluid depends on the saturation of the other fluids within the porous media as shown in Figure 2-5. At the residual water saturation ($S_w = S_{wi}$), only oil will flow through the given pore. As the water saturation starts to increase, the flow of water will start causing the relative permeability to water will

increase and the relative permeability to oil will decrease. Finally, at residual oil saturation, the flow within the pore will be dominated by water causing a negligible flow of water causing the relative permeability to oil is zero. At this stage, the relative permeability of water will be maximum. In many cases, the relative permeability data for a given porous media may not be available. Hence, researchers proposed different analytical models for different scenarios. The details can be found in the literature (Ahmed, 2019). Also, based on the relative permeability formulation, the capillary pressure can be expressed as a function of the phase saturations. The analytical models can be found in the literature, among those, the Brooks-Corey model is the most commonly used to estimate capillary pressure, it is given by,

$$p_c = p_e(S_{eq})^{-1/n_b} \qquad 2.12$$

where $p_e$ is entry pressure, $S_{eq}$ is a saturation of the wetting phase and $n_b$ is the pore size distribution index.

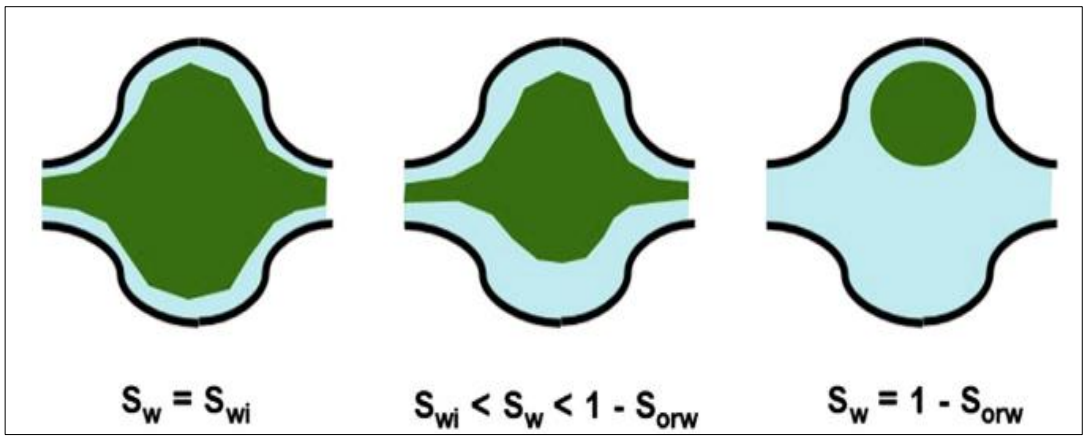


Figure 2-5 The effect of water saturation on the flow and distribution of oil through a pore (Ahmed, 2019).

## 2.4 Review of Experimental works related to swelling porous media

There is some evidence of the experimental work that has been done to study the changes in permeability as a result of swelling. Rodríguez et al. (2008) experimentally studied the steady state and transient permeabilities of the jute fibre mats. The unidirectional flow setup was used to estimate the permeabilities in both rigid conditions and swelling conditions. During the experiments, it is observed that the permeability decreases in unsaturated conditions for the samples that have porosity values less than 0.75.

There is a variety of experimental work done that focuses on the performance of fabrics, such as wettability tests, vertical and horizontal wicking tests, horizontal

spreading tests, moisture management, and forced flow tests. All these tests are used to predict the absorption and transport properties of woven fabrics. Wettability and vertical wicking test are the most common methods used for testing the fabrics (Tang et al., 2017). The permeability testing of the fabrics is studied by a few researchers, Oğulata and Mavruz (2010) proposed an analytical model to determine the permeability and porosity of the knitted fabric and conducted a series of permeability tests with an air permeability tester for a constant pressure drop of 100 Pa. Shih and Lee (1998) studied the effect of different arrangements of fibre on permeability. The study included the measurement of in-plane permeability for different structures of fabrics. Further, a microscale image analysis is done to observe the flow patterns. Xiao et al. (2012b) focused their work on the prediction of dynamic permeability. A series of experiments were done using an arrangement similar to an air permeability tester. The experimental results revealed the dynamic permeability is larger than the static permeability for loose textiles, and lower for tight fabrics. Patanaik and Anandjiwala (2009) conducted falling head permeability tests on non-woven flax fabrics and measured the pore size with a capillary flow porometer. The obtained results for velocity are then compared with a developed FEA model. Huang and Qian (2008) (2007) compared different test methods to measure the water vapour permeability of fabrics. The main objective of the work was to determine the thermal comfort properties of clothing systems. In their work, the results from the upright cup method, inverted cup method, dynamic moisture permeation cell method etc. are compared with a newly proposed method. The most of work related to permeability testing of fabrics is focused on air permeability testing to determine the comfort and air-breathing characteristics. Although, some people studied the moisture absorption and wicking performance of the fabrics but there is a gap in knowledge of actual permeability of these fabrics.

There are few studies on swelling measurement reported in the literature. Moore et al. (1950) investigated the swelling of cotton in water. The study included the microscopic investigation of changes in the cross-section of raw cotton fibres as a result of swelling. Also, their work includes a study of the changes in the circularity of the single fibre as a result of swelling. It is seen that for a single raw fibre the percentage change in the circularity ranges from 3.1 to 10.1% for mature and immature cotton fibres. This study is focused on the swelling performance of raw cotton fibres.

Hence, this work may not be useful to predict the porosity or permeability changes in the case of woven cotton fabrics. A few investigators, however, reported the prediction of changes in permeability as a result of fibre swelling. Masoodi and Pillai (2012b) experimentally characterised the effect of swelling on the jute fibres under different test liquids. The swelling of jute fibres is examined under the microscope to capture the changes in fibre diameter. Based on this work, Masoodi et al. (2012a) in their other efforts estimated the changes in the volumetric porosity and permeability with suitable analytical models. Further, to measure the changes in the permeability experimentally, a constant volume flow test setup is developed and changes in the inlet pressure are analysed to predict the real-time permeability changes. Later it is observed that for the shorter times the models based on estimated porosity and permeability changes showed good agreement with experimental results but for the longer times, the associated error increased. Similar work is done by Francucci et al. (2010) by considering humidity absorption. All these works mentioned above are done on the natural or conventional fibres used in composite materials. Also, there is limited data available for the changes in porosity as a result of swelling. Further, there are very few studies focused on the swelling measurement of cotton fabrics; the majority of the studies are focused on the reaction of cotton fibres with different chemicals. Cuissinat and Navard (2006) analysed the behaviour of the cotton cellulose fibres in water mixtures to observe the swelling and dissolution mechanisms such as ballooning. Ramadevi et al. (2017) investigated the swelling of cotton fibres as a result of treatments with aqueous glycine solutions. They analysed the effect of glycine solution treatments and their influence on the regain properties and cross-section morphology of cotton fibres. Their analysis included factors such as the effect of PH values of a solution on ribbon width, cross-sectional area and moisture regain.

## 2.5 Review of Numerical modelling

### 2.5.1 Numerical modelling of the flow-through non-absorbing swelling porous media

The numerical modelling of LCM processes has been used by many researchers to determine the optimal process parameters such as inlet gates and vents and to minimize the total mould-filling time (Zade and Kuppusamy, 2019). Researchers adopted different numerical methods to study the different LCM processes. The LCM mould-filling process is usually considered as the moving boundary problem while numerical

modelling. The LCM mould-filling process can be modelled by using two basic approaches. The first approach is the moving mesh approach, in which the domain near the liquid flow front is re-meshed during each time step (Saad et al., 2018). Coulter and Guceri (1988) developed the numerical code based on the boundary-fitted coordinate finite difference method and on the homogenized porous media approach to simulate the two-dimensional isothermal resin flow. A numerical model based on the boundary element method is proposed by Yoo and Lee (1996) and Um and Lee (1991) to simulate the mould-filling process. Chang and Hourng (1998) proposed the numerical model based on the Finite Element Method to study the non-isothermal and isothermal mould filling but the applications were limited to the rectangular mould geometries. All these numerical models mentioned above are based on the moving mesh approach. The accuracy of the moving mesh approach is good, but the major barrier in numerical modelling was the huge computational cost because, the numerical model with few thousand elements required many hours of the calculation. Also, it became difficult to handle cases where multiple injection gates and inserts are used (Saad et al., 2018).

The second approach is the fixed mesh approach, where the liquid flow front tracking is done on the fixed unique mesh throughout the simulation. It is based on the finite element (FE) and control volume (CV) method. This method becomes computationally efficient for modelling the mould-filling process because of recent developments in computing one does not need to re-mesh the domain since the fixed mesh is used. Trochu et al. (1993) developed a numerical model based on nonconforming finite elements to simulate the mould-filling process. The flow front tracking in this method has been done using a fixed mesh scheme. The work included the development of numerical models for different mould designs such as rectangular mould, mould with inserts and obstacles and mould tested with multiple injection ports. The predictions from the proposed numerical models are validated against the experimental data for total mould filling time. Shojaei et al. (2003) used the Finite element control volume (FE/CV) method for the mould-filling simulations. In their work, the pressure equation was solved using finite element formulation while the flow front tracking was done using control volume formulation. The proposed method is extended to model the resin flow in different mould geometries to study the different injection strategies. The results showed switching injection methods lead to the

maximum reduction in total mould filling time and a minimum number of vents. The FE/CV method became the base for commercial software packages such as PORE FLOW, LIMS, RTM-Worx and PAM-RTM which have been applied to non-isothermal flow (Bruschke and Advani, 1994). Lately, Saad et al. (2018) adapted the fixed mesh approach to model the Resin Transfer Moulding (RTM) process including the heat transfer effects and concluded that the optimisation of the locations for the injection gates is the practical way to minimise the mould fill time. Similar work is conducted by Boyard (2016), the work included a numerical simulation methodology that involves multiphysics and multiphase flow modelling using Finite difference and Finite volume methods.

An alternative to the FE/CV approach is the Eulerian free surface modelling techniques to specify the flow front advancement. The volume of fluid method (VOF) is another method used by researchers to simulate the LCM processes. Porto et al. (2012) developed a CFD model based on the VOF method to simulate the RTM (Resin Transfer Moulding) and LRTM (Light Resin Transfer Moulding). The study is focused on the mould-filling times in both processes. The results showed that due to a higher-pressure gradient, the LRTM process has less mould-filling time than RTM. Yang et al. (2015) developed a 3D model for compression resin transfer moulding (CRTM) using VOF and a dynamic mesh model. The resin flow is modelled employing source terms to the standard code. In addition to that, the deformation of the cavity is modelled as well. The developed model is used to analyse the relation between resin injection times and clamping forces. The results showed that while designing the mould for the CRTM process, the open gaps lead to lower clamping forces and fewer injection resin times. Using a similar approach, Yang et al. (2016) proposed a 3-D model for the resin infusion process. In both studies, the thickness of the preform is taken as a variable in the process, which leads to the use of the dynamic mesh method to account for the changes in preform porosity and permeability. Zade and Kuppusamy (2019) recently developed 2D CFD models to simulate the mould-filling processes. The combination of the Finite Volume Method and Volume of Fluid Method is used to model the process. The main purpose of this work is to demonstrate the possibility of Ansys Fluent to perform mould filling simulations and to quantify the sensitivity of flow front propagation and mould filling time with respect to variation in raw material parameters. The results suggested using lower velocities of

resin during mould filling to avoid the micro voids also the mould fill time is directly proportional to the viscosity of the resin. Finally, the study highlighted the need for user-defined functions to model the advanced flow scenario during LCM mould filling.

The adoption of the swelling effect into numerical simulation is rarely studied. Masoodi et al. (2012b) used FE/CV-based numerical simulations to study the effect of fibre swelling on the fluid flow in porous media. In their first efforts, a computer programme (based on the FE/CV approach) is used to model the wicking process in swelling porous media. The simulation utilised a novel form of the continuity equation, which included the effect of liquid absorption and fibre swelling in conjunction with Darcy's law to track the flow front. They proposed a new method for estimation of the time-varying permeability which was used to modify the permeability of the element behind the moving flow front. The numerical model is used to predict wicking heights for the case paper strips with a different weight percentage of carboxymethyl cellulose (CMC). The results showed good agreement with experimental data with a maximum error of 10%. However, the study is limited to a 1D flow case, and the authors highlighted the need for a suitable numerical approach to reduce the errors. In this case, the thickness of the porous media (paper) was not constant as a result of swelling; however, the thickness of porous media is constant in LCM. Also, the permeability is assumed to be a function of time only. This limits the application of these approaches while simulating the LCM mould-fill process.

Masoodi et al. (2012a) in further efforts, assumed constant thickness of porous media and a non-homogenous form of permeability to simulate the LCM mould fill process. The non-homogeneous local permeability and porosity functions are proposed which are based on the wetting time of fabric (porous media) that is $K=K(x, t)$. The two common LCM cases (constant flow rate and constant injection pressure) are studied. The time dependant permeability was found using both indirect estimation and direct measurement. The numerical results obtained for isothermal; non-reacting conditions showed that the numerical models based on a measured value of permeability predicted accurate liquid front locations. The results demonstrated assumption of rigid porous media is not always correct. The limitation of their studies is the assumption 1-D flow scenario, however, in practice, the flow scenarios are more advanced. Also,

the study lacks do not include the effect of orthotropic permeabilities on flow front propagation. A similar study is conducted by Francucci et al. (2014) using the finite element and volume of fluid method, but it was also limited to a 1D constant injection pressure case.

### 2.5.2 Numerical work on the wicking in rigid and swelling porous media

Wicking is the spontaneous absorption of liquid in a porous matrix under the action of capillary pressure. This flow scenario can be called the system of multiphase flow as it involves at least two phases: a wetting phase, which is the liquid that enters the porous domain, and a non-wetting phase, which gets displaced by the wetting phase. During the wicking process, the difference in surface energies of dry and wet porous matrix causes the generation of a capillary force at the fluid interface that moves the liquid or wetting phase into the porous matrix (Masoodi and Pillai, 2012a). Wicking performance is an important factor in absorbent porous materials, where the primary goal of the products is to absorb and retain the maximum amount of liquid (Masoodi et al., 2012c).

There are two main mathematical models available to study wicking. The first and oldest approach is the Lucas-Washburn approach, which assumes the porous media as the bundle-aligned capillary tubes of the same radius. As a result of this model, a linear relationship is obtained between the absorbed liquid mass and the square root of the time when the gravity effect is negligible (Lucas, 1918). Szekely et al. (1971) proposed a modified version of the Lucas-Washburn equation based on the energy balance to include the gravitational and inertial effects and developed an ordinary differential equation that predicts the wicking rate. Further, Masoodi et al. (2008) proposed a method to improve the wicking predictions of polymer wicks by showing that the hydraulic and capillary radii should be measured separately when using the capillary model. Research has shown that the suggested equation is also valid for absorbing porous media (Masoodi et al., 2011). Although the Washburn equation is important for modelling absorption in porous media, it is limited to one-dimensional flow cases along the direction of capillary tubes. Furthermore, the equation relies on the assumption of straight flow paths of liquid and is not accurate for real porous media, which have complicated and random paths (Masoodi et al., 2011).

Another approach in mathematical modelling of the wicking flow in porous media is based on Darcy's law, which proposes a simple relationship between pressure drop and averaged velocity of liquid while modelling the flow of water through a sand column. Darcy's law is a well-established approach and it has been widely used to model the single-phase flow through porous media (Bear, 2013). To do so, first, Darcy's law is coupled with the continuity equation to obtain the velocity and pressure fields. Masoodi et al. (2007) used Darcy's law-based approach to model the wicking flow in porous media by imposing the capillary pressure at the liquid front. The capillary pressure is calculated using two different approaches. The First approach is based on the balance of viscous dissipation and surface energy, whereas the second approach assumes porous media as a bundle of capillary tubes. Zarandi et al. (2018) proposed a new theoretical model for the transversely isotropic porous media to predict the flow front locations using Darcy's law approach. The results showed that the proposed model works best for the assumption of a fully saturated region behind the moving liquid front, but it fails to account for partial saturation effects due to the inhomogeneity of the porous media. Zarandi and Pillai (2021) in their latest efforts, investigated the effects of microstructure on the wicking performance of porous media by considering the three different types of wick structures; a) Sintered bed b) Fibrous wick (low porosity) and c) Fibrous (High porosity). The wicking predictions from the previously proposed analytical model for highly porous wicks were observed to be inaccurate due to the assumption of a sharp-liquid front. As result, they highlighted the need for numerical modelling of the wicking flow to study time-dependent wicking.

The approaches mentioned above assume a single-phase formulation where only the liquid phase is considered. In the cases where wicking flow through porous media is considered a multiphase flow scenario, the existence of several phases leads to the formulation of a momentum balance equation that considers the multiphase effects on the fluid dynamics (Santagata et al., 2020). The Richards equation, which describes the motion of liquid in porous media, has been widely used in modelling soil mechanics problems, such as the moisture distribution in soil. The Richards equation is a reduced form of a complex two-phase fluid problem that uses variable capillary pressure in a partial differential equation (Wein et al., 2019). The Richards equation can be derived by applying the general Darcy's law for two different fluids

simultaneously; hence such an approach can also be termed Darcy's law-based approach. Note that in Darcy's equation, the pressure is a single variable, but the Richards equation includes a term involving the moisture content. For a given porous material, the important term in the context of multiphase flow assumption is the saturation curve, which must be measured experimentally for different fluid combinations and fitted using non-linear empirical expressions. The Richards approach is hard to use if these parameters are not known, as complex experiments need to be done to measure the relative permeability, capillary pressure, and value of moisture diffusion coefficient (Diersch et al., 2011).

Computational fluid dynamics (CFD) is an effective tool for predicting the performance of porous materials. CFD solvers, based on some mathematical models mentioned above, have been successfully used to model the wicking flow through a porous medium. Different methods are used to solve the sets of equations numerically, and many examples can be found in the literature. Among all methods, finite element-based methods (FEM and FE-CV) are widely used to model wicking flow through the porous medium. The homogenized porous media approach has proven to have the capability to simulate complex flow processes in porous media, such as the ability to include swelling effects.

Masoodi et al. (2011) developed Darcy's law-based single-phase model using the finite element control volume method (FE-CV) to model the 3-D liquid imbibition into polymer wicks. The simulation results were validated against the experimental data as well as analytical solutions of Washburn and Darcy's law. The developed numerical model is further extended to model the wicking process in wicks with variable cross-sections. The numerical results showed the effects of sudden changes in an area on the total mass absorption of liquid by the wick. It is observed that reducing the wick diameter at the correct places allows for controlling the wicking rate. Although the predicted results showed the capability of the method, this study only considered a one-dimensional flow case. In another effort, Masoodi et al. (2012c) adopted the same approach to model the wicking flow in paper-like swelling porous media, where the swelling effect was included by assuming permeability to be time-dependant. Mendez et al. (2010) also modelled imbibition in a fan-shaped porous membrane by considering a 2-D flow scenario, adopting Darcy's law-based approach, and using the finite element method. The study included the experimental investigation of liquid

absorption in fans shaped porous membranes. The analysis presented in this study is divided into two parts. The first part focuses on the liquid imbibition in rectangular strips whereas the second part focuses on liquid imbibition in a circular-shaped section. The main purpose of their study was to identify the limits of the Lucas-Washburn approach due to an increase in non-wetted pore volume.

Most recently, Santagata et al. (2020) modelled 3-D absorption of liquid in swelling porous media using the finite scaling size method. The developed model was based on an approach developed by Diersch et al. (2011), where Richard's equation was used to solve mass and momentum. The flow was assumed to be multiphase, where three different phases (gas, liquid, and solid) coexist in the porous domain. The interesting thing about this work is the modelling of changes in the dimensions of the porous domain because of swelling action. This flow condition has been modelled by solving the mass equations for the solid phase that considers a term related to swelling. The numerically predicted liquid acquisition time and liquid distribution were in good agreement with the experimental data. As mentioned previously, to develop such a model, parameters like relative permeability, viscosity, and swelling ratio need to be measured and included in the model. These parameters need to be measured experimentally to develop accurate numerical models. Zarandi and Pillai (2018) developed a model based on Richard's Equation to predict the distribution of saturation along the length of the wick. They adopted a pore-scale simulation-based approach to determine the traditional properties of the porous media such as capillary pressure and relative permeability. Later, based on these obtained properties, the numerical simulations based on Richard's equations were performed in 1D with Mathematica and in 2D with COMSOL. These efforts demonstrated the applicability of Richard's equation in modelling the liquid imbibition process in dry porous media. The motivation behind this work is to overcome the shortcomings of their previous work i.e. prediction of flow front locations under partially saturated porous media (Zarandi et al., 2018).

The Finite Volume Method (FVM) is rarely used while modelling the wicking flow in porous media using the homogenised porous media approach. Li et al. (2016b) modelled the multiphase flow in porous media using the Eulerian approach. The main objective of their study was to analyse the performance of a reservoir and wells. The study presented 1-D, 2-D, and 3-D cases that mimicked actual reservoir conditions.

Different models, such as Brookes-Corey and Buckley-Leverette models, were used to model the capillary pressure. The results showed water/oil volume fractions at different values of injection velocities. FVM is mostly used in pore-scale simulations where flow is simulated through a real structure of the porous medium to study the interaction between different fluids. These types of simulations are used to study the details of flow and to determine relative permeability curves. Ashari and Tafreshi (2009) used the FVM and Eulerian multiphase modelling approach to study the rate of fluid transport in a partially saturated fibrous porous medium. They used a 3-D microscale model of 750 ×750 ×750 voxel with a single voxel size of 2 μm and selected the Leverette J model for capillary pressure estimation with proper values of empirical coefficients. As a result of the conducted simulations, a set of general mathematical relationships for capillary pressure and relative permeability is proposed which is valid for a range of fibre diameters (10-25 μm) and solid volume fraction (5-12.5%). In another effort, Ashari et al. (2010) used a similar approach to model and study the radial spreading of liquid in a fibrous porous medium and motion-induced fluid release. Ranjan et al. (2012) developed a CFD model using a combination of the finite volume method and thin film evaporation model for the wicking process at the microscale/pore scale. In this work, the CFD models are developed to predict the capillary pressure, permeability, and thin-film evaporation rates of various micro-pillared geometries of wicks used in heat pipes. A comparison between three different micro-pillared geometries– conical, cylindrical, and pyramidal is presented and compared to the performance of conventional sintered particle wicks. It was concluded that the use of a micro-pillared wick structure leads to considerable enhancement in the heat transport capacity of the device.

## 2.6 Chapter Summary

In summary, a variety of approaches have been used to model the liquid imbibition process in porous media under different conditions; a) non-absorbing swelling porous media b) absorbing rigid porous media and c) absorbing swelling porous media. For the case of flow-through non-absorbing swelling porous media, the computational models excluded the swelling effects as a result of liquid absorption by fibres. Very few researchers included the swelling effects in the computational model, but their study was limited to the 1D flow scenario only. The Finite Element Control Volume (FE/CV) Method is widely used to model this flow scenario with single-phase flow

assumptions. Although the numerical study of the flow through swelling porous media has been performed in literature by some researchers., there is still a lack of numerical models to simulate the flow in 2-D swelling porous media. Some studies considered the porosity as a function of process parameters, such as compression forces but they did not include the permeability changes in the preform as a result of liquid absorption. A limited number of researchers focused their study on the modelling of swelling effects, but the majority of study is limited to 1D flow scenarios. Hence, the adaption of the fibre swelling effect into numerical simulation is crucial for the successful design of the mould and will help to eliminate trial and error, which are time-consuming and costly. Another group of researchers developed a two-phase flow model to track the wicking flow in swelling porous media. The predicted results showed good agreement with experimental data, but the mathematical model requires several fitting parameters. A specific set of experiments is needed to calculate these parameters, limiting its applications (Mirnyy et al., 2012). Further, the majority of numerical models for both cases were developed using finite element based inhouse built codes such as PORE-FLOW, PAM-RTM etc. whose use is limited to particular applications. The existing commercial software such as ANSYS does not have an inbuilt model that can account for swelling effects in porous media.

For the remaining flow cases (absorbing rigid/swelling porous media), some researchers have used a single-phase flow formulation whereas others have used a multiphase flow formulation to model these flow scenarios. The most popular method is the finite element control volume (FE/CV) method based on Darcy's law, where the liquid imbibition is viewed as a single-phase flow. Methods based on the single-phase formulation consider the one-dimensional flow scenario only for most cases. When imbibition is considered a system of multiphase flow, the methods based on Richard's equation and Eulerian methods have been used. Finite Volume and Volume of Fluid-based models are rarely used to model the liquid imbibition process. Mostly, this method is used for pore-scale simulations. There is evidence that the FVM can be applied along with the Eulerian method to model the liquid absorption process. However, in this case, a lot of fitting parameters need to be estimated with a series of experiments or simulations, and it might become difficult to model the liquid absorption process accurately if these parameters are not known correctly(Diersch et al., 2011) (Li et al., 2016a). Recently, Zarandi and Pillai (2021) used a microscale

simulation-based approach to estimate the fitting parameters such as relative permeability, capillary pressure-saturation curves etc. However, the predictions from the resulting numerical model showed deviations from experimental data for wicking height. Hence, the applicability of the Richards approach and the Eulerian-Eulerian approach is heavily dependent on the accuracy of fitting parameters.

Further, there are a variety of experimental works have been done in terms of performance testing of fabrics. The majority of them are based on the standard testing methods or equipment named air permeameter etc. Further, reviewed literature shows that the majority of studies are focused on the testing of the fabrics to determine the fundamental factors that contribute towards the comport which are focused on moisture absorption only. Although the main aim of these tests is to determine the transport properties of the fabric, mostly the permeability measurement is excluded. Overall, the existing work on the testing of fabrics is focused on clothing applications. Another important factor is the swelling measurement of fabrics, there are few experimental studies available for the swelling measurement of fabrics. These studies included the measurement of changes in fibre diameter and permeability as a result of swelling action. However, the measurement of real-time changes in porosity is mostly neglected. Hence it is essential to study the swelling behaviour of the fabrics to estimate the consequent effects on their performance.

# Chapter 3 Analytical models

This chapter presents an overview of the different analytical models used in this study. The analytical models are presented for the case of forced imbibition (LCM mould-filling processes) and natural imbibition processes (wicking flow). In the case of the forced imbibition process, the analytical models for two different injection conditions as proposed in Masoodi et al. (2012a); a) constant volume flow rate and b) constant pressure injection is presented. Further, for the case of natural imbibition or wicking flow, the analytical model from Masoodi et al. (2007) is taken. For the wicking flow, the capillary forces act in opposite direction to that of gravitational forces. Finally, in this chapter, the new analytical model is proposed for the liquid draining case where capillary forces and gravitational forces act in the same direction. This is the extension of the analytical model presented by Masoodi et al. (2007). Finally, the corrected version of an analytical model for the 3D imbibition in porous media by Xiao et al. (2012a) is proposed. The analytical models presented in this chapter are used to validate the proposed numerical methodology. The use of each model is cited in the latter part of the thesis.

## 3.1 Analytical models for forced imbibition case

In each LCM process, the mould is filled with the fibrous medium (preform) through which the resin is forced to impregnate such a preform. The single-phase flow of Newtonian liquid in the porous medium is the common approach used to model the resin flow in the LCM process. There are two fluids present in the mould: The resin is the one that is invading the pores by displacing the air in the next pores. The assumptions are based on the fact that there is a sharp interface, behind which the whole region is occupied by the resin while ahead of which the pores are completely filled by air. The single-phase flow in rigid porous media is governed by the following expressions of Darcy and the continuity equation (Masoodi et al., 2012a). Upon rearranging equation 2.1 we have,

$$u = -\frac{K}{\mu}\nabla p \qquad 3.1$$

The continuity equation is given by,

$$\nabla . u = 0 \qquad 3.2$$

The flow of resin through preform is the best example of forced liquid imbibition through porous media. Resin-like test liquids are frequently made to flow through flat rectangular moulds by line injection from one side of a rectangular stack of fabric layers, also known as preform to study LCM flows under controlled conditions as shown in Figure 3.1. Such a flow scenario is viewed as 1D flow as the flow variables change along the direction of flow (Masoodi et al., 2012a) (Shojaei et al., 2003).

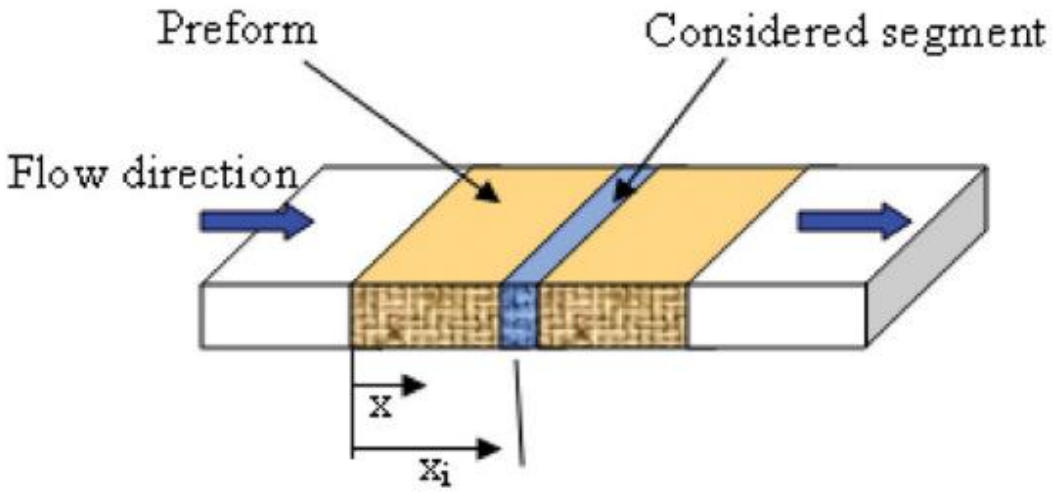


Figure 3-1 The flow front propagation in a preform made up of a stack of layers during one-dimensional flow through a mould cavity (Masoodi et al., 2012a).

### 3.1.1 Constant volume flow rate condition

For 1-D flow cases, test liquids (resin) are made to flow through the flat rectangular moulds in which the liquid is injected from one side of a rectangular stack of fabric layer (preform). For such flow under a constant volume flow rate, the mass balance is given by,

$$Q = A_f \, \varepsilon \frac{dx_f}{dt} \tag{3.3}$$

Where Q is the mass flow rate of the resin, $x_f$ is the flow front location along the x-direction. Upon integration and rearranging the variables, we have,

$$x_f = t \frac{Q}{A_f \, \varepsilon} \tag{3.4}$$

where $t$ is the filling time, and $A_f$ is the cross-sectional area of the preform. This equation holds valid for both non-swelling porous media and swelling porous media. The consideration of the swelling effect is not necessary for the prediction of flow

front locations in the case of volume flow rate conditions. Darcy's velocity behind the moving flow front can be taken as,

$$\frac{du}{dx} = 0 \rightarrow u = constant = \frac{Q}{A_f} \qquad 3.5$$

To find the pressure field, the constant Darcy's velocity *(u=Q/A)* is substituted into equation 2.1 which results in,

$$p_{in} = \frac{\mu}{\varepsilon_o K}\left(\frac{Q}{A_f}\right)^2 t \qquad 3.6$$

For swelling porous media, the inlet pressure is a function of time, but the permeability is a function of the wetting time, which is $K=K\,(t - t_w)$ for $t > t_w$ where $t_w$ is the time when the local fabric is wetted by the invading liquid and $t$ is the time related to current flow front location. Hence the above equation modifies to,

$$p_{in} = \frac{Q^2\mu}{\varepsilon_o {A_f}^2}\int_0^t \frac{dt'}{K(t')} \qquad 3.7$$

Note that in the derivation of equation 3.4, the permeability of preform in the wetted region is assumed as homogeneous and the function of time only which is $K=K\,(t)$. However, in practice, it is the function of both space and time. The space dependence of permeability can be expressed in terms of local wetting time values that vary along with the flow front (Masoodi et al., 2012a).

### 3.1.2 Constant injection pressure condition

For the case of resin flow through rigid porous media under constant pressure conditions, the combination of equations 3.1 and 3.2 leads to the Laplace equation for pressure in the following form.

$$\nabla^2(p) = 0 \qquad 3.8$$

Upon solving equation 3.5 for a 1-D case, and replacing the pressure gradient in equation 3.1 the flow front location $(x_f)$ for 1-D rigid porous media in case of constant permeability conditions can be expressed as (Masoodi et al., 2012a),

$$X_f = \sqrt{\frac{2P_{in}Kt}{\varepsilon_o \mu}} \qquad 3.9$$

where $P_{in}$ is the injection pressure and $t$ is the injection time. For swelling porous media, the permeability $K$ is not constant which leads to following the elliptic equation for pressure.

$$\nabla(K(\nabla p)) = 0 \qquad 3.10$$

The expression for flow front locations in the case of the 1-D swelling porous medium is given by,

$$x_f = \sqrt{\frac{2P_{in}}{\varepsilon_o \mu} \int_0^t K(t')dt'} \qquad 3.11$$

## 3.2 Analytical models for natural imbibition case

Wicking is the transport of the liquid into porous media as a result of capillary suction created at the interface. The generation of capillary suction pressure arises due to the wetting of the solid matrix by the wetting phase. The natural imbibition can be categorised into two different processes as shown in Figure 3.2; a) wicking flow, where capillary forces act opposite to gravitational forces (Masoodi et al., 2007). b) draining flow, where capillary forces act in the same direction as that gravitational forces. The analytical model proposed by Masoodi et al. (2007) for the case of wicking is used in this study for wicking flow conditions and extended to the draining case.

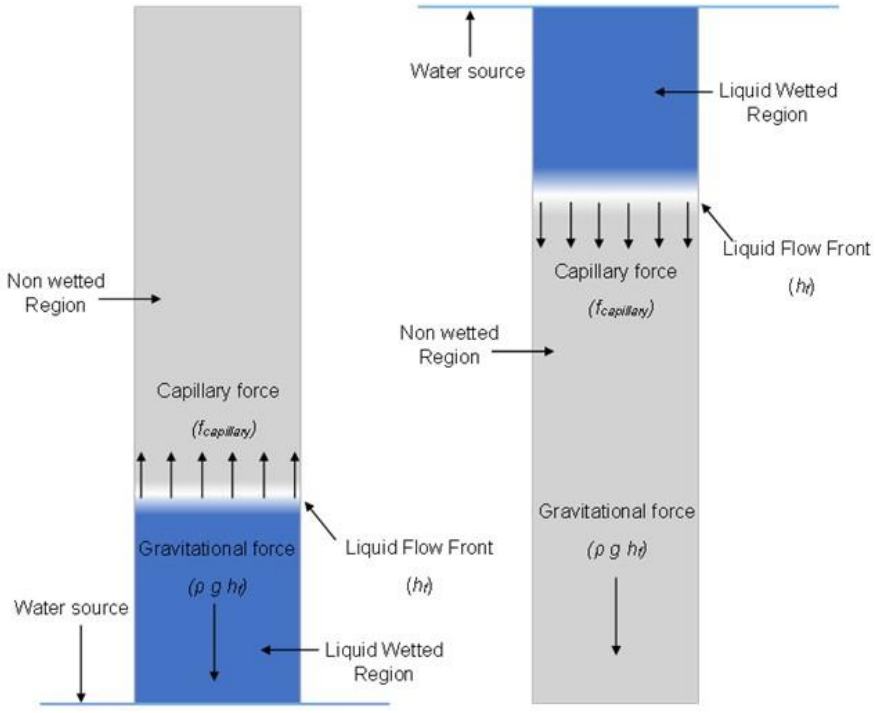


Figure 3-2 Schematic view of 1D flow for a) an upward wicking case and b) a draining case

### 3.2.1 When capillary forces act the same as gravitational forces (1D Draining case)

Considering the 1D fluid motion in a simple wick as shown in Figure 3.2. When the porous media is assumed to be rigid with constant viscosity, the combination of equation 3.1 and equation 3.2 leads to the following Laplace equation for pressure (Masoodi et al., 2007).

$$\nabla^2(p) = 0 \qquad 3.12$$

As shown in Figure 3.2, for the 1-D flow scenario, when the liquid is being absorbed against the force of gravity, the above Laplace equation modifies as,

$$\frac{d^2P}{dh^2} = 0 \qquad 3.13$$

where *P* is the modified pressure due to the pore-averaged hydrodynamic pressure and gravity-induced motion in the porous domain. The modified pressure is expressed as,

$$P = p_{pore} + \rho g h \qquad 3.14$$

where *h* is the height of a point at the liquid fluid interface, $\rho$ is the fluid density, and $p$ *is* the pore-averaged hydrodynamic pressure. Equation 3.13 is solved with the following boundary conditions in terms of the pore-averaged hydrodynamic pressure

$$p_{pore} = p_{atm} \quad \text{at} \quad h = 0 \qquad 3.15$$

$$p_{pore} = p_{atm} + p_s \quad \text{at} \quad h = h_f \qquad 3.16$$

The term $p_s$ is the suction pressure created at the liquid-air interface because of the capillary force action. The capillary forces present at interfaces are responsible to pull the liquid interface regardless of the direction of the flow. Using equation 3.13, equations 3.14,15 can be rewritten as,

$$P = p_{atm} \quad \text{at} \quad h = 0 \qquad 3.17$$

$$P = (p_{atm} + p_s) + \rho g h_f \quad \text{at} \quad h = h_f \qquad 3.18$$

The general solution of equation 3.10 using the boundary conditions 3.14 and 3.15 leads to the following expression for the modified pressure,

$$P(h) = p_{atm} + \rho g h + p_s \frac{h}{h_f} \quad 3.19$$

The solution of this expression is valid for $0 \leq h \leq h_f$. when the liquid front $(dh_f / dt)$ speed is related to Darcy's velocity the resulting differential equation is given by,

$$\frac{dh_f}{dt} = \frac{K}{\mu\, \varepsilon}\left(\frac{p_s}{h_f} + \rho g\right) \quad 3.20$$

When the equation is solved with the initial condition as $h_f\,(t=0)$. The final equation for the liquid front height $h_f$ is obtained as,

$$p_s \ln\left|\frac{p_s}{p_s + \rho g h_f}\right| + \rho g h_f = \frac{\rho^2 g^2 K}{\varepsilon \mu} t \quad 3.21$$

Once the locations of the liquid flow front are known then the above equation can be used to estimate the absorbed mass of liquid with respect to time. Note that the above equation is valid when the inflow and capillary forces and gravitational forces act in the same direction which is called a liquid draining case.

### 3.2.2 When capillary forces act opposite to gravitational forces (1D Wicking case)

Using the same approach, the analytical model for the case of wicking flow is proposed by Masoodi et al. For the wicking case, the equations 3.14 and 3.15 gets modified as (Masoodi et al., 2007) (Masoodi et al., 2011),

$$P = p_{atm} \quad \text{at} \quad h = 0 \quad 3.22$$

$$P = (p_{atm} - p_s) + \rho g h_f \quad \text{at} \quad h = h_f \quad 3.23$$

Here, the negative sign for suction pressure $p_s$ indicates that the capillary forces and gravitational forces are acting in opposite directions to each other. Hence, using these boundary conditions the equation that predicts the flow front locations in case of wicking flow is given by (Masoodi et al., 2007) (Masoodi et al., 2011),

$$p_s \ln\left|\frac{p_s}{p_s - \rho g h_f}\right| - \rho g h_f = \frac{\rho^2 g^2 K}{\varepsilon \mu} t \quad 3.24$$

### 3.2.3 Analytical model for 3D imbibition in semi-infinite porous media.

In this section, the analytical model for the 3D imbibition in isotropic porous media is derived The analytical model proposed by Xiao et al. (2012a) is corrected in this study.

Xiao et al. (2012a) in their efforts, proposed an analytical model based on the assumption of physical velocity. Here, we modify the equation by using Darcy's velocity in the formulation. Following are the assumptions made while proposing the model

1). As shown in Figure 3.3, the analytical model assumes a point source from which the liquid is absorbed within the spherical porous media. 2) The shape of flow front advancement for this case is assumed to be hemispherical and the porous medium is isotropic. 3). The effect of the hydrostatic pressure on the flow front advancement is neglected.

The liquid flow rate through the advancing flow front is given by,

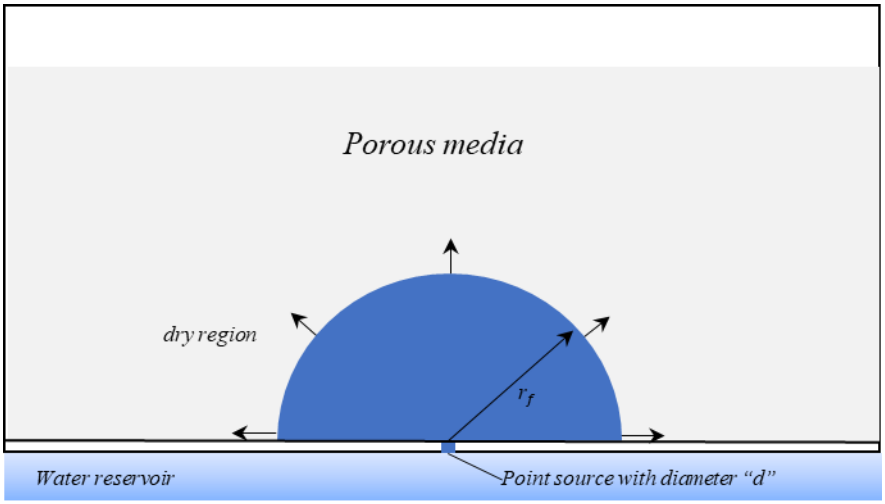


Figure 3-3 Details of the hemispherical imbibition process in a semi-infinite porous domain. The liquid is absorbed from the point source of diameter d.

$$Q = u2\pi r_f^2 \qquad 3.25$$

where $r_f$ is the advancing front and $u$ is the superficial velocity (Darcy velocity) of liquid and it is given by,

$$u = u_r \varepsilon_o \qquad 3.26$$

where $u_r$ is the physical velocity of the liquid flow and $\varepsilon_o$ is the porosity of the porous media.

From equations 3.24 and 3.25, the expression for the radial velocity is given as a function of pressure gradient according to the well-known Darcy's law,

$$\nabla p = \frac{\mu}{k} . \left( \frac{Q}{2\pi r_f^2} \right) \qquad 3.27$$

Assuming the atmospheric conditions at the source ($p_{atm}$), and suction pressure at the interface (Masoodi and Pillai, 2012a) or liquid flow front. Hence pressure at $r=r_f$ will be $p_{atm} - p_s$. Equation 3.27 can be integrated with respect to the radius of the wetted region to get the pressure by assuming the initial flow front to be $r = r_o$ to obtain the expression for the pressure.

$$p_s = \frac{\mu\, Q}{2\pi K_o}\left(\frac{1}{r_o} - \frac{1}{r_f}\right) \tag{3.28}$$

By combining equations 3.27, 3.25, and 3.24, we get

$$r_f^2 \frac{dr_f}{dt}\left(\frac{1}{r_o} - \frac{1}{r_f}\right) = \frac{K_o p_s}{\varepsilon\mu} \tag{3.29}$$

Upon integrating equation 3.28 by assuming the wetting front to be $r = r_o$, an expression for the wetting front can be derived. This equation can be used to calculate the time by assuming the values of the initial flow front radius and the corresponding range of wetting front radius values.

$$\frac{1}{3r_o}\left(r_f^3 - r_o^3\right) - \frac{1}{2}\left(r_f^2 - r_o^2\right)\frac{\mu\varepsilon}{p_s K_o} = t \tag{3.30}$$

where $r_f$ is the flow front radius, $r_o$ is the initial flow front, $K_o$ is permeability in rigid conditions, and $p_s$ is capillary suction pressure.

## 3.3 Chapter Summary

In this chapter, the analytical models for forced imbibition and natural imbibition are presented. For the case of natural imbibition, the newly developed model for the liquid draining case is proposed. This is done by extending the work proposed by Masoodi et al. (2007). The work is mainly focused on the development of an analytical model for the wicking flow case where capillary forces act in opposite direction to gravity. Darcy's law-based approach has been used by Masoodi et al. (2007) to derive such an expression. In the present study, the model is extended by considering capillary forces and gravitational forces acting in the same direction. Finally, this chapter also introduces the modified version of the analytical model proposed by Xiao et al. (2012a) for 3D imbibition in isotropic porous media. The model is corrected by replacing the physical velocity with Darcy velocity. The analytical models for forced imbibition and natural imbibition will be used in chapters 6 and 7 respectively.

# Chapter 4 Experimental method

This chapter presents the details of the experimental works conducted to meet the aims as stated in Chapter 1. The experimental works include the testing of the cotton fabric samples to obtain the properties of the porous media. In brief, the measurements of the fibre diameter, capillary pressure, porosity, and permeability are carried out under rigid and swelling conditions. The literature highlighted the need for experimental investigation of the swelling behaviour of cotton fabrics. The data relating to changes in the diameter of individual fibres, porosity, and permeability of any porous media is needed to model the flow through swelling porous media. Experimental investigation of these parameters would help to develop accurate CFD models of hygiene products such as baby diapers, sanitary napkins etc. This chapter proposes a novel approach to measure the changes in porosity as a result of swelling effects. Further, the two new correction factors to account for the effects of inter-fibre interactions on the total swelling rate of fabric are proposed. Finally, this chapter presents the performance measures of cotton samples under swelling conditions. To study and analyse the flow through swelling porous media experimentally, the parameters of the porous media should be measured carefully. These parameters are Fibre diameter, porosity, permeability, and capillary pressure. The experimental procedures to measure these parameters are described in the next subsections.

## 4.1 Cotton fabric

A wide variety of properties are used to design new hygiene products. The product developers have to optimise a set of characteristics such as shape, absorption potential, breathability, durability, cost, etc. Pure cotton or cotton blends with polyester are among the commonly used materials in absorbent fabrics. The cotton fabric used in this study was selected based on the scope of this study, and the design of hygiene products. Hence, muslin squares (used as nappies for baby care products) made up of 100% cotton were selected for the study. As specified by the manufacturer, these fabrics are woven using extra-long-staple cotton (ELS) that provides a tight weaving pattern and better absorbency. Since the α-cellulose content of a typical cotton fibre ranges from 88.0% to 96.5%, the cotton tends to swell upon water absorption.

To make a sample out of the fabric sheets, several pieces of fabric were cut to a specified size and sewed together to make one overlocked piece. Each overlocked

piece was made up of seven individual pre-cut pieces. Finally, to make a sample out of overlocked pieces, nine of these were stacked together to make one sample, as shown in Figure4.1. This total gave a sample thickness of 25 mm. The sample was compressed near the edges (sewing line) but was almost uniform and isotropic in the other areas.

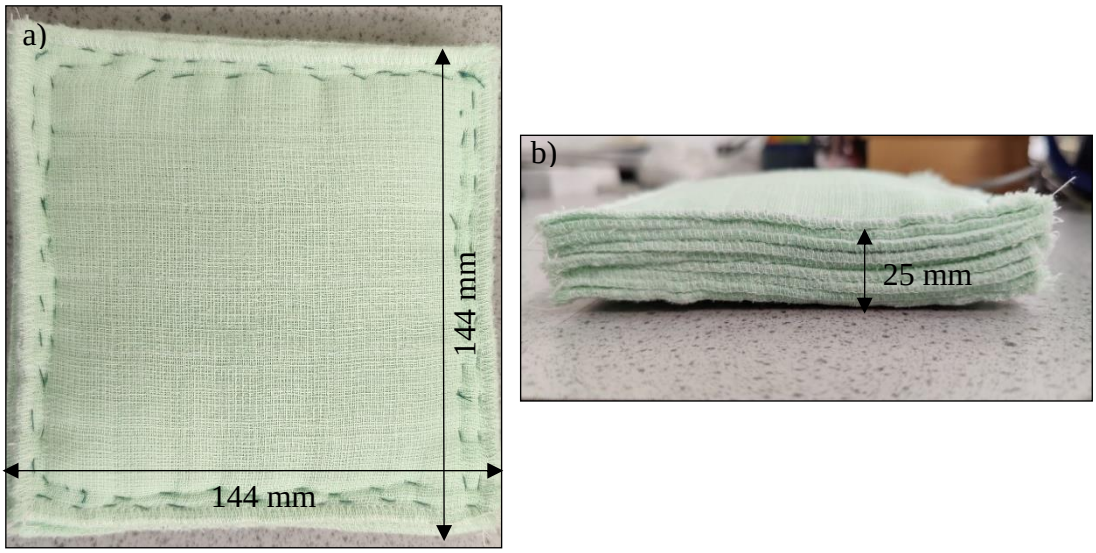


Figure 4-1 The front and top view of the prepared sample for the liquid absorption experiments

Several samples were made to measure the porosity, permeability, capillary pressure, and liquid absorption performance of the cotton fabrics. The use of this sample is presented in the next subsections.

## 4.2 Measurement of the Fibre diameter

The swelling of the fibres as a result of the swelling has a great effect on the porosity and permeability of the fabrics. Hence investigation of the swelling effect on the fibre is the first step in the study. Firstly, the swelling of the individual fibre was measured using the method proposed by Masoodi et al. The swelling of individual fibres was analysed using the Nikon metallurgical microscope eclipse lv150N at a magnification of 10×, along with the live recording camera to examine the cotton fabric behaviour due to water absorption. The microscope was calibrated within a range of 3µm as specified by the manufacturer.

Several 150 mm cotton fibre samples/slides were prepared by securing both ends using a suitable adhesive strip and placed under the microscope as shown in Figure 4.2. The diameters of fibre at the different locations were recorded in the dry state and its

averaged diameter is taken as the pre-swelled diameter $D_o$. Once this was measured, the samples were exposed to the water. The wetting process was recorded for a total of 1 minute. Once recorded, the photographs were taken every 1 or 2 seconds. The diameters (D) were then measured at different time values. The photographs are compared with the reference measurement $(D_o)$ using the same calibrated scale, allowing for the observation of any diameter growth. The process was repeated 5 times. Finally, the results were extracted in terms of relative changes in diameter $(D/D_o)$ with time. For the swelling measurement, water is used as the test liquid as it induces the swelling in cotton fabric

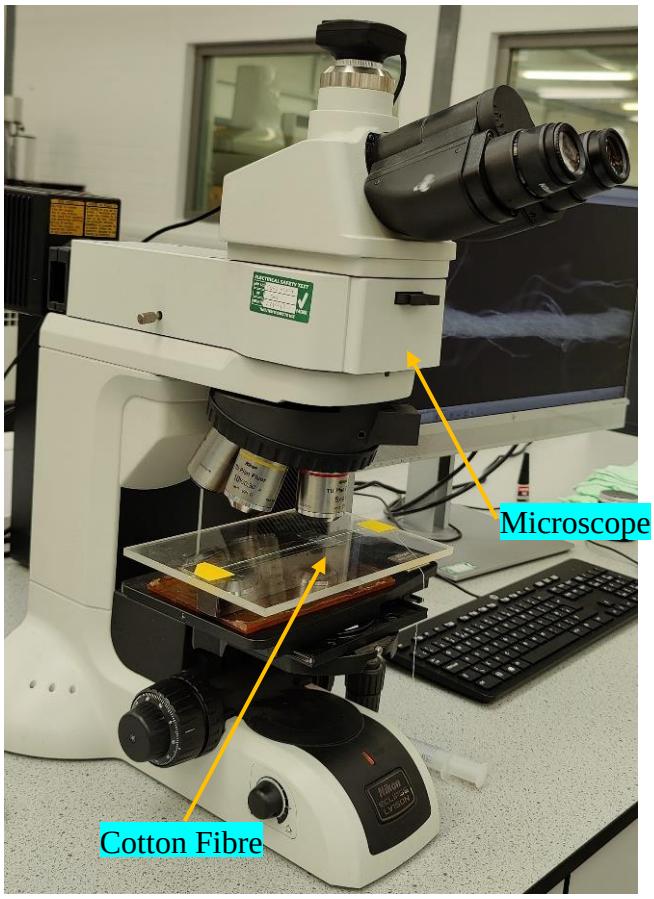


Figure 4-2 Microscopic arrangement to record the wetting process of individual cotton fibre

Figure 4.3 shows the evolution of the average fibre diameter of cotton when exposed to water. It demonstrates that when fibres were unrestricted, they swelled up to 10%. From Figure 4.3, it is clear that the maximum swelling of cotton fibre occurred within a shorter period of time due to its super absorbency. The α-cellulose content of a typical cotton fibre ranges from 88.0% to 96.5%. The polar group on the cellulose molecule attracts water molecules by hydrogen bonding, resulting in moisture build-

up in the cell wall and fibre swelling. The predictions related to the changes in the diameter of cotton fibre could be useful while predicting the porosity and permeability changes analytically; such predictions would help engineers to design and optimise the products made up of cellulose-based fabrics. Based on the obtained results, the expression that predicts the changes in cotton fibre diameter when exposed to water is given as:

$$\frac{D}{D_o} = 1.115 - 0.1257e^{-0.3189t} \qquad 4.1$$

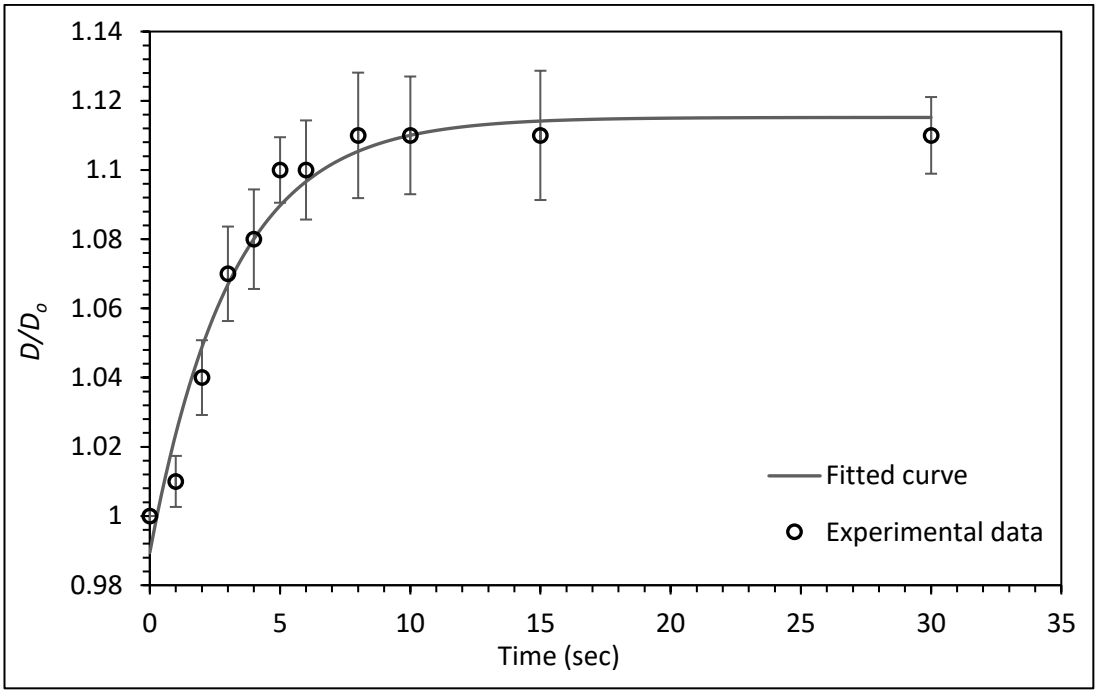


Figure 4-3 Swelling of cotton fibres in water: the current averaged diameter of the fibres is $D_o$ = 0.000272 m; the error bars show a confidence interval of 95%.

## 4.3 Measurement of the porosity

### 4.3.1 Porosity and capillary pressure measurement under rigid conditions

The porosity in the study is measured under rigid and swelling conditions. Firstly, the porosity is measured under rigid conditions by using the imbibition method. The method is simple; in this method, the weight of the dry porous sample is first recorded then the sample is immersed in the oil that the porous sample tends to imbibe. Once the sample is fully saturated by the oil the corresponding weight is recorded again. As described earlier, water induces swelling in cotton fabrics hence it cannot be used to measure the porous media properties under rigid conditions. To measure the porosity correctly, two different test liquids are used in this study. As a substitute for water, the oil is used as a test liquid for the measurements under rigid conditions. To check if the

cotton swells in oil, the same process as described in the previous section is followed. The cotton fibres are exposed to oil and observed under the microscope to look for any changes in diameter. The multifunctional oil WD-40 is used for the measurements under rigid conditions. Once the weight of the sample under saturated conditions is recorded, the porosity under the rigid conditions is calculated using the following expression,

$$\varepsilon_o = \frac{(W_s - W_d)/\rho_{oil}}{V_{sample}} \qquad 4.2$$

where $\rho_{oil}$ is the density of the oil, $V_{sample}$ is the volume, $W_s$ and $W_d$ are the weight of the sample in saturated *(s)* and dry *(d)* conditions.

The prepared samples as described in the previous section were used for the porosity measurement in rigid conditions. The weight of the sample in the dry and saturated state was recorded for each test and the porosity was calculated using Equation (1). The five different tests were conducted to measure the porosity to report the results with a confidence level of 95%. Finally, the average porosity was found to be 0.88. Table 4.1 below shows the experimental results for the porosity measurement under rigid conditions.

Table 4.1 Experimental results for the porosity measurement in rigid conditions

| **Test** | **Weight (dry) (kg)** | **Weight (saturated) (kg)** | **Pore volume ($m^3$)** | **Sample volume ($m^3$)** | **Porosity** |
|---|---|---|---|---|---|
| 1 | 0.155 | 0.472 | $3.88\times10^{-4}$ | $4.40\times10^{-4}$ | 0.881 |
| 2 | 0.155 | 0.472 | $3.88\times10^{-4}$ | $4.40\times10^{-4}$ | 0.881 |
| 3 | 0.155 | 0.472 | $3.87\times10^{-4}$ | $4.40\times10^{-4}$ | 0.879 |
| 4 | 0.155 | 0.472 | $3.87\times10^{-4}$ | $4.40\times10^{-4}$ | 0.879 |
| 5 | 0.155 | 0.472 | $3.87\times10^{-4}$ | $4.40\times10^{-4}$ | 0.879 |

### 4.3.2 Porosity measurement under swelling conditions

The porosity is also measured under swelling conditions, for this case water is used as the test liquid. Several samples of the cotton fabric cell (24mm×24mm) were pasted on the slide with their all ends secured using the adhesive as shown in Figure 4.4

Next, the prepared slides are placed under the Nikon metallurgical microscope eclipse lv150N at 10x magnification. Finally, small amounts of water are injected within the

unit cells using a syringe. The whole wetting process was recorded, and photographs were taken every second. This is the first time that porosity measurement is done under swelling conditions. The obtained photographs are then characterised using the tool called Image J. As discussed earlier, due to the effect of swelling, the porosity of the fabric reduces. As a result, the solid volume fraction increases by decreasing the available pore area. This reduction in the pore area is captured by using the image segmentation technique. The thresholding method is the simplest method of image segmentation. Thresholding is a technique to divide the image into two or more classes of pixels.

Figure 4-4 Unit cells of the cotton fabric used to measure the porosity reduction

For the present study, the thresholding technique is applied to binary image segmentation. The advantage of having a binary image is that it only has two possible intensity values. Numerically, these values are either 1 or 255 for white and 0 for black. For the current study first, the obtained image is converted into an 8-bit image. Once converted to an 8-bit image, the threshold values are adjusted to track the pore area for each image. Finally, from the pore area, the porosity is estimated. The figure below shows the steps in the image segmentation process. This process is repeated for each recorded image and porosity reduction is estimated.

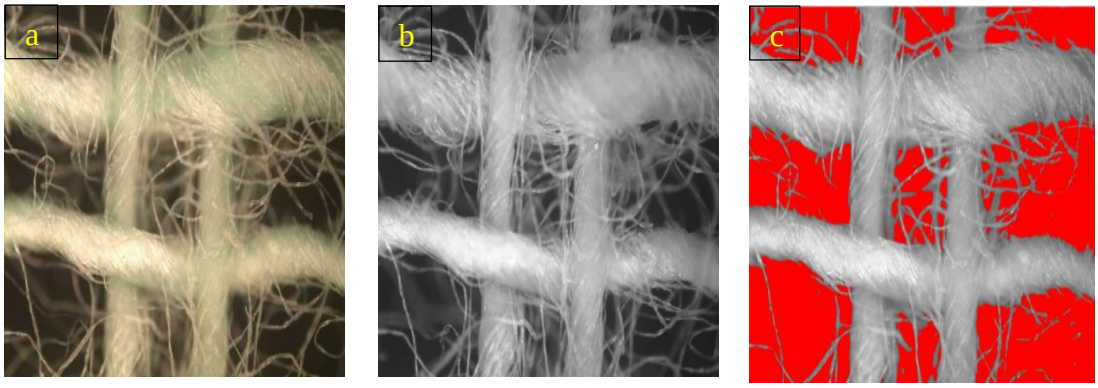


Figure 4-5 Characterization process of the image to calculate the pore area: a) original image, b) black and white image, and c) Pore area tracking

Figure 4.6 shows the reduction in the porosity as a result of swelling when exposed to water. The initial or dry state porosity ($\varepsilon_o$) of the unit cell is found to be 0.436 which is the average of five measurements. Upon water absorption, the porosity rapidly reduces over a shorter period of time. This behaviour is also observed in the case of individual fibre swelling. The relative changes in the porosity are plotted against time. The relative porosity is the ratio of final porosity at a given time to the initial porosity ($\varepsilon/\varepsilon_o$). Figure 4.6 shows that the relative porosity reduces by 11%. It is also observed that the porosity rapidly reduces till 6 seconds and becomes then becomes constant.

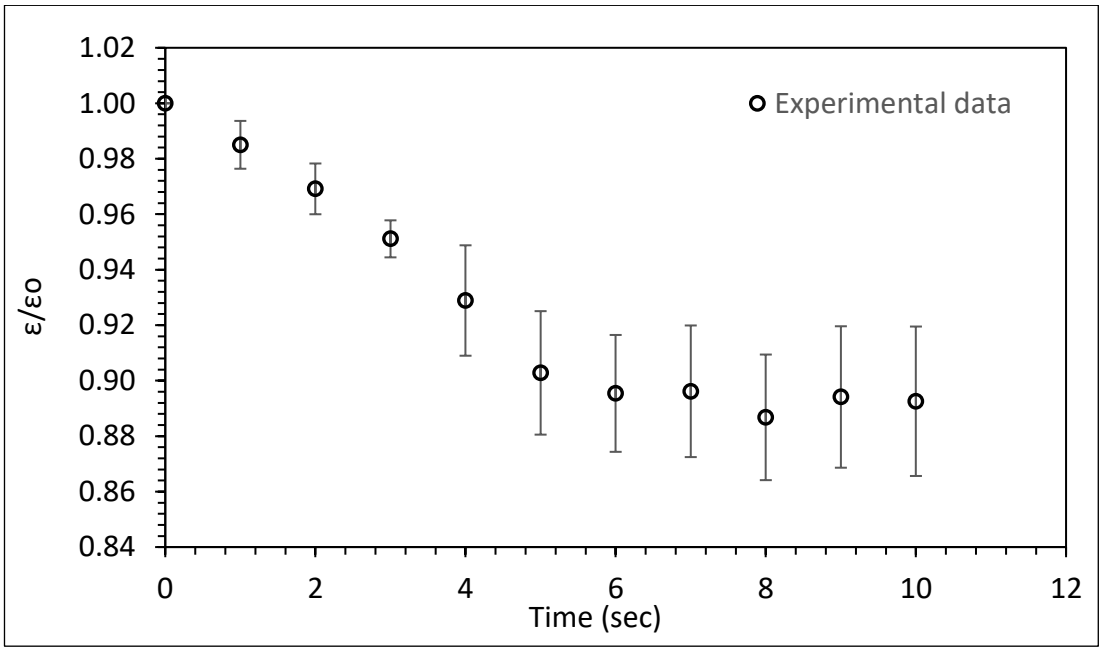


Figure 4-6 Swelling of the unit cell of cotton fabric in water: the current averaged initial porosity ($\varepsilon_o$) of a unit cell is = 0.436; the error bars show 95% confidence intervals

Based on the obtained results for porosity reduction, a fitting expression that predicts the reduction in porosity when exposed to water is given by,

$$\frac{\varepsilon}{\varepsilon_o} = 0.0015t^2 + 0.0266t + 1.0085 \qquad 4.3$$

The porosity reduction can be also predicted analytically. Masoodi et al. (2012a) proposed an expression that determines the reduction in porosity as a result of swelling. The equation is derived using the simple approach in which it is assumed that the fibre swells independently without any interference from other fibres. The equation proposed by Masoodi et al is given as,

$$\varepsilon = 1 - (1 - \varepsilon_o)\left(\frac{D}{D_o}\right)^2 \qquad 4.4$$

where $D_o$ and $\varepsilon_o$ are the initial fibre diameter and porosity of the fabric. If the changes in the relative diameter ($D/D_o$) with respect to time are known, then Equation 4.4 can be used to predict changes in porosity. Figure 4.7 compares the analytical predictions for porosity reduction using equation 4.4. and Experimental results. Equation 4.4 is overpredicting the reduction in the porosity. The porosity reduction is predicted around 30% by Equation 4.4 which is higher than the experimentally determined values. The reason behind this can be related to the assumptions made while deriving Equation 4.4. It does not take inter-fibre interaction into account. In reality, there are restrictions within the porous matrix due to the dense network of the fibres which affects the swelling of fibres.

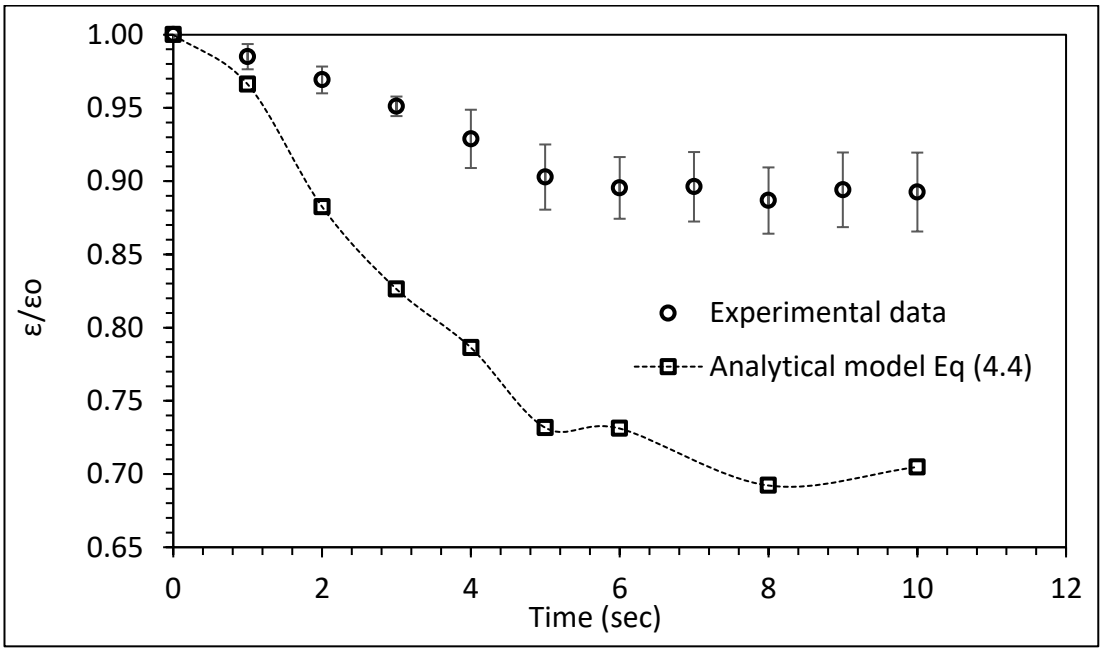


Figure 4-7 Comparison between analytical predictions with Experimental data for porosity reduction

To account for these miscellaneous effects, the corrections factors are proposed in this study. The correction factors are selected based on the nature of the graph. Using the regression analysis, the values of constants *a* and *b* are optimised as presented in Table 4.2 below. Following are the two different correction factors (*$C_1$ and $C_2$*) proposed,

$$\mathrm{C}_1 = \left( a \left( \frac{\varepsilon}{\varepsilon_o} \right)^{1-b} \frac{\varepsilon}{\varepsilon_o} \right) \tag{4.5}$$

$$\mathrm{C}_2 = \left( e^{\left( a \times \left( b - \frac{\varepsilon}{\varepsilon_o} \right) \right)} \frac{\varepsilon}{\varepsilon_o} \right) \tag{4.6}$$

Equation 4.4 is then modified by adding these correction factors, The modified equation is given by,

$$\varepsilon = 1 - (1 - \varepsilon_o) \left( \frac{D}{D_o} \right)^2 \mathrm{C}_{n\,(n=1\ or\ 2)} \tag{4.7}$$

Table 4.2 Values of the constants a and b for the correction factors

| Correction factor | *a* | *b* |
|---|---|---|
| *$C_1$* | 1 | 0.67 |
| *$C_2$* | 0.997 | 0.82 |

Figure 4.8 shows the comparison between the experimental results and the predictions from the corrected analytical model given by Equation 4.7. It is observed that the corrected predictions are in excellent agreement with the experimental results. The results demonstrated the applicability of such correction factors in analytical models for the correct the existing analytical models.

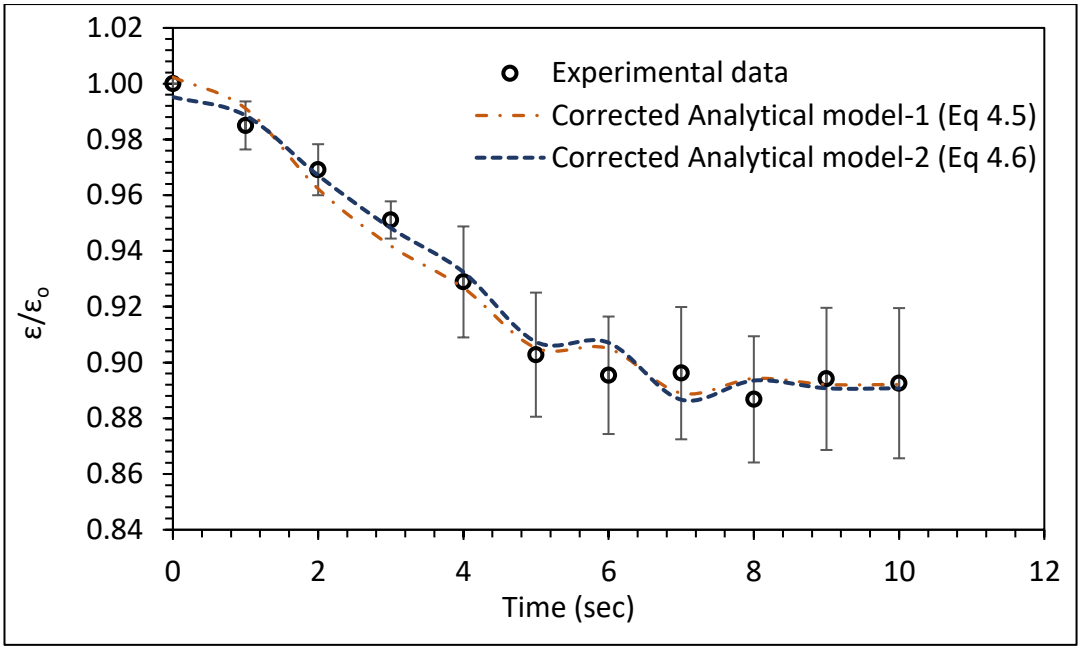


Figure 4-8 Comparison between experimental and modified analytical predictions with proposed correction factors

## 4.4 Measurement of Capillary pressure

The capillary pressure is also measured for the samples. The simple vertical wicking test method is used to measure capillary pressure. As a result of wicking, the liquid is absorbed within the porous sample against gravity. The final wicking height is then used to calculate the hydrostatic pressure which can be taken as the capillary pressure. The hydrostatic pressure related to the final wicking height is calculated using the well-known formula.

$$P_c = \rho_w \, g \, h \qquad 4.8$$

Where $\rho_w$ is the density of water and $h$ is the final wicking height

The measured value of capillary pressure is 1412.64 Pa which is the averaged value of five tests for a total wicking height of 0.144 m.

## 4.5 Measurement of the permeability

The permeability of the prepared samples is measured by using the Falling head permeability tests. Falling head permeability is an effective and simple technique to measure the permeability of porous materials. As shown in Figure, for the falling head permeability tests, the liquid is made to flow through the sample under fully saturated conditions. The exit tube of the sample holder is maintained at atmospheric conditions which makes the exit head 0. Once the steady state is reached, the initial and final

heights *($h_o$* and *$h_1$)* of the liquid column and the respected time values *($t_o$* and *$t_1$)* are recorded. Using the recorded values, the permeability coefficient can be calculated using the following expression,

$$K = \frac{a\,L}{A\,t}\,ln\left(\frac{h_o}{h_1}\right) \qquad 4.9$$

where *a* is the diameter of the pipe, *L* is the thickness of the sample, *A* is the cross-sectional area of the sample, $h_o$ and $h_1$ are the initial and final heights of the liquid column in the pipe and *t* is time. Rearranging the above equation we get,

$$\ln\left(\frac{h_o}{h_1}\right) = \left(\frac{A}{a\,L}\,K\right) \qquad 4.10$$

The coefficient of permeability is also calculated using a well-known equation,

$$K = \left(\frac{k\ \times \rho\ \times g}{\mu}\right) \qquad 4.11$$

where *k* is the permeability of the fabric sample, $\rho$ is the density of the test liquid and $\mu$ is the dynamic viscosity of the test liquid. Upon combining above Equations 4.10 and 4.11 we get

$$\ln\left(\frac{h_o}{h_1}\right) = \left(\frac{A}{a\,L}\right)\left(\frac{k\ \times \rho\ \times g}{\mu}\right)t \qquad 4.12$$

Equation 4.12 is later used to calculate the exact value of permeability for the prepared sample.

For the present study, a house-made falling head permeameter is developed as shown in Figure 4.8 (b). The permeability is measured under rigid and swelling conditions using the developed apparatus. As explained earlier, to measure the permeability under rigid and swelling conditions, WD-40 oil, and water are used as test liquids respectively.

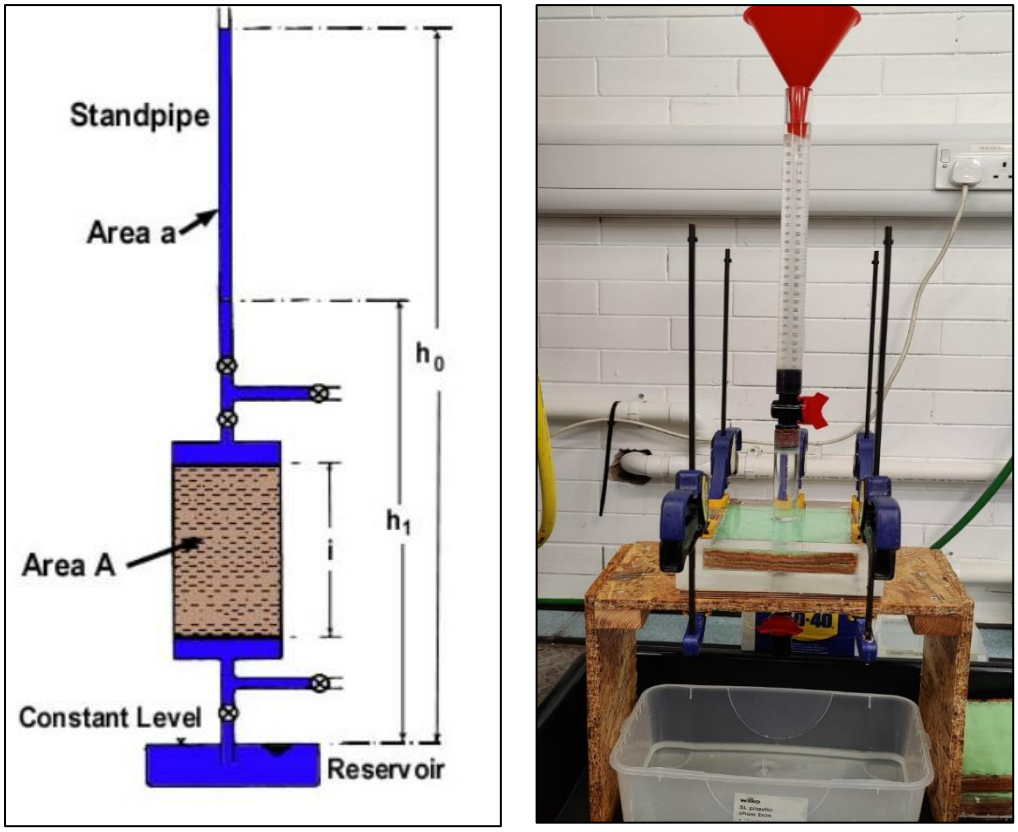


Figure 4-9 The falling head permeability test setup

The table below shows the details of the in-house built falling head permeability test setup and the properties of test liquids.

Table 4.3 Details of apparatus and test liquids

| | | |
|---|---|---|
| Tube diameter | 0.02 | m |
| Area of the tube ($a$) | 0.0003142 | $m^2$ |
| Length of Sample ($L$) | 0.022 | m |
| Width of the sample ($w$) | 0.142 | m |
| Area of sample ($A$) | 0.020164 | $m^2$ |
| Volume of the sample ($V$) | 0.0004436 | $m^3$ |
| Density of oil ($\rho_{oil}$) | 817 | $Kg/m^3$ |
| Viscosity of oil ($\mu_{oil}$) | 0.0010 | $N\text{-}s/m^2$ |
| Density of water ($\rho_{water}$) | 1000 | $Kg/m^3$ |
| Viscosity of water ($\mu_{water}$) | 0.0013 | $N\text{-}s/m^2$ |

### 4.5.1 Permeability measurement under rigid conditions

The measurement of the permeability under rigid is done using the in-house-built apparatus. First, the permeability is measured under rigid conditions by using oil. The sample is held in the sample holder or mould and saturated with the oil. After saturating the sample, the initial head of 260 mm is maintained in the tube and slowly the valves are opened. The time is recorded for the liquid column depths of 60 mm,120 mm,180mm and 250 mm respectively. The following table shows readings of the falling head permeability test done under rigid conditions. Note that the results shown are the averaged values of five tests.

Table 4.4 Readings obtained for the falling head permeability tests for rigid conditions

| Initial head (m) | Final head (m) | Depth (m) | Time (sec) | Permeability coefficient (m/sec) | Permeability ($m^2$) |
|---|---|---|---|---|---|
| 0.260 | 0.200 | 0.600 | 1.2 | $7.31\times10^{-5}$ | $9.12\times10^{-12}$ |
| 0.260 | 0.140 | 0.120 | 2.1 | $9.73\times10^{-5}$ | $1.21\times10^{-11}$ |
| 0.260 | 0.180 | 0.180 | 3.2 | $1.25\times10^{-4}$ | $1.56\times10^{-11}$ |
| 0.260 | 0.100 | 0.250 | 4.4 | $2.53\times10^{-4}$ | $3.15\times10^{-11}$ |

From the obtained readings, the dimensionless parameter $ln\ (h_0/h_1)$ is plotted against time as shown in Figure 4.9.

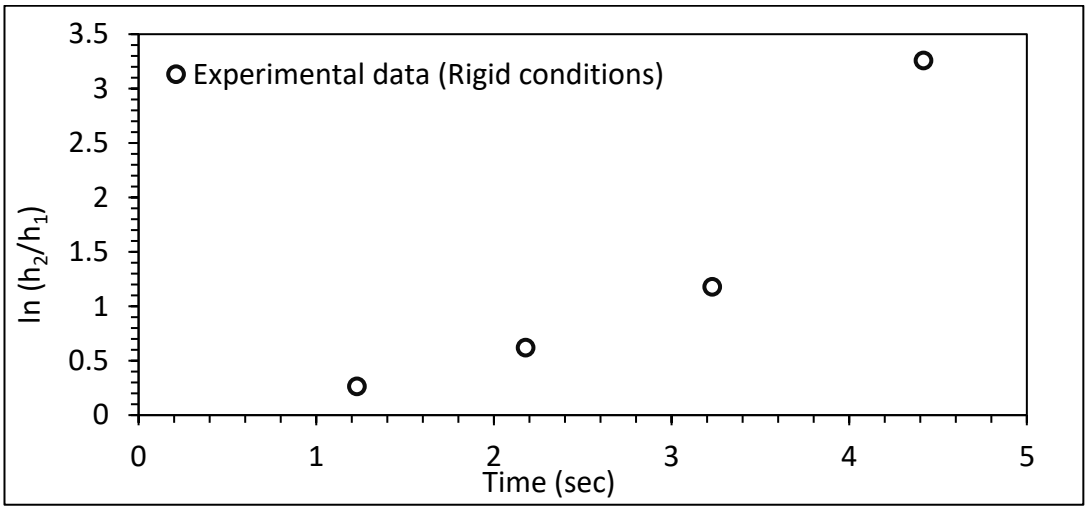


Figure 4-10 Variation of dimensionless parameter $\ln(h_0/h_1)$ with time for rigid case

To calculate the permeability using the obtained readings, Firstly, the permeability coefficients are calculated using Equation 4.9. Finally, Equation 4.11 is used to calculate the permeability values. Note that, permeability coefficient and permeability are two different concepts. The permeability coefficient is also known as Hydraulic

conductivity which is denoted as *K*. Table below shows the obtained permeability coefficients and Permeability values for a rigid case. The Figure shows the variation of the permeability with depth.

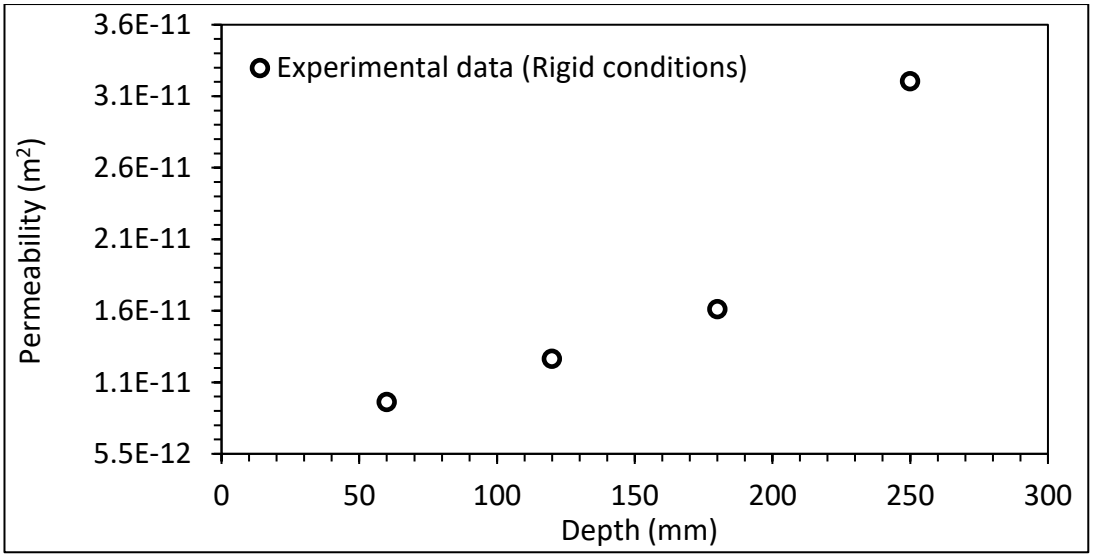


Figure 4-11 Variation of the permeability with depth for rigid conditions

The permeability is calculated using Equation 4.12. The slope of the $ln\ (h_0/h_1)$ is calculated and equated with the RHS of Equation 4.12. This gives the permeability value of $3.91\times10^{-11}m^2$ which is closer to the calculated permeability value for 0.250m depth. Hence, the measured permeability of the prepared sample under rigid conditions is finalised to be $3.91\times10^{-11}m^2$

### 4.5.2 Permeability measurement under swelling conditions.

The permeability is also measured under fully swollen conditions using the same apparatus and process as stated in the previous subsection. For the swelling case, water is used as the test liquid as it induces swelling in the cotton fabrics. The sample is first saturated with water and then time values are recorded for different depths once the steady state is reached. The following table shows the readings of the falling head tests conducted under swelling conditions. Note that the readings shown in the table are the averaged value of five tests.

Table 4.5 Readings obtained for the falling head permeability tests for swelling conditions

| Initial head (m) | Final head (m) | Depth (m) | Time (sec) | Permeability coefficient (m/sec) | Permeability ($m^2$) |
|---|---|---|---|---|---|
| 0.260 | 0.200 | 0.600 | 1.7 | $4.28\times10^{-5}$ | $6.67\times10^{-12}$ |
| 0.260 | 0.140 | 0.120 | 3.5 | $5.82\times10^{-5}$ | $9.18\times10^{-12}$ |
| 0.260 | 0.180 | 0.180 | 5.6 | $7.01\times10^{-5}$ | $1.11\times10^{-11}$ |
| 0.260 | 0.100 | 0.250 | 8.5 | $1.27\times10^{-5}$ | $2.005\times10^{-11}$ |

From the obtained readings, the dimensionless parameter *ln* $(h_0/h_1)$ is plotted against time as shown in Figure 4.11. Further, Figure 4.12 shows the variation of the permeability with depth for the swelling conditions. Upon comparing the results with the rigid case, the effect is swelling can be seen as a result of swelling,

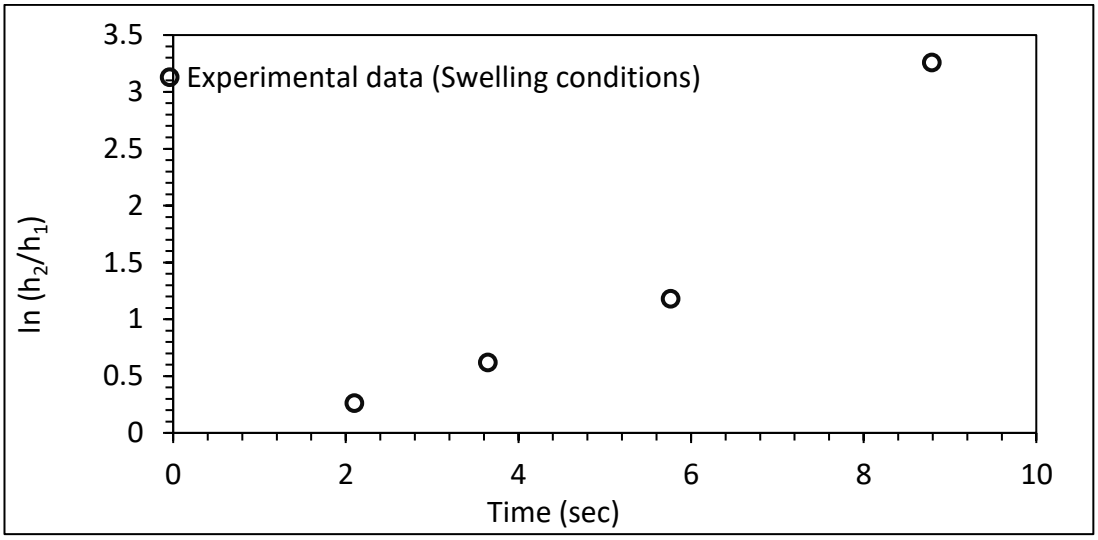


Figure 4-12 Variation of dimensionless parameter $\ln(h_o/h_1)$ with time for swelling case

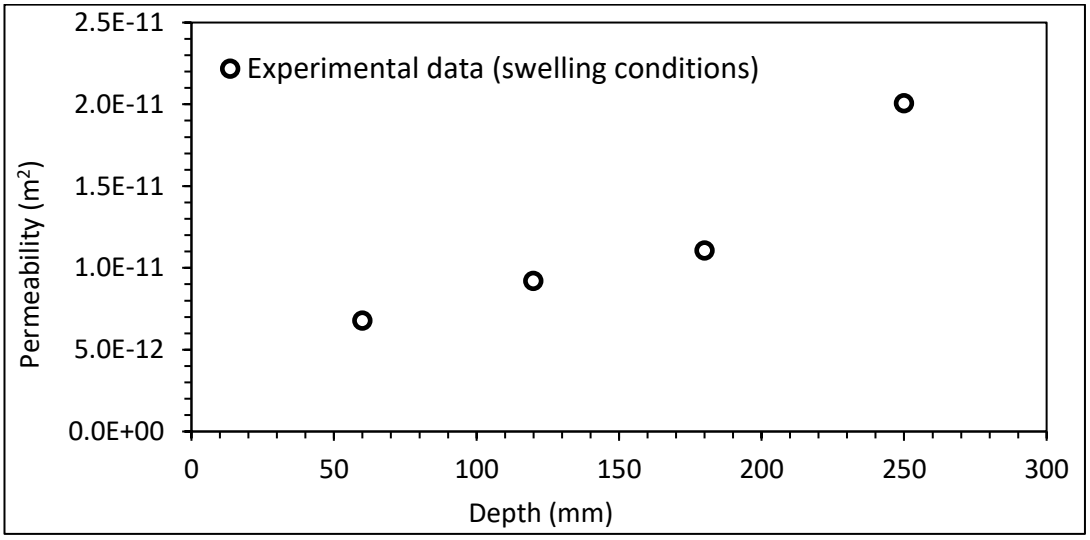


Figure 4-13 Variation of permeability with depth for swelling case

The permeability for the swelling case is estimated using the same approach as the rigid case using Equation 4.12 as explained in the previous subsection. The obtained value of permeability under fully swollen conditions is $2.40\times10^{-11}m^2$which is closer to the calculated permeability value for 0.250m depth It can be observed that the permeability is reduced by almost 60 % than the rigid case. This demonstrates the effect of swelling on the cotton fabrics due to water absorption.

The presented results only show the total reduction in permeability of prepared samples under fully swollen conditions. Hence, in this study different analytical models of permeability are used to predict the changes in the permeability with time. Masoodi and Pillai (2010) proposed different models that can be used to predict the changes in permeability because of swelling. Equation 2.3 is the general form of permeability which is the function of porosity and fibre/bead diameter. Masoodi and Pillai (2010) modified the equation by replacing the constant c in the porosity function with the ratio of permeabilities $(K/K_o)$. The table below shows the different models available to predict permeability.

Table 4.6 The final forms of the permeability expressions for porous media made up of packed particles as cited in Masoodi and Pillai (2010)

| Author and Year | Suggested relation for $\varphi(\varepsilon)$ |
|---|---|
| Blake (1922), Kozeny (1927), Carman (1937) | $K_o\left(\frac{\varepsilon}{\varepsilon_0}\right)^3\frac{1-\varepsilon_0}{1-\varepsilon}$ |
| Zunkar (1920) | $K_o\frac{\varepsilon}{\varepsilon_0}\frac{1-\varepsilon_0}{1-\varepsilon}$ |
| Terzaghi (1925) | $K_o\left(\frac{\varepsilon-0.13}{\varepsilon_0-0.13}\right)^2\left(\frac{1-\varepsilon_0}{1-\varepsilon}\right)^{0.3}$ |
| Fehling (1939) | $K_o\left(\frac{\varepsilon}{\varepsilon_0}\right)^4\frac{1-\varepsilon_0}{1-\varepsilon}$ |
| Rose (1945) | $K_o\left(\frac{\varepsilon}{\varepsilon_0}\right)^{4.1}\frac{1-\varepsilon_0}{1-\varepsilon}$ |
| Rumpf and Gupte (1971) | $K_o\left(\frac{\varepsilon}{\varepsilon_0}\right)^{5.5}\frac{1-\varepsilon_0}{1-\varepsilon}$ |

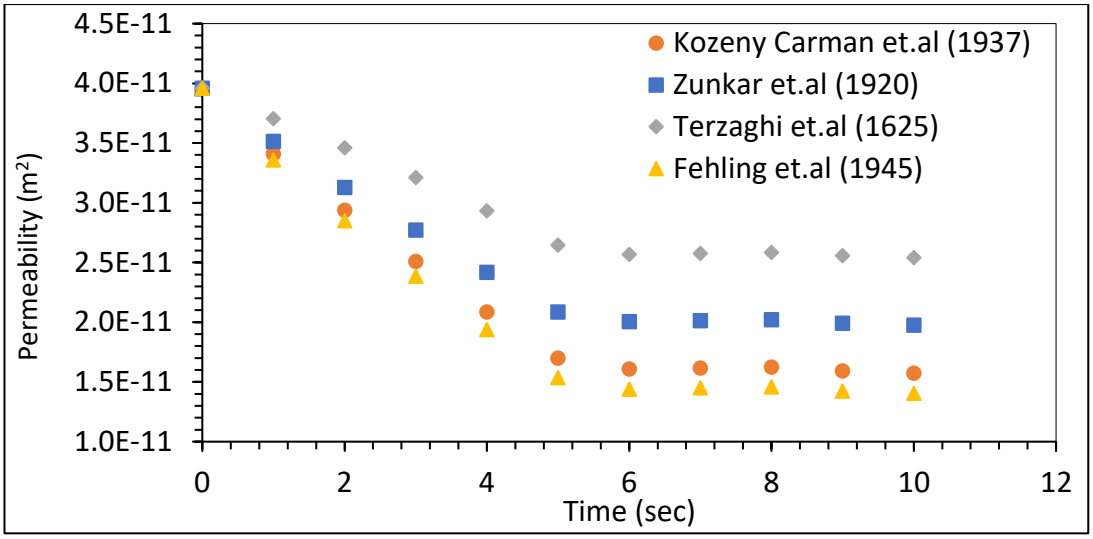


Figure 4-14 the predicted changes in the permeability of the sample using the formulations proposed for spherical porous media

Table 4.7 The final forms of the permeability expressions for fibrous porous media cited in Masoodi and Pillai (2010)

| Author and Year | Suggested relation for $\varphi(\varepsilon)$ |
|---|---|
| Devis (1952) | $K_0\left(\frac{1-\varepsilon_0}{1-\varepsilon}\right)^{0.5}\frac{1+56(1-\varepsilon_0)^3}{1+56(1-\varepsilon)^3}$ |
| Chen (1955) | $K_0\frac{\varepsilon}{\varepsilon_0}\ln\frac{(1-\varepsilon_0)^2}{(1-\varepsilon)^2}$ |
| Bruschke and Advani (1993) | $K_0\frac{\psi(\eta)}{\psi(\eta_0)}\frac{\eta}{\eta_0}$ where $\eta_0=\frac{4}{\pi}(1-\varepsilon_0)$ and $\psi(\eta)$ $=\frac{(1-\eta)^2}{\eta^3}\left(\frac{3\eta\cdot\tan^{-1}\sqrt{(1+\eta)/(1-\eta)}}{\sqrt{1-\eta^2}}+\frac{\eta^2}{2}+1\right)^{-1}$ |
| Gebart (1992) | $K_0\frac{1-\varepsilon}{1-\varepsilon_0}\left[\left(\sqrt{\frac{1-\varepsilon_{min}}{1-\varepsilon}}-1\right)/\left(\sqrt{\frac{1-\varepsilon_{min}}{1-\varepsilon}}-1\right)\right]^{5/2}$ $where\ \varepsilon_{min}=1-\frac{\pi}{2\sqrt{3}}$ |

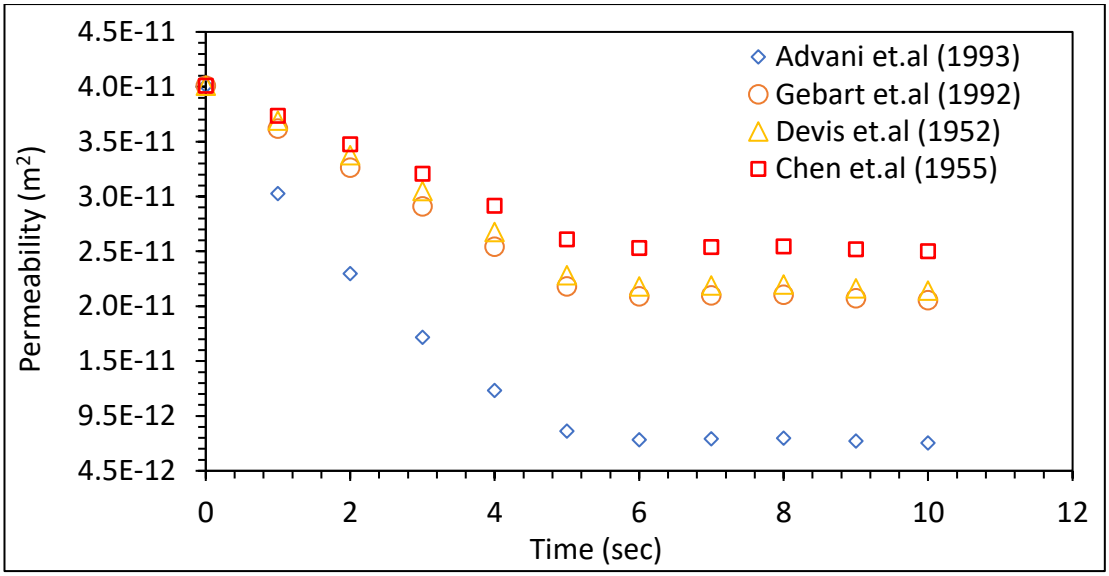


Figure 4-15 the predicted changes in the permeability of the sample using the formulations proposed for fibrous porous media

Figure 4.13 and 4.14 shows the predicted changes in permeability with time using the analytical models presented in tables 4.7 and 4.8. In this study, the permeability is not measured as a function of time, hence the applicability of these models will be confirmed by either numerical simulations or the sets of experiments.

## 4.6 Water absorption tests

The water absorption tests are conducted to analyse and study the performance of the cotton fabrics under swelling conditions. For the tests, a simple setup is developed as shown in Figure 4.16. The test setup includes the sample holder, camera system, water reservoir, supply pipes and computer. As shown in Figure 4.17 (a), the water is mixed with the red food colouring so that, its flow front propagation can be tracked easily during the injection process. The acrylic square box is used as a sample holder. The top face and bottom of the acrylic box have the engravings as shown in Figure 4.17 (a). The main purpose of having engravings on the top is to track the water flow front propagation correctly. Further, Figure 4.17(b) shows the details of the water reservoir used in the experiments. As seen in Figure 4.16, at the top face of the reservoir the pipe is attached which provides a continuous source of water. This is arrangement is used to maintain the constant liquid level in the water reservoir.

To record the liquid absorption process, the camera arrangements on top and bottom are used as shown in Figure 4.15. To avoid errors in the measurement, the cameras are started before injecting the water into the sample. The Logitech webcam (HD 1080p

60 fps) is used as the top camera and for the bottom face due to space restrictions, a mobile camera (HD 720p 30 fps) is used. Note that, the camera times are synced by starting them together at the same time. The top camera is attached to the laptop to record the process. The process is started by opening the valve as shown in Figure 4.15. The water is injected within the sample through a 3mm nozzle. For the present study, two different values of water heads (0.52 m and 1.3 m) are selected. The water level is measured by an attached scale

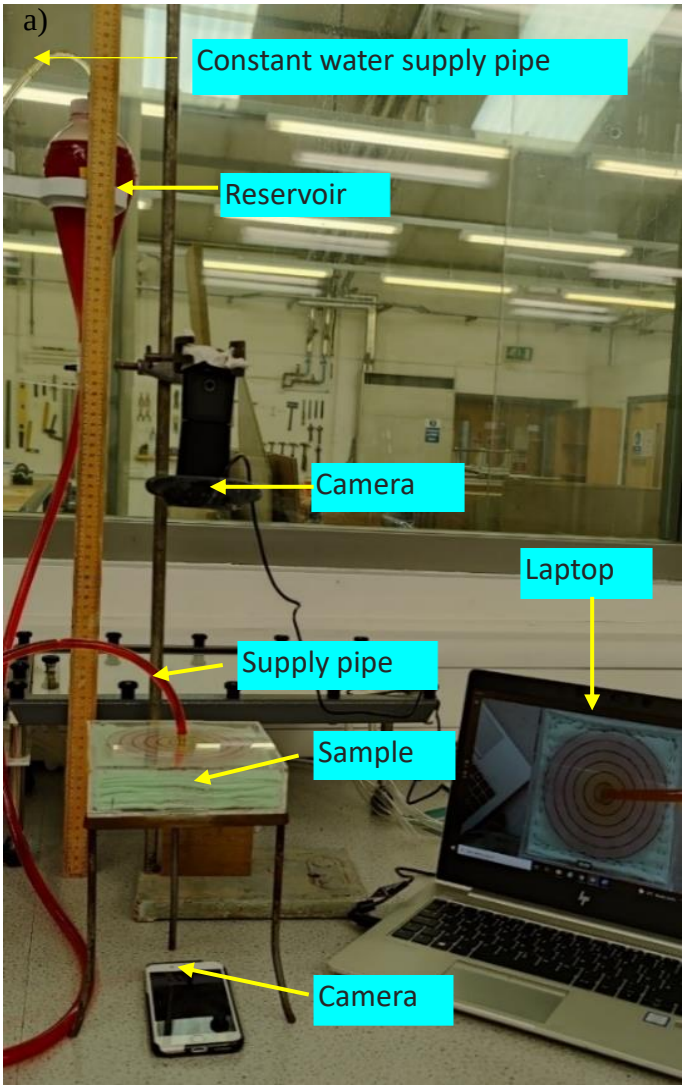


Figure 4-16 The setup to test the water absorption performance of the fabrics

Figure 4.17 and Figure 4.18 shows the obtained flow front locations for the water absorption test for two different water head values (0.52 m and 1.3 m). The results include the water flow front propagation on the top and bottom face of the sample. The graph shows the flow front advancement is more dominant on the bottom face of the sample than on the top face. It takes almost 250 sec for the water flow front to

reach 60 mm on the top face whereas on the bottom face it takes 144 sec. The dominant flow front propagation on the bottom face is related to the effect of the gravitational forces.

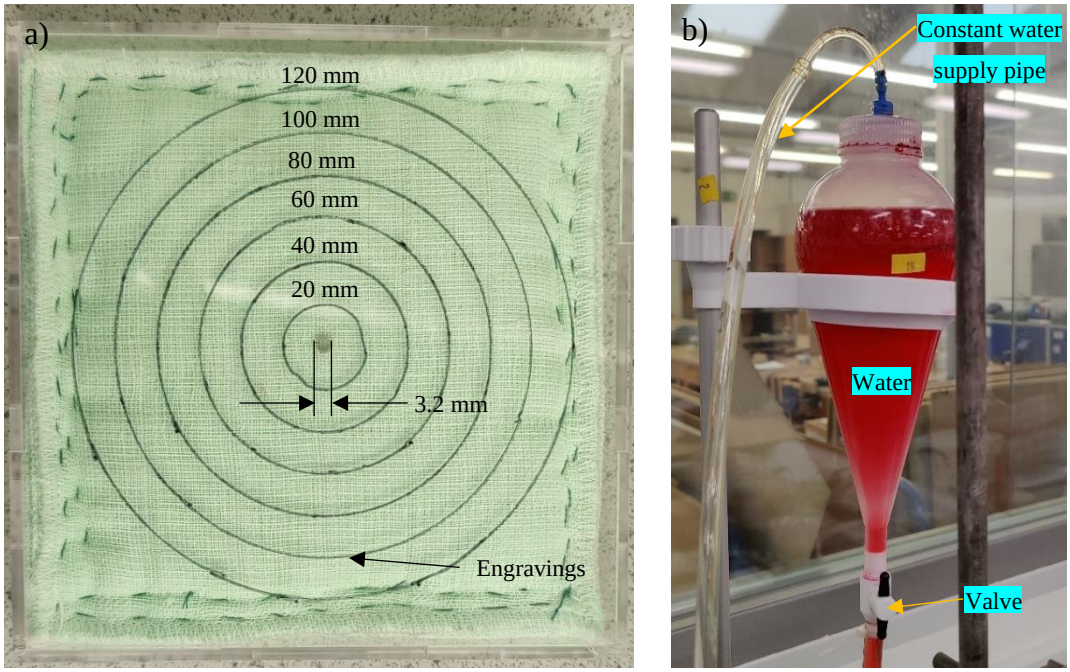


Figure 4-17 Details of a) Top view of sample holder b) water reservoir

The measured capillary pressure for the given sample is 1418 Pa, As the capillary forces along with the gravity and inflow force are in the same direction, the liquid absorption in the downward direction becomes dominant causing the faster flow on the bottom face. Further, it can be observed that changes in the water head affected the flow front advancement on both faces. The flow front propagation is faster for the case of 1.3 m water head, it can be seen that the total time to reach a 60 mm front radius is reduced by 20 % on both faces. From the figures, it can be observed that errors related to flow front propagation bottom face are larger. As mentioned earlier, the samples are made by stacking the different layers of pre-cut cotton fabric together by hand sewing process. This may be the reason behind the large error bars as the stacking pressure may not be constant and the same for each sample. As a result, the water absorption between interlayers is affected. If the stacking pressure is not uniform throughout the sample, it could lead to inconsistent water absorption. Also, as a result of water absorption, it was observed that the middle part of the sample swells up which could another reason behind the error bars. It is expected that for machine-sewed samples, this error may reduce. As the stacking pressure will be uniform and constant throughout the samples. Also, the samples were dried and reused for some tests; it was

observed that the size of samples after reuse changed slightly, which could be a reason behind the errors. Note that these results are the averaged values of five experiments and error bars are 95% confidence intervals. Finally, Figure 4.19 shows the flow front locations from the experiments for the top and bottom faces of the sample. Note that, the thick black lines that appear in the figures is stand.

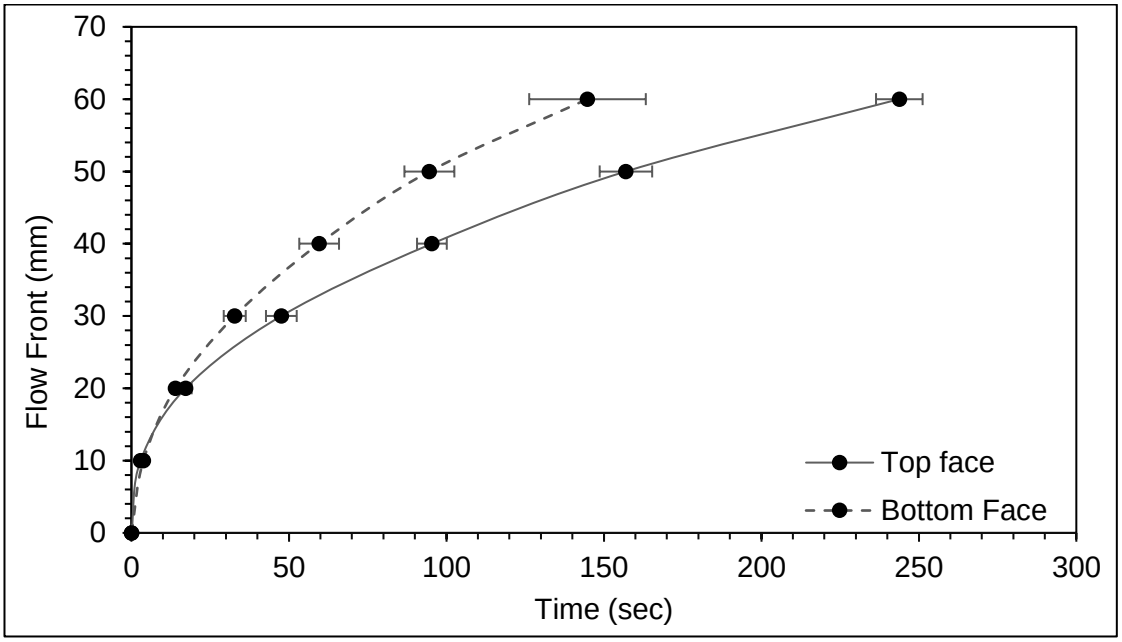


Figure 4-18 The experimental observation of water flow front locations at constant pressure inlet water head 0.52 m

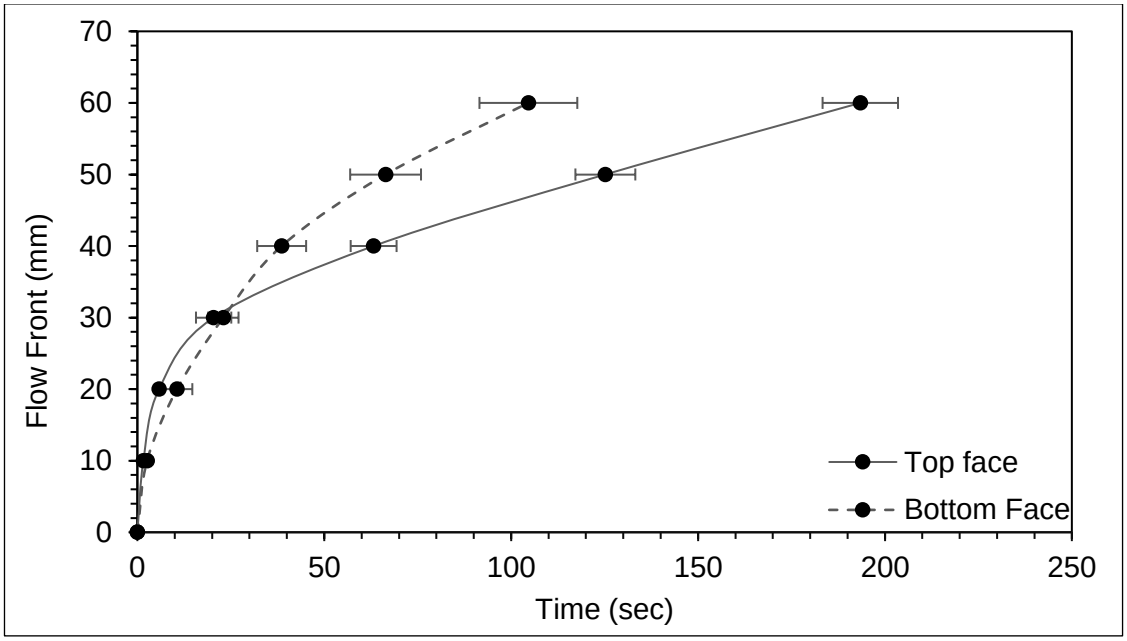


Figure 4-19 The experimental observation of water flow front locations at constant pressure inlet water head 0.13 m

| Flow front Radius (mm) | Time (sec) | Top face | Time (sec) | Bottom face |
|---|---|---|---|---|
| 10 mm | 2.9 | 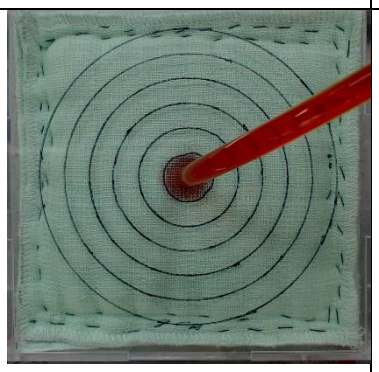 | 3.8 | 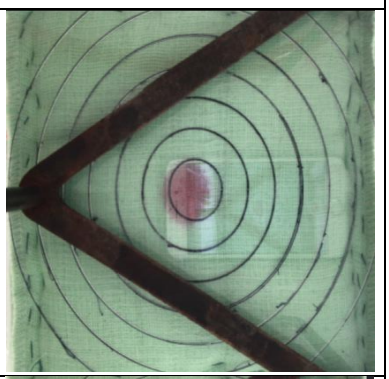 |
| 20 mm | 17 | 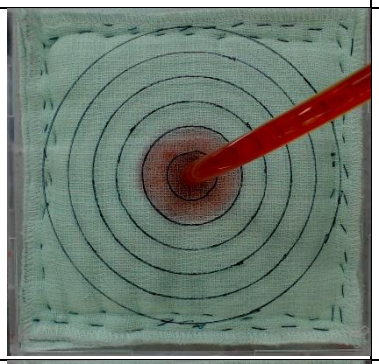 | 14 | 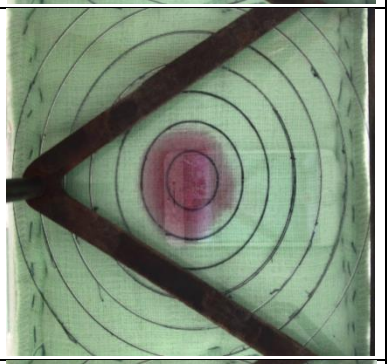 |
| 30 mm | 46.5 | 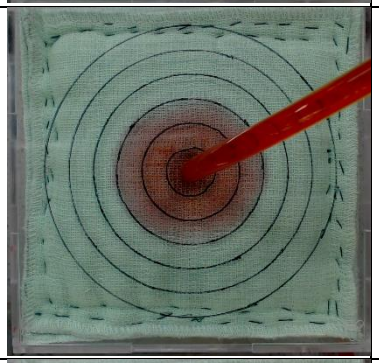 | 32 | 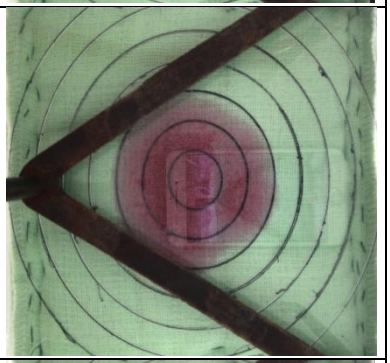 |
| 40 mm | 95.4 | 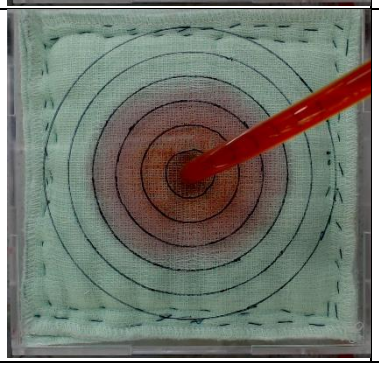 | 59 | 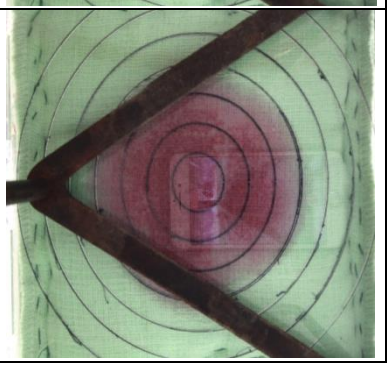 |

| | | | | |
|---|---|---|---|---|
| 50 mm | 157 | 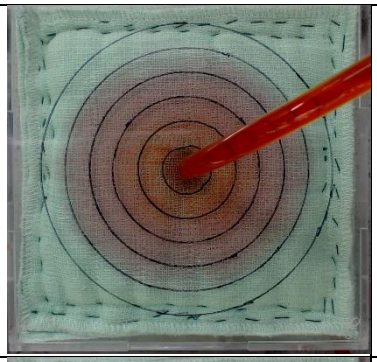 | 94 | 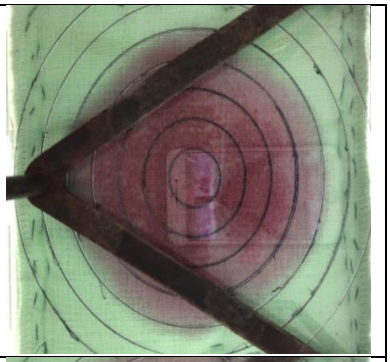 |
| 60 mm | 243 | 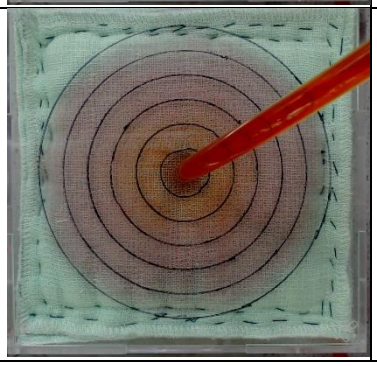 | 144 | 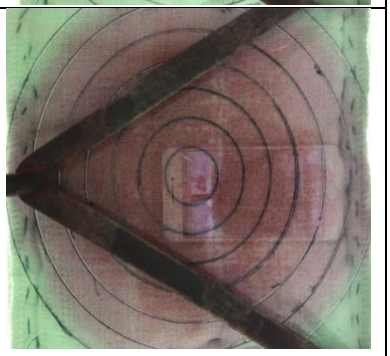 |

Figure 4-20 Experimental results for the flow front propagation of water for 0.52 m water head

## 4.7 Chapter Summary

In this chapter, we analysed the swelling of the cotton fibres in water. To study the effect of swelling, the changes in the fibre diameter, porosity and permeability were experimentally investigated. The swelling of cotton fibres caused the porosity and permeability of fabric samples to decrease. Finally, the water absorption test was conducted for two water heads to analyse the absorbency of fabrics.

Thick fabric samples were made by stacking overlocked pieces of cotton fabric. Changes in the diameter of cotton fibre upon absorption of water were first analysed using microscopic images. It was seen that the fibres swelled quickly upon the application of water. It was observed that the cotton swelled about 11% when exposed to water. One fitting equation was found to capture the changes in fibre diameter. The initial porosity in the rigid conditions was measured by the imbibition method. The oil was used as a test liquid as it does not typically cause swelling in the fibres. The obtained porosity was 0.8801 for the sample. Further, the changes in the porosity were recorded using microscopic images at different time values. These changes were then characterised by a novel method that allowed us to track the changes in the pore area of the unit cell of a fabric. Several slides of accurately cut unit cells were prepared and placed under the microscope and the water absorption process was recorded. Further, using an image characterisation method, the changes in the pore area of the unit cell

were tracked. It was observed that the swelling action reduced the porosity by 12%. Finally, an equation predicting the porosity as a function of time was proposed. The obtained experimental results were then compared with predictions from a modified analytical model that used data from fibre diameter measurement. To account for the factors such as fibre-fibre interactions etc., two correction factors were proposed to modify an existing analytical equation. As a result, the predictions from the modified analytical model improved by a great margin.

The permeability of the prepared samples was measured using the falling head permeability measurement technique. It was seen that the permeability of samples decreased by 60.85% under fully swollen conditions. The changes in the permeability were also predicted analytically based on the data obtained for relative porosity reduction. The predictions showed a similar permeability reduction as that of the experimental results. Finally, the water absorption test was performed to analyse the performance of the fabric under swelling conditions. To do so, a simple test setup was developed that maintained the water reservoir at a constant level and recorded the absorption process with camera arrangements on top and bottom. The liquid absorption performance of fabric was tested for the two different values of the water heads (i.e., 52 cm and 130 cm). As a result, the effect of changes in the water head was seen on the flow front advancement on the upper and lower face of the sample. It was also observed that gravity considerably affected the water absorption behaviour of the fabric, causing faster flow front propagation on the lower face of the sample. Based on the data obtained for relative porosity reduction. The predictions showed a similar permeability reduction as that of the experimental results. Finally, the water absorption test was performed to analyse the performance of the fabric under swelling conditions. To do so, a simple test setup was developed that maintained the water reservoir at a constant level and recorded the absorption process with camera arrangements on top and bottom. The liquid absorption performance of fabric was tested for the two different values of the water heads (i.e., 0.52 m and 0.130 m). As a result, the effect of changes in the water head was seen on the flow front advancement on the upper and lower face of the sample. It was also observed that gravity considerably affected the water absorption behaviour of the fabric, causing faster flow front propagation on the lower face of the sample.

These findings related to the liquid absorption performance of the fabrics under swelling conditions are useful in the hygiene industries where the design of products is mainly based on the liquid absorption performance.

# Chapter 5 Numerical method

This chapter describes details of the numerical method and the respected theories used to model the flow through porous media under different flow conditions. ANSYS Fluent 2020R is used to perform the CFD simulations. This chapter briefly covers the governing equations of mass and momentum conservation, it also covers the details of the volume of fluid approach to model the liquid imbibition in porous media. Further, it explains the extension of the basic modelling framework to include the swelling and capillary pressure effects through User-defined functions (UDFs).

## 5.1 Introduction to Computational Fluid Dynamics (CFD)

Numerical modelling uses a set of mathematical equations to describe the behaviour of the engineering system. In engineering, numerical models are often used for a variety of objectives, including interpretive, design, and predictive research. When numerical models are employed to explain the rationale behind field or laboratory data, the study is referred to as an interpretative study. For design-related objectives, numerical models are used to compare the relative performance of various systems. Finally, the predictive numerical models are used to predict the efficacy of the experimental data of the actual system (Barbour and Krahn, 2004)

There are three approaches available to solve the governing equations of heat and mass transfer and fluid flow problems, those are analytical, experimental, and computational. The analytical solutions of governing equations of momentum, and continuity is available in the literature. However, the analytical solutions are limited due to the requirement of complex derivations and substantial mathematical efforts. Despite that, analytical modelling is used by engineers to understand the fundamental laws to control and understand the behaviour of many applications. Finally, the analytical modelling can also be used as an initial step towards the validation of CFD models. In the experimental method, the relevant measurement tools and equipment are required to predict the physical process. Full-scale experiments are time-consuming, expensive, and sometimes difficult to perform (Barbour and Krahn, 2004).

In the computational approach, Computational fluid dynamics (CFD) modelling techniques have emerged and played an essential role in solving complicated flow problems for a wide range of technical applications. Computational Fluid dynamics

(CFD) is a numerical approach to solving a set of governing mathematical equations to predict the solutions to problems ranging from fluid dynamics, heat transfer and chemical reactions. CFD techniques replace PDE systems with a set of algebraic equations that can be solved using a digital computer to provide suitable ways to simulate real fluid flows. The CFD techniques complement theoretical and experimental fluid dynamics by providing an efficient way to test the fluid flow systems. The main advantage of CFD modelling is that it allows us to model and test conditions that are extremely difficult to measure experimentally and are not described by analytical methods (Hu, 2012).

For the present study, CFD techniques are used to model the flow through porous media. The combination of the Finite Volume Method and Volume of fluid method is used to model the liquid imbibition in porous media under different conditions that include rigid, swelling, absorbing etc. For CFD modelling, ANSYS Fluent 2020 R1 solver is used. The macroscopic porous media approach is adapted for this study. The user-defined functions are used wherever the existing features of the solver are modified. The details of the modelling approach are mentioned in the subsections below.

## 5.2 Governing equations

In the present study, the flow through rigid or swelling porous media is assumed as laminar. For the case of Liquid Composite Moulding processes (forced imbibition case) and in the case of industrial wicks and hygiene products (natural imbibition case) the flow has a low Reynolds number ($R_e < 1$) (Zarandi, 2019) (Ranjan et al., 2011) (Saad et al., 2018). For all cases considered in this work, the fluid is assumed to be Newtonian. When porous media is considered to be in swelling condition, it is assumed that the fibres swell upon absorption of liquid and do not shift due to resin flow. For applications considered in the present study (LCM mould filling, industrial wicks and diapers), the flow of liquid is usually slow which can be taken as the inertia less viscous low (Stokes flow). The inertia effect is negligible as the Reynolds of resin flow is less than one. The total imbibition process is assumed as isothermal. Hence, based on these assumptions, the problem can be formulated as follows,

### 5.2.1 Mass and momentum conservation

The formulation for the conservation of the mass and momentum in case of flow through porous media is given by (Fluent, 2020),

$$\nabla.(\vec{u}) = 0 \tag{5.1}$$

For the absorbing porous media, the continuity equation changes as, (Masoodi et al., 2012a),

$$\nabla.(\vec{u}) = -S - \frac{\partial \varepsilon}{\partial t} \tag{5.2}$$

where the sink term, *S*, is related to the absorption rate of the liquid/resin by fibre matrix. The second term $\left(\frac{\partial \varepsilon}{\partial t}\right)$ is related to the porosity reduction of the fibre matrix as a result of swelling action. If $v_f$ is the total volume fraction of the fibres, the sink term *S* and the rate of increase in fibre volume $\left(\frac{\partial v_f}{\partial t}\right)$ as a result of swelling action can be related using,

$$S = b\frac{\partial v_s}{\partial t} \tag{5.3}$$

where $v_s$ is the solid volume fraction and b is the absorption coefficient of the porous media that ranges between 0 to 1 (if the increase in total solid volume is caused by another effect, then the b can be taken beyond unity). Here, the *b=1* case indicates that the rate of increase of solid matrix volume is equal to the volumetric rate of liquid absorption by porous media and the *b=0* case indicates no absorption of liquid in the fibre matrix. Upon using equation 5.3 in equation 5.2 and considering the relation $v_f + \varepsilon = 1$, the final continuity equation for the liquid-absorbing swelling porous medium is given by (Masoodi and Pillai, 2010),

$$\nabla.(\vec{u}) = (b-1)\frac{\partial \varepsilon}{\partial t} \tag{5.4}$$

The previous works on the modelling of swelling porous media (Masoodi and Pillai, 2010) (Masoodi et al., 2012c) (Javadi et al., 2012) assumed the value of *b=1* which led to acceptable results with a good agreement with the experimental data. Hence in the present work, for the case of swelling fibrous porous medium, the value of *b* is assumed as 1. Hence equation 5.4 reduces to equation 5.1 which will be used to model the flow through a porous medium in the present study.

The momentum equation can be expressed as (Fluent, 2020),

$$\frac{\partial}{\partial t}(\rho\vec{u}) + \nabla.(\rho\vec{u}\vec{u}) = -\nabla p + \nabla.(\bar{\bar{\tau}}) + S_i + f \qquad 5.5$$

where $p$ *is* the fluid pressure, $\rho$ is the fluid density, $\bar{\bar{\tau}}$ is viscous stress tensor and $S_i$ is the source term associated with the porous media conditions and $f$ is the external source term. The source term that models pressure drop through porous media is composed of two different parts. A) viscous loss term (the first term on the right-hand side of the equation) and b) Inertial loss term (the second term on the right-hand side of the equation) (Fluent, 2020).

$$S_i = -\left(\frac{\mu}{K}\overrightarrow{u} + C_2\frac{1}{2}\rho|\vec{u}|\vec{u}\right) \qquad 5.6$$

The second term on the left-hand side of equation (5.6) is the non-linear convection term which can be ignored as for the selected applications of porous media Reynold's number related to flow is less than 1. On the other hand, the second term in equation (5.5) can be ignored as the flow is dominated by viscosity. Hence the resulting equation that characterises the single-phase flow through porous media is given by (Fluent, 2020),

$$\frac{\partial}{\partial t}(\rho\vec{u}) = -\nabla p + \nabla.(\bar{\bar{\tau}}) - \left(\frac{\mu}{K}\overrightarrow{u}\right) + f \qquad 5.7$$

## 5.3 Finite volume method

This section focuses on the application of the finite volume method (FVM) to discretise the partial differential equations presented in the previous section. The FVM is a numerical method for evaluating the elliptic, parabolic, and hyperbolic partial differential equations which are in algebraic form. In the finite volume method, the solution subdomain is divided into small non-overlapped volumes that cover the entire space domain as shown in Figure 5-1. In the finite volume method, the continuum variables presented in the previous section are replaced by the discretised volume average variables in the space and time domain at specified locations. The vertex-centred approach is adapted to discretise the domain into control volume (in this case the nodes of the mesh act as the centre of the controlled volume whose boundaries are created through connecting the centroids and midpoints of each element and their edges respectively).

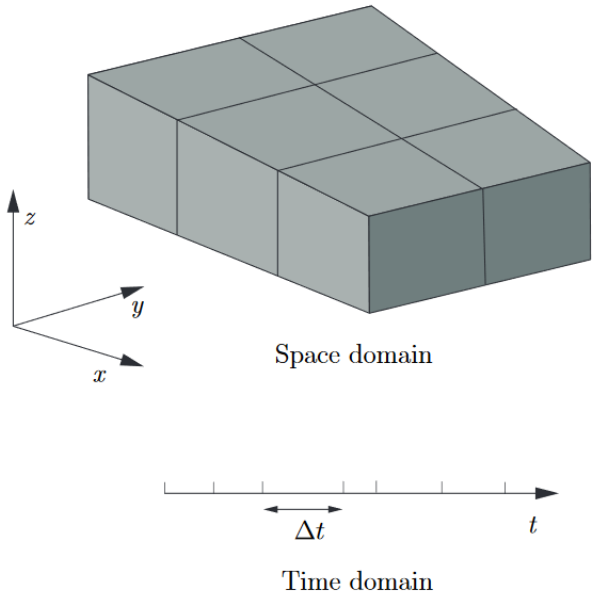


Figure 5-1 Discretisation of the solution domain (Aboukhedr, 2019)

After the domain discretisation, an integral form of the balance equations and approximation of integrals by numerical integration is required for each control volume. The equations written for each control volume are then assembled to obtain the unique algebraic system which needs to be solved by suitable numerical methods to obtain the unknown variables (Aboukhedr, 2019) (Aleksendric and Carlone, 2015).

## 5.4 Volume of fluid method

The Volume of Fluid method (VOF) is a surface-tracking technique applied to fixed Eulerian mesh. It is designed for two or more immiscible fluids where the position of the interface between two fluids is of interest. In the VOF method, a single set of momentum equations is shared by the fluids, and the volume fraction for each fluid is tracked in each cell throughout the domain. In this method, the primary and secondary phases (non-wetting phase and wetting phase respectively) are identified by their volume fractions $\alpha_w$ and $\alpha_{nw}$ in a computational cell. If $\alpha_w = 1$, the cell is full of wetting fluid; if $\alpha_w = 0$, the cell is full of the other phases (non-wetting); and if $0 < \alpha_w < 1$, the cell contains the interface between the non-wetting phase and wetting phase (Chattopadhyay and Guthrie, 2014).

The velocity for the mixture phase in the volume of fluid method is obtained by the solution of a single set of momentum equations,

$$\frac{\partial}{dt}\left(\rho_{fluid}\vec{u}\right) + \nabla.\left(\rho_{fluid}\vec{u}\vec{u}\right) = -\nabla p + \nabla.\left(\bar{\bar{\tau}}\right) + S_i \qquad 5.8$$

Where the subscript fluid refers to the corresponding fluid, which can be any one of two phases or a mixture. Assuming the incompressibility, the conservation of mass is described by equation (5.1). In the volume of the fluid method, the interface between the wetting and non-wetting phase is tracked by solving the continuity equation for the volume fraction as:

$$\frac{\partial \alpha}{\partial t} + \nabla.\left(\vec{u}\alpha\right) = 0 \qquad 5.9$$

where α indicates the volume fraction of the corresponding phase. The effective physical properties of the fluid $\phi$ (*viscosity* $\mu_e$, *density* $\rho_e$) in a computational cell are expressed as volume-weighted average (Srinivasan et al., 2011).

$$\phi_e(s,t) = \alpha(s,t).\phi_w + [1 - \alpha(s,t)].\phi_{nw} \qquad 5.10$$

where *s* indicates the position *(x and y)* and subscript *w* and *nw* indicate the wetting and non-wetting phase respectively. From equations (5.7), (5.8) and (5.9), the VOF model can be established for solving the two-phase flow in porous media is given by,

$$\frac{\partial}{\partial t}(\rho_e\vec{u}) = -\nabla p + \nabla.\left(\bar{\bar{\tau}}\right) - \left(\frac{\mu_e}{K}\overrightarrow{u}\right) \qquad 5.11$$

The framework presented above is a generalised structure of volume of fluid approaches that have been employed in a wide range of two-phase flow situations with different degrees of success and various adjustments. In the next subsections, an extended version of the basic framework is presented; its applicability and validity are demonstrated through the different case studies which address the numerically challenging scenarios cited in the literature.

## 5.5 Modelling the swelling and capillary pressure effects

To model the swelling effects and capillary pressure effects, equation 5.11 is modified by adding the source terms using the User-defined functions. The user-defined functions allow us to modify the existing features of the solver. This basic framework does not include the swelling effects of porous media. As mentioned earlier, for the volume of fluid method a single set of the momentum equation is solved at the mixture level. Unlike the Euler-Eulerian multiphase modelling approach, the basic formulation of VOF does not have the capillary pressure term in the momentum equations. As described in Masoodi et al, the capillary pressure always acts at the interface due to

differences in the surface energies of the wet and dry surfaces of porous media. The next subsections present the modification in the basic framework of VOF formulation to include the effects mentioned above.

### 5.5.1 Modelling the swelling effects.

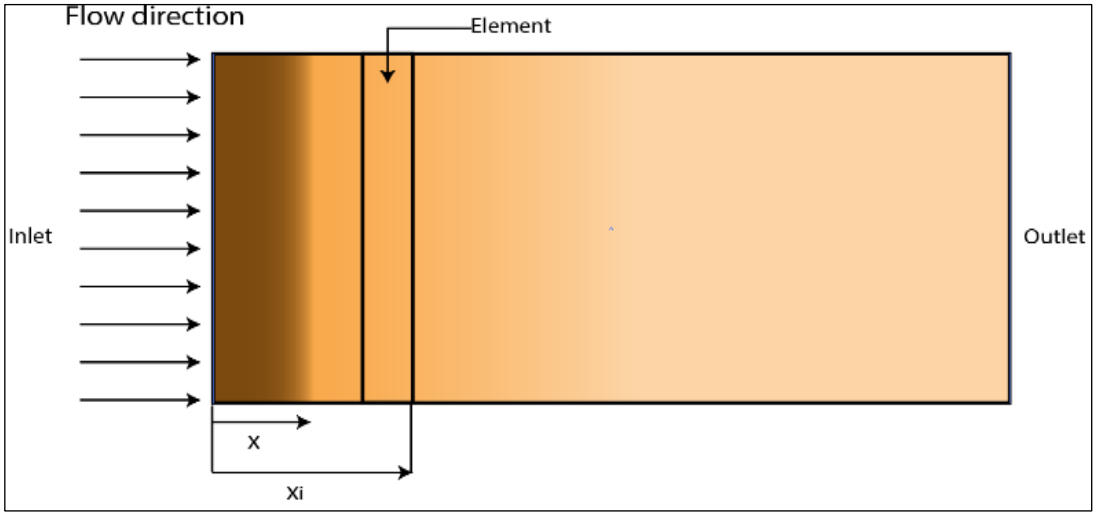


Figure 5-2 Problem setup for rectilinear flow in swelling porous medium

Figure 5.2 shows the schematic arrangement for rectilinear flow, considering the element (porous cell zone) located at $x_i$ from the inlet which gets wet when resin flow front $x$ passes through it. The permeability in the wetted region starts to decrease as a result of fibre swelling. If $t_w$ is the time when the element becomes wet, then the following expression holds true for permeability in the wetted part (Masoodi et al., 2012c).

$$(K) = \begin{Bmatrix} K_o & t < t_w \\ f(t) & t \geq t_w \end{Bmatrix} \qquad 5.12$$

Where $K_0$ is the permeability of dried preform in $m^2$, $f$ is the analytically or experimentally estimated function of time for a change in permeability (in units of $m^2$), and $t$ is the time in seconds. The function $f(t)$ is heavily related to the accuracy of the model. For the present studies, the function is either taken from the literature data or estimated analytically. The detailed use of this function is presented in the next chapters. Upon hooking the UDF-based function, the permeability term in equation 5.11 gets modified at each time step in transient simulations.

### 5.5.2 Modelling the capillary pressure effects

To include the capillary pressure effects at the interface, an additional source term is added to the solver via user-defined functions. The source term is based on the following expression,

$$f = \nabla \alpha_L \ (P_s) \tag{5.13}$$

where $\alpha_L$ is the volume fraction of the wetting phase and $P_s$ is the applied capillary pressure. The developed udf is split into two parts. The first part calculates and stores the volume fraction gradients at each time step and stores them in the user-defined memory locations. The second part hooks the source terms to the momentum equations. The capillary pressure can either be calculated from the analytical approaches as mentioned in Masoodi et.al (2012c) or it can be directly measured from experiments. For the case of the analytical approach, equation 5.13 modifies to the following forms. Referring to equations 2.7 and 2.8 and combining them with equation 5.13 we get,

i. For the case of flow across a bank of the same radius fibres,

$$f = \nabla \alpha_L \ \frac{1-\varepsilon}{\varepsilon} \frac{\gamma \cos \theta}{r_{fb}} \tag{5.14}$$

ii. For the case of flow across a porous medium made of spherical particles

$$f = \nabla \alpha_L \ 3 \frac{1-\varepsilon}{\varepsilon} \frac{\gamma \cos \theta}{r_{sp}} \tag{5.15}$$

where $\alpha_L$ is the volume fraction of liquid $r_{fb}$ and $r_{sp}$ are the radius of fibres and spherical beads respectively.

## 5.6 Algorithm Implementation

This section presents the general implementation of the modified framework to model the flow through porous media under different flow scenarios. Following are the three different flow scenarios considered in the present study:

a) Modelling of the flow-through swelling porous media under the non-absorbing condition where the effect of capillary pressure can be neglected. Example: Liquid composite moulding process. For this case, UDF is primarily employed to calculate the permeability reduction at each timestep. The UDF then makes

the real-time changes in the permeability *(K)* in Equation (5.11) as the solution progresses. The approach is implemented in Chapter 6.

b) Modelling the wicking flow through rigid absorbing porous media where the flow is mainly driven by the capillary forces. Example: Commercial wicks used in industries, tissue papers. For this case, UDF applies the specified capillary pressure at the interface between liquid and gas.

c) Modelling the flow through absorbing porous media under swelling conditions where the inflow forces and capillary forces both play an important role. Example: hygiene products such as baby diapers. This flow condition is the combination of the previous two flow scenarios. In this case, user-defined functions from cases a and b are combined to include swelling and capillary pressure effects.

Figure 5.3 shows the general numerical algorithm to model the different flow scenarios mentioned previously. For the transient simulations, the timestep size is selected based on the resulting courant number value. The courant number, which is the ratio of distance travelled by moving front to for a given time value to the cell size. For VOF models, the maximum allowed courant number is 250 near the interface (Fluent, 2020). For all simulations, the suitable timestep values are selected so that the result courant number would be 3. A combination of the PISO algorithm for pressure velocity coupling and a second-order upwind scheme for the determination of momentum is selected for all models. PRESTO! and Geo-reconstruct discretisation schemes are selected for pressure interpolation and volume fraction respectively. The multiphase flow problems do not usually converge to extremely low residual values such as $10^{-6}$ (Hussein et al., 2019). For the present study, the numerical simulation is considered to be converged when scaled residuals of mass, and velocity components are less than $10^{-4}$. For all cases of flow, the air is assumed as a non-wetting phase (primary phase) and wetting phases are defined according to porous media applications. The details of the mesh and simulation input are described in the respected chapters.

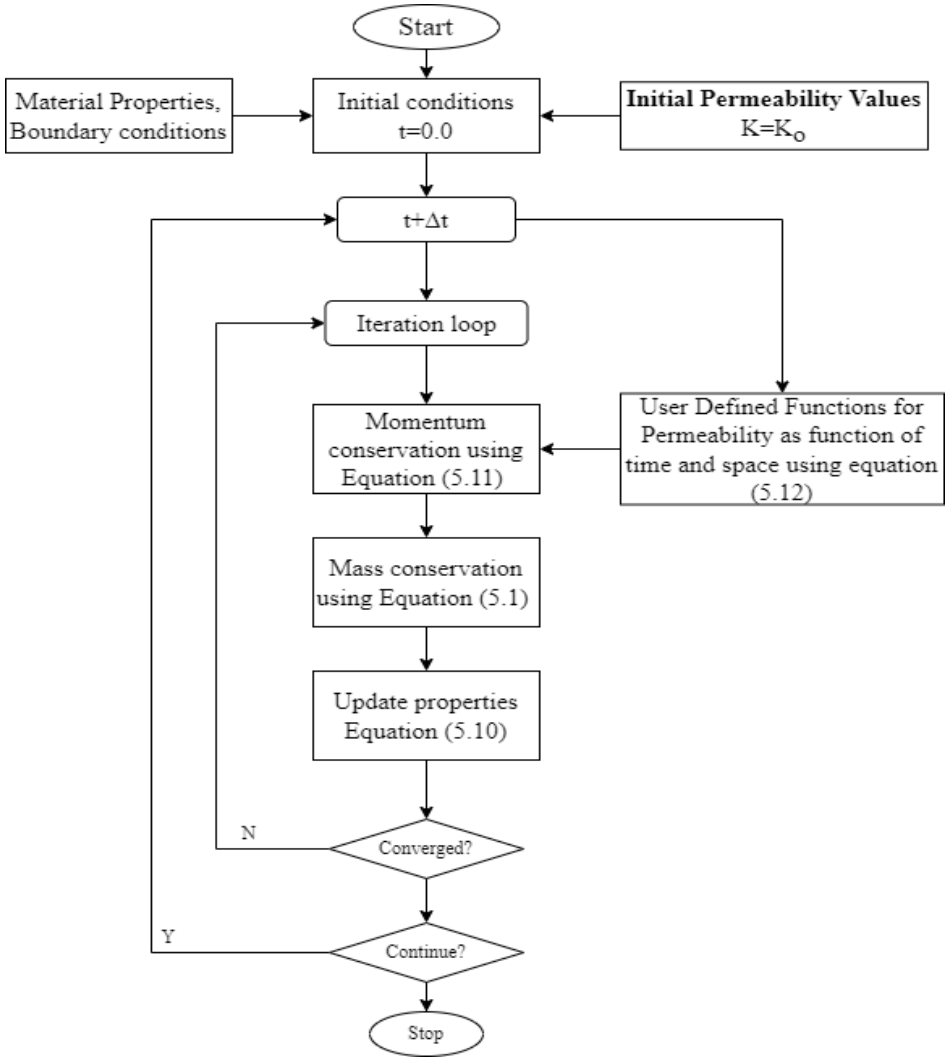


Figure 5-3 Numerical algorithm employing user-defined functions to model the flow through swelling porous media

## 5.7 Chapter summary

This chapter highlighted and discussed the numerical method employed for the present study. The governing equations are presented which are used to model the flow through porous media under different conditions. The volume of the fluid method is also presented in this chapter. Further, the use of user-defined functions (UDF) to modify the existing features is explained for the different flow cases that are; a) flow through swelling porous media, b) flow through absorbing porous media under rigid conditions and c) flow through absorbing porous media under swelling conditions. The details of the expressions to develop the udf are presented and discussed in this chapter. In summary, this chapter described the numerical methodology employed to investigate the flow through porous media using the combination of the finite volume method and Volume of Fluid method.

# Chapter 6 Numerical Modelling of the Flow in a Swelling Preform During LCM Filling

The composite industry increasingly uses natural fibres because of their environment-friendly advantages. Numerous studies have shown that Natural fibres such as jute, kenaf etc. can be used as a reinforcement in bio-based composites. These natural fibres may swell during the mould-filling process when they absorb resins. The phenomenon of swelling of natural fibres as a result of liquid absorption adds a new dimension to the research of Liquid Composite Mould filling simulations. As a result of swelling, the porosity and permeability of the preform reduce over the period of time. In any LCM mould-filling simulation, the permeability of the preform is a very important parameter. The design of moulds is heavily dependent on the nature of flow through the porous preform. The conventional method of designing the mould is based on a series of experiments which is costly and time-consuming. Hence, computational modelling of the flow-through swelling porous media would be useful to model the different mould-filling processes with the swelling effect. This chapter demonstrates the possibility of using CFD to study the effect of swelling on LCM mould filling in isotropic and orthotropic porous media. An empirical relation for local permeability changes is used to model the flow of resin under a constant volume flow rate and constant injection pressure conditions. To validate the proposed methodology, the CFD predictions for flow front locations are compared against the experimental data obtained for constant volume flow rate and constant injection pressure case. Further, the CFD predictions for changes in inlet pressure are also compared against experimental data for constant volume flow rate conditions. The comparison showed good agreement between CFD predictions and experimental data. The modelling approach is further extended to capture flow front advancement in 2D. To do so, two different arrangements employing point injection are considered. The CFD models are developed for the isotropic and anisotropic porous media conditions. It was observed that the volume fraction of resin in the swelling porous medium is 6% less than that of the rigid porous medium at any given time. It was also observed that the location of the inlet and outlet has a considerable effect on the flow front advancement.

## 6.1 Physical Description

For the validation case, the simple 1D flow scenario is considered. The experimental setup developed by Masoodi et al is selected for this study. The experimental setup consists of a 1D flow setup and an RTM machine. The reinforcement of the experiment is made by stacking several layers of the jute fibre mates. The experiments are performed for constant pressure injection and constant volume flow rate conditions for 1D flow conditions. For the experiments under constant pressure injection, three different values of injection pressure are used (8kPa,12kPa and 14kPa). For the case of constant volume flow rate tests, three different values of flow rate are used (Q=1ml/sec, 2 ml/sec and 3 ml/sec). For the present simulations, a mould shaped like the rectangular domain is used. During the experiments, the flow front locations of resin are measured with time for constant injection pressure cases. For the case of constant volume flow rate conditions, the changes in the inlet pressure are measured. Hence, for the validation activity, these results will be compared against CFD results. Figure 6.1. shows the details of the physical setup of the 1D flow experiment. Further, for the case studies, two different arrangements are used. To capture the flow front advancement in the 2D, the physical setups with circular injection ports are selected for the case studies as shown in Figure 6.2.

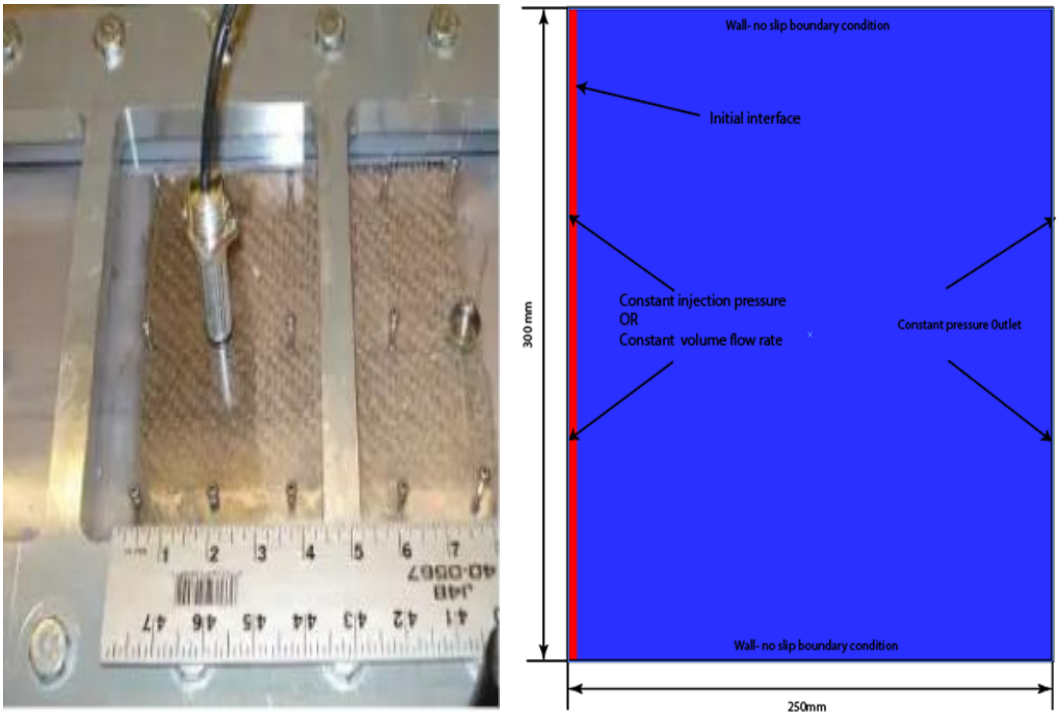


Figure 6-1 Geometrical details of the arrangements used for 1D CFD simulations (a) Experimental arrangement (b) Computational domain

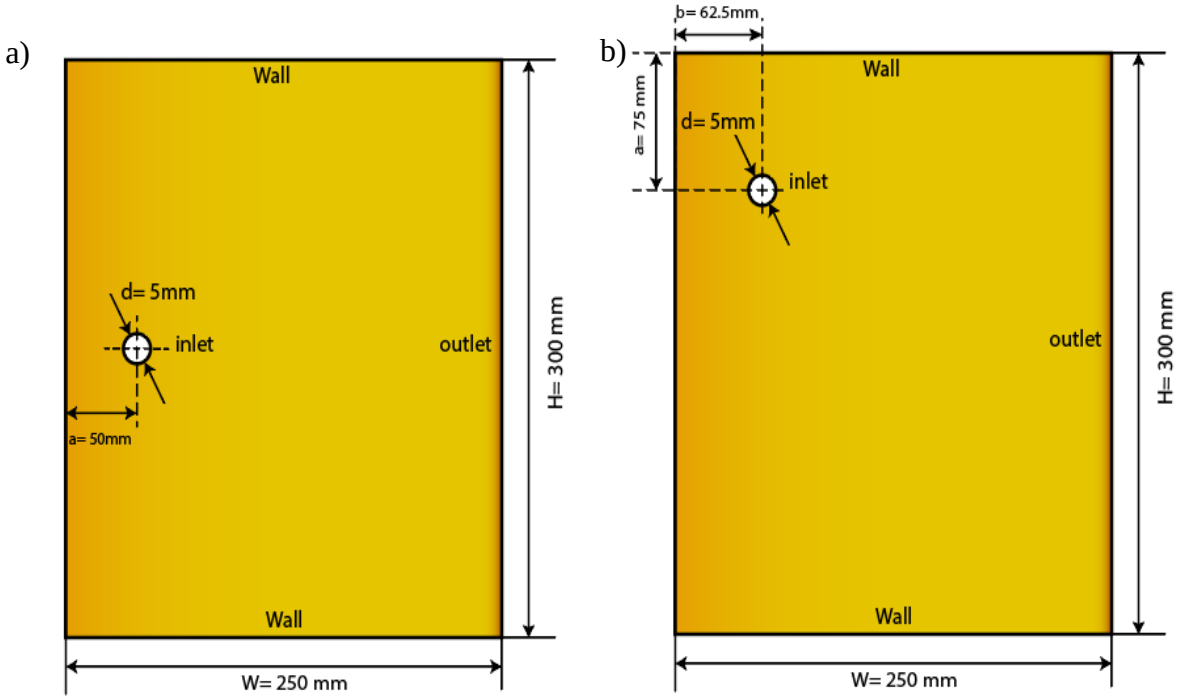


Figure 6-2 Geometrical details of the arrangements used for 2-D CFD simulation (a) Central injection arrangement (b) Eccentric injection arrangement

## 6.2 Computational Description

Figure 6.1 and 6.2 shows the details of the boundary conditions used for the 1D and 2D CFD simulations. The details of the mesh for each case are shown in Figure 6.2. For all cases of flow, the quad type of mesh is used. The reason behind the use of finer mesh everywhere in the domain is that the liquid and air interface is not stationary. To perform the mesh sensitivity tests, the CFD results for constant injection pressure cases are generated. The simulations are performed for the cell sizes of 0.35 mm and 0.7 mm for 14 kPa injection pressure. Figure 6.4 shows the comparison between the predicted flow front locations for two different cell sizes. Figure 6.4 clearly shows that the resulting flow front locations for both cell sizes have minor differences. Hence, all computations are done using the cell size of 0.7 mm.

The porous media model with the volume of fluid method is used for simulating the flow for all cases. The properties/inputs of the porous media model are taken from Masoodi et.al (2012). The porosity of the domain is defined as 0.88 and the initial permeability is defined as $6\times10^{-10}$ $m^2$. To include the swelling effects in simulations, the user-defined functions (UDF) based on the methodology indicated in section 5.5.1

are hooked to the solver. The experimentally generated function proposed by Masoodi et al. (2012a) used UDF to include the permeability changes which are given by,

$$K = \begin{cases} 6 \times 10^{-10} & \boldsymbol{t < t_w} \\ 3.7 \times 10^{-15}(t - t_w)^2 - 1.75 \times 10^{-12}\ (t - t_w) + 6 \times 10^{-10} & \boldsymbol{t \geq t_w} \end{cases} \qquad 6.1$$

where $t_w$ is the wetting time of the element and t is the current time. As indicated in Masoodi et al. (2012a), for all the cases the effect of capillary pressure is neglected as the resulting capillary pressure is 83Pa using which is calculated using the equation

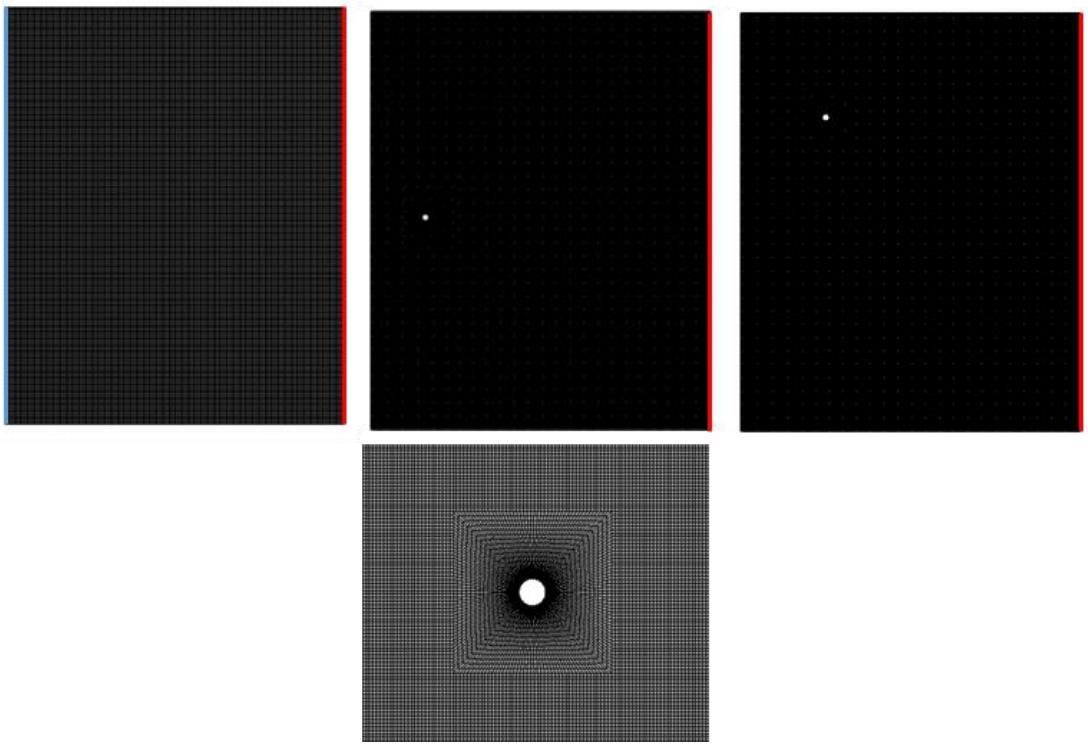

Figure 6-3 Representative computational mesh for the domain a) Details of mesh for 1D flow validation case (blue and red lines represent the position of inlet and outlet respectively) b) Details of mesh near inlet for the case studies

For the simulations discussed in this chapter, the following are the general boundary conditions defined at different boundaries.

**Inlet:** The velocity inlet and Pressure inlet boundary conditions are defined for the case of constant volume flow rate and constant injection pressure respectively.

**Outlet:** The pressure outlet boundary condition is defined at the outlets where flow exits the domain.

**Wall:** For walls, no-slip boundary conditions are defined for all flow cases

To capture the movement of the interface accurately in the transient simulations, the size of time step $\Delta t$ must be small enough so that a fluid particle should move only a fraction part of cell spacing $x_c$ with the fluid velocity $u$ at each step, which is given by,

$$\Delta t = C_{FL}\frac{x_c}{u} \qquad 6.2$$

where $C_{FL}$ is the Courant flow number, and it is kept in the range of 0.5-1 during the computation. For the simulation, the resin and air are defined as the wetting phase and non-wetting phase. The resin has a density of 1235 kg/m$^3$ and a viscosity of 0.0179kg/m. s.

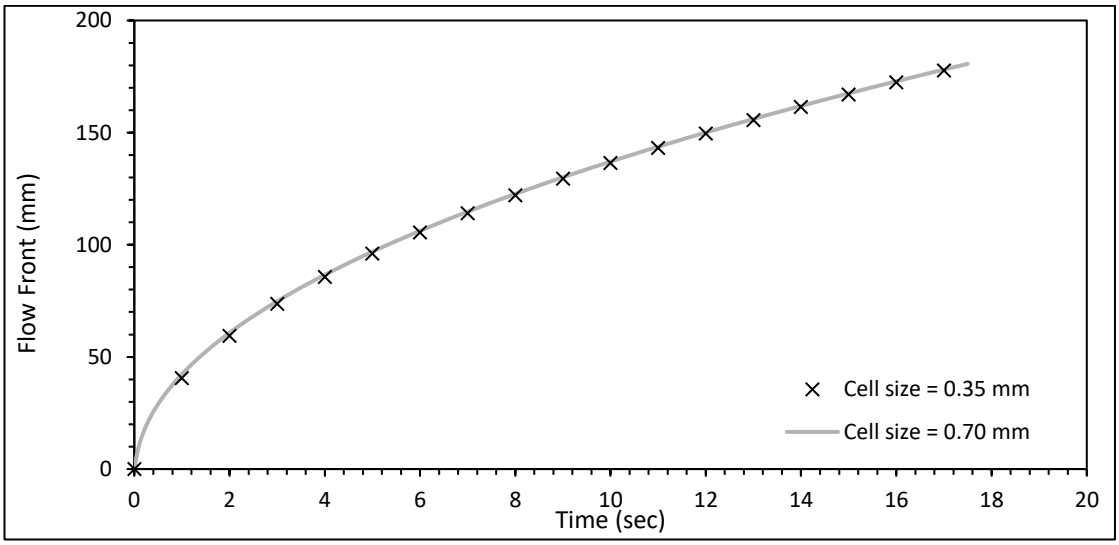


Figure 6-4 Comparison between Predictions of flow front locations for the case of constant injection pressure of 14kPa for two different cell sizes

## 6.3 Validation

To validate the numerical methodology, the experimental data for constant volume flow and constant inlet pressure conditions are compared with CFD simulation results. The computational domain and important boundary conditions are illustrated in Figure 6.1. The computational domain is a rectangular box with dimensions of $250 \times 300$ (mm), the resin is injected from the inlet and air is removed from the outlet. To characterise the flow, permeability in both directions *($K_{xx}$, $K_{yy}$)* is assumed to be equal.

Figure 6.5 shows a comparison between experimental data and CFD results for the liquid flow front locations in the case of the constant injection pressure condition. Here, the three different injection pressure values *(8 kPa, 12 kPa and 14 kPa)* are used and the permeability is taken as a function of time and space. The experimental data are taken from Masoodi et al. (2012a). There is some discrepancy between the two

sets of experimental data. The reason behind this could the inconsistent parameters such as injection pressures, permeabilities etc. Also, it has been stated that the error bars were not estimated in the study. It can be seen that the CFD results are in good agreement with the experimental and numerical results by Masoodi et al. (2012a) with an average percentage error of 2.7 %.

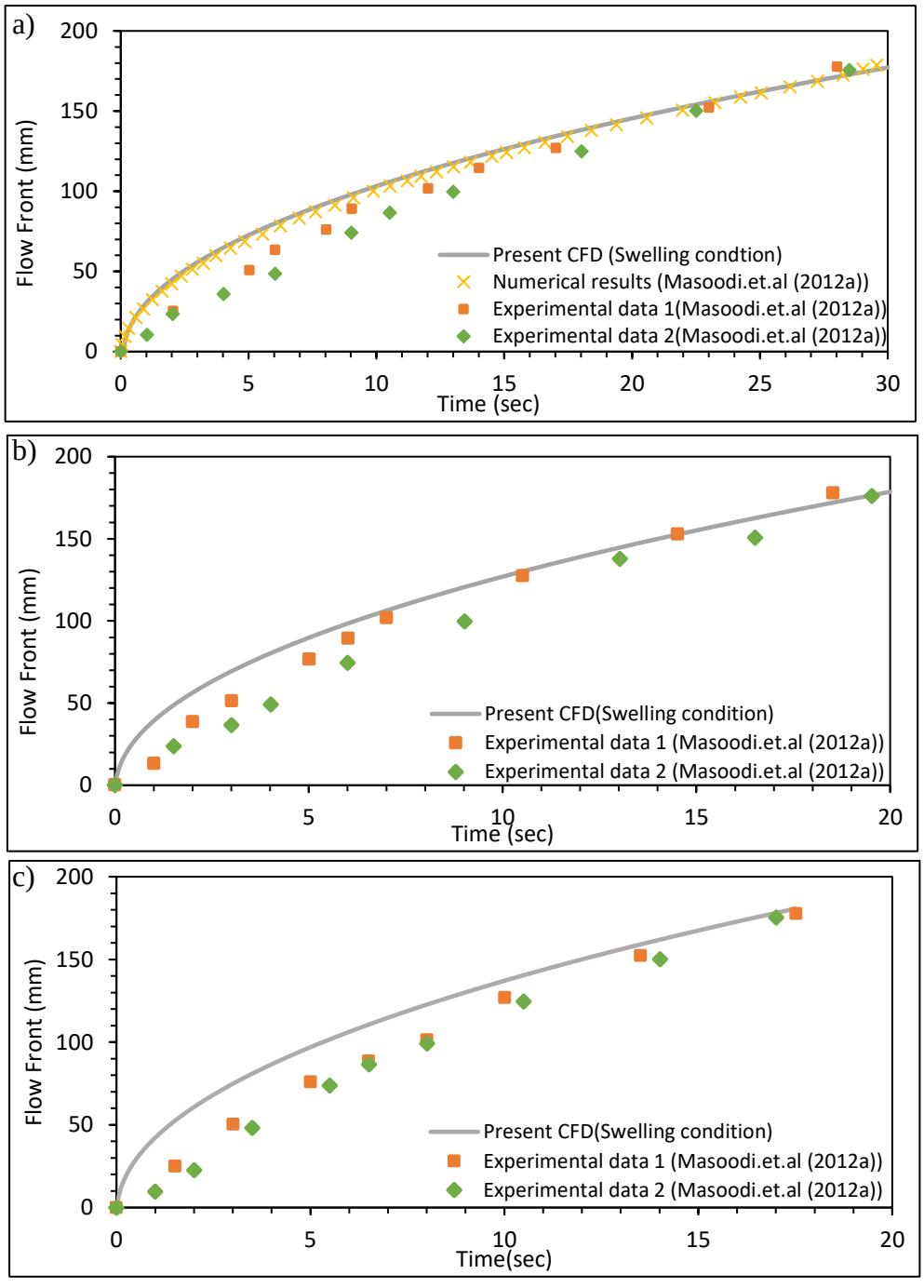


Figure 6-5 The comparison between experimental and CFD predictions for liquid-front locations for 1-D constant injection pressure conditions (a) $P_{inj}$=8kPa (b) $P_{inj}$ =12kPa (c) $P_{inj}$ = 14kPa

Further, Figure 6.6 shows the experimental and CFD predictions of flow front locations for constant volume flow rate conditions. As stated by Masoodi et al. (2012a) the effect of swelling does not have a considerable effect while the prediction of flow front locations in case of constant volume flow rate conditions. As expected, the CFD predictions are in good agreement with experimental data from Masoodi et al. (2012a). For this case as well, the permeability is assumed to be a function of time and space.

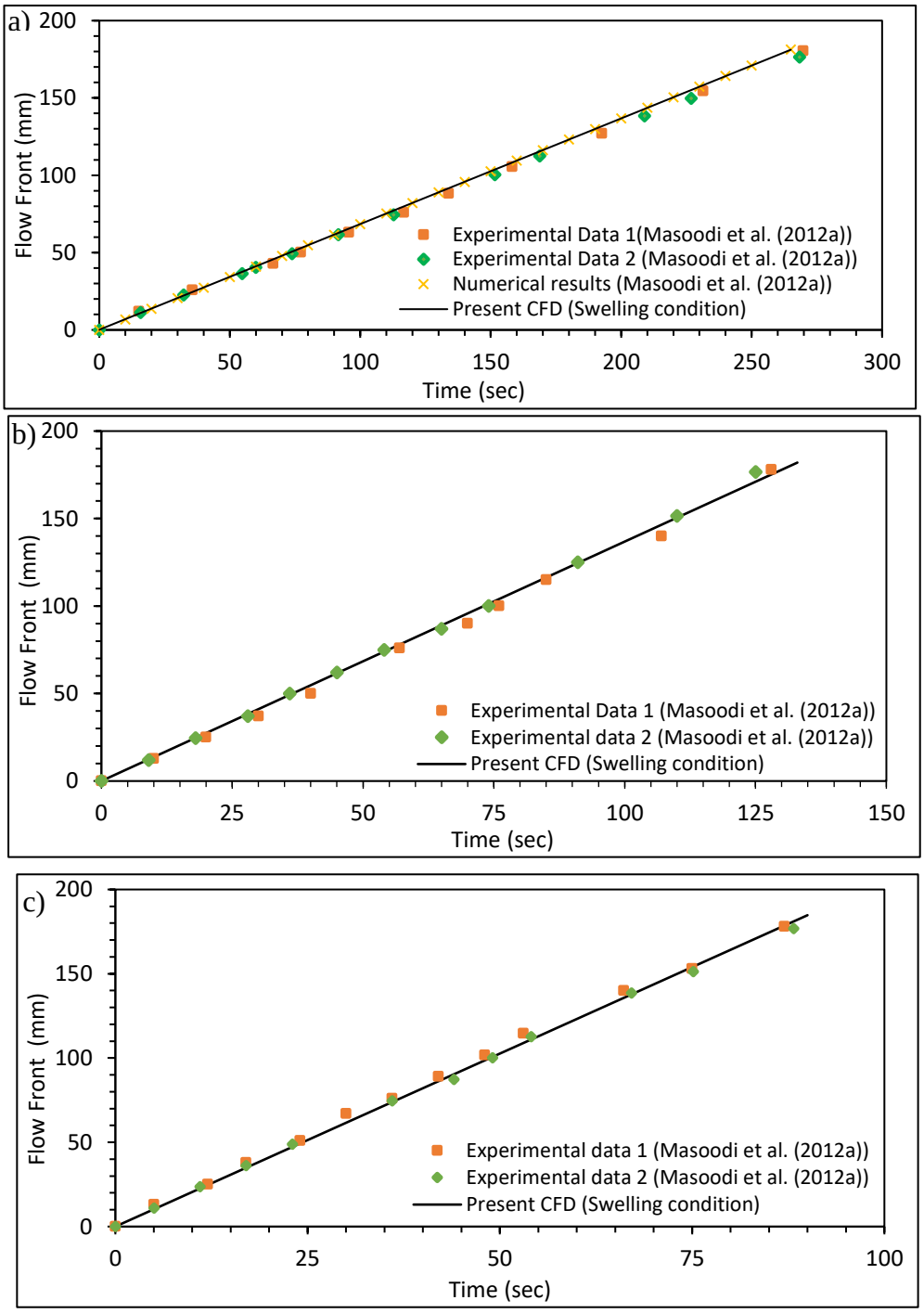


Figure 6-6 The CFD predictions for resin front locations for the 1-D constant volume flow rate conditions (a) Q = 1ml/s (b) Q = 2ml/s (c) Q = 3ml/s

Figure 6.7 shows the evolution of inlet pressure as a function of time for three different flow rates *(Q = 1 ml/s, 2 ml/s and 3 ml/s)*. It is clear from the graphs that predicted results are in good agreement with experimental data (Masoodi et al., 2012a) with an error margin of 5%. This demonstrates the validity of the present method to model the flow in swelling porous media. For the experiments, Masoodi et al. (2012a).used woven jute fabrics to make the preform which can be considered as the two-scale or dual-scale porous media that consists of a fibre bundle of lower permeability and higher permeability in the gaps between bundles. This scenario can be treated as a combination of two different porous media. It is expected that including these dual scale effects would yield a better comparison with experimental data for the case of constant injection pressure conditions.

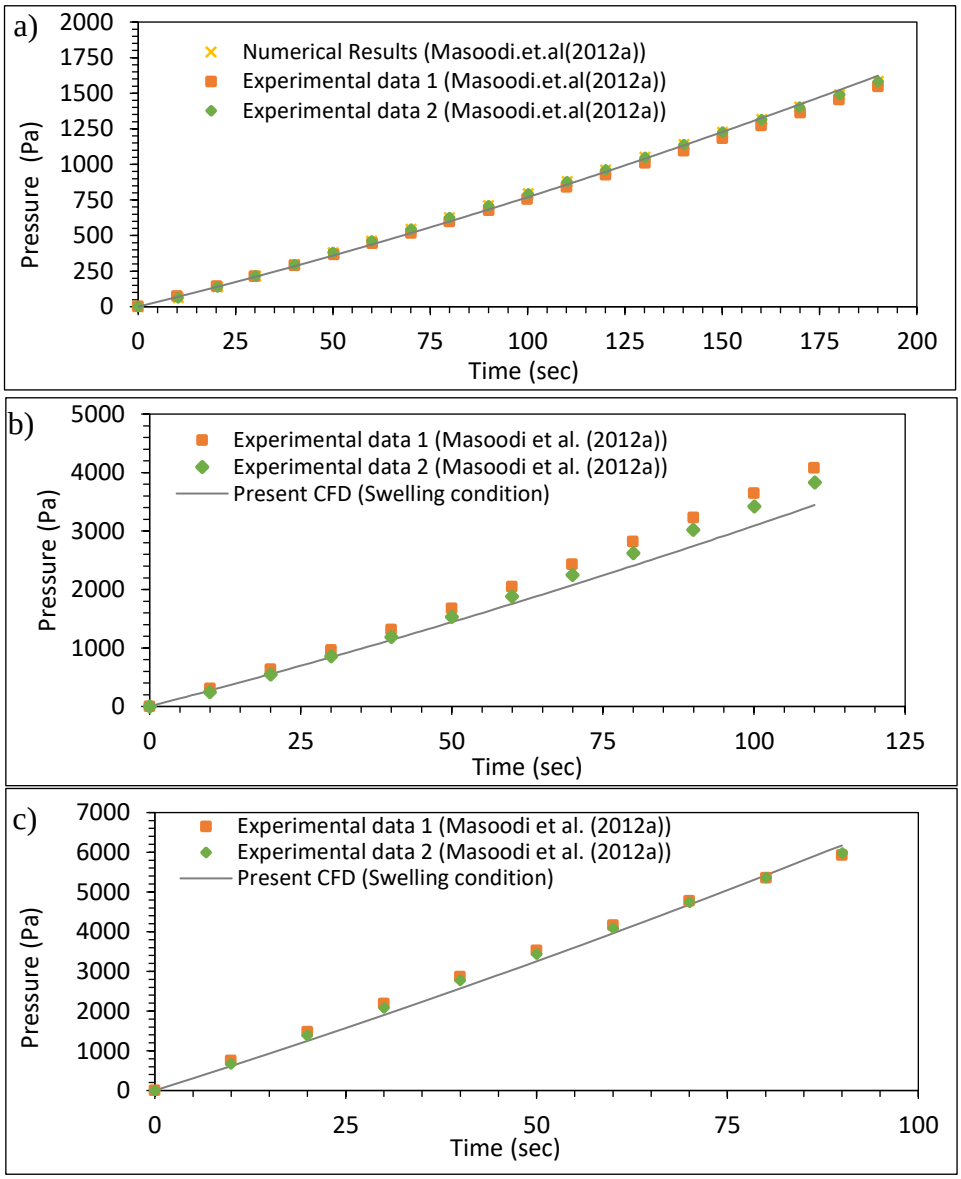


Figure 6-7 The Experimental and CFD predictions for the changes in the inlet pressure for constant volume flow rate conditions (a) Q = 1ml/s. (b) Q = 2 ml/s. (c) Q = 3 ml/s.

## 6.4 Results and Discussions

### 6.4.1 Two-dimensional mould filling in the isotropic porous media

To explore the ability of the present method to capture the 2-D flow patterns, point-type injection instead of boundary-type injection is used for simulations. For this purpose, two different cases are considered for the condition of constant injection pressure. Arrangement 1: Central injection arrangement and Arrangement 2: Eccentric injection arrangement. Figure 6.2 shows the details of the geometry used for both arrangements. For the case studies, the constant injection pressure conditions are considered as it shows the effect of swelling on the flow front propagation through the preform as demonstrated in the previous section. The simulations are performed for the rigid and swelling conditions. All the porous media properties and inputs are the same as that of the validation case. For this case study, the isotropic porous media conditions are assumed where permeability is the same in the x and y directions ($K_{xx}$=$K_{yy}$).

Figures 6.8 and 6.9 show the transient contours of resin flow for both arrangements for an isotropic condition. The red colour shows the resin-impregnated region, and the blue colour shows the completely unsaturated region. From the circular injection port, the radial resin flow pattern is observed until it touches the top and bottom walls. The swelling effect is not so dominant in early simulation time (until 10 sec). As time progresses forward, the swelling effect becomes dominant for both cases, and after t = 30 seconds one can spot the differences in the flow front locations in terms of resin volume fraction. Also, it is observed that, as the flow front reaches the outlet, its advancement becomes slow. It is expected that for larger dimensions of a porous domain, the swelling effect may be seen as dominant; the reason can be explained by the experimentally generated function for permeability reduction. For higher values of time, the permeability reduces by a higher amount. Also, the position of the inlet gate affects the total mould-filling time.

Figure 6.10 plots the variation of the resin volume fraction with time for central and eccentric injection arrangements. The time at which the domain (mould) gets fully saturated by the resin is called the total mould fill time. Figure 6.10 shows that, for case central injection and eccentric injection, the total mould fill times are 60 seconds and 100 seconds, respectively when the preform is assumed to be under non-swelling rigid conditions upon impregnated by resin. For this case, the rigid permeability of the

preform is defined as $6\times10^{-10}m^2$. The main reason behind simulating flow under the rigid case is to analyse the flow front locations and how they will be affected because of swelling

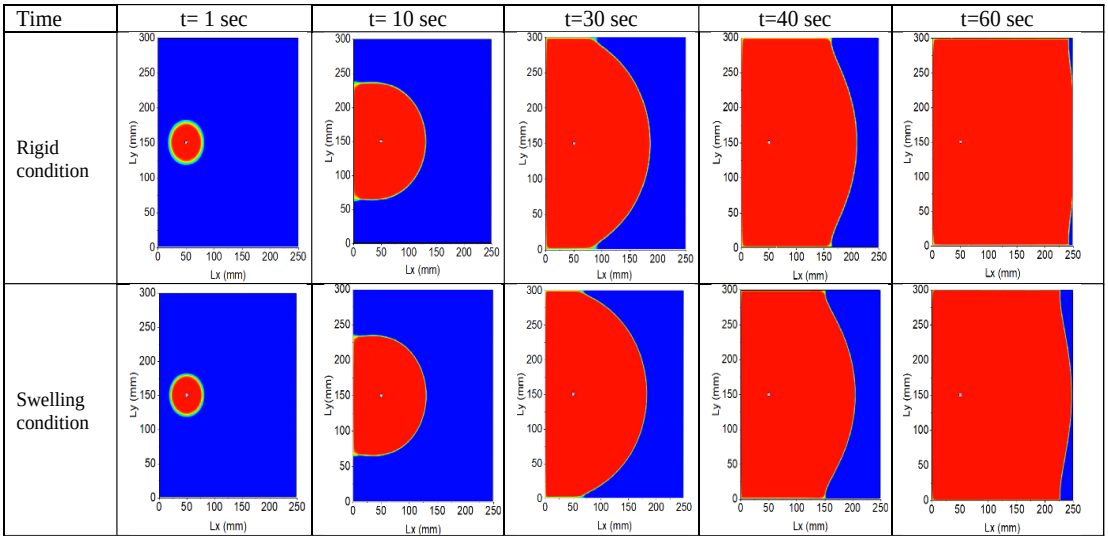


Figure 6-8 Transient contours of resin volume fraction for both rigid and swelling conditions for 14 kPa inlet pressure case (Central injection case) (isotropic porous media

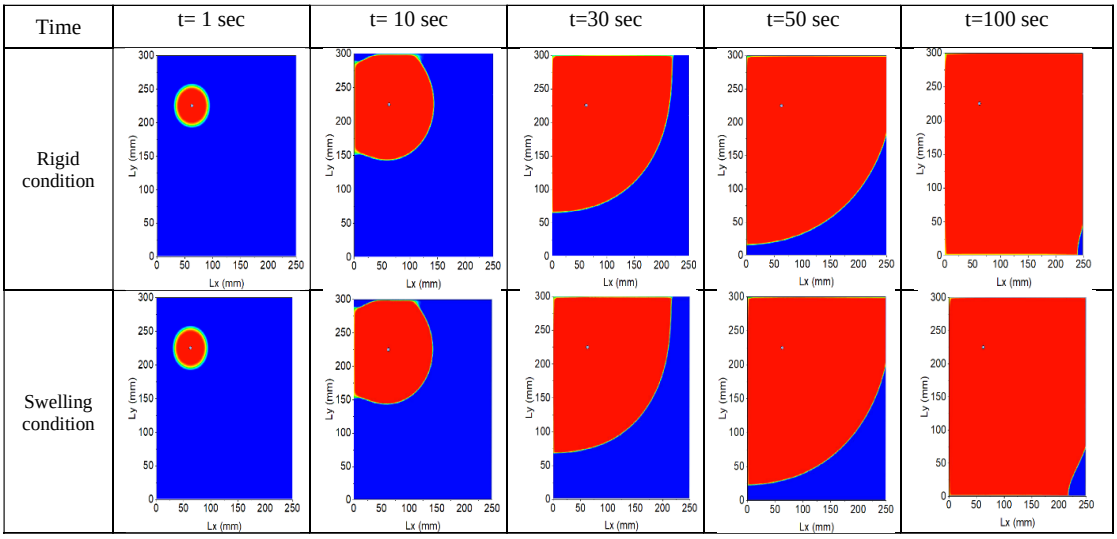


Figure 6-9 Transient contours of resin volume fraction for both rigid and swelling conditions for 14 kPa inlet pressure case (Eccentric injection case) (isotropic porous media).

For swelling conditions, these values increase to 70 seconds and 120 seconds respectively. It can be seen from Figure 6.10 that the advancement of the resin flow front is considerably affected by the position of the inlet. There is a considerable difference between trends followed by resin volume fractions for both arrangements. For the case of central injection, the trend is somewhat similar to that of the rectilinear case, because in late simulation time the flow front starts to follow the rectilinear case trend, as mentioned in the previous section. Hence one can deduct from these results

that the flow front advancement is not greatly affected by the swelling effect in early simulation. The differences in resin volume fractions can be used to design and optimise the LCM processes in terms of numbers, positions, and even size of the inlets.

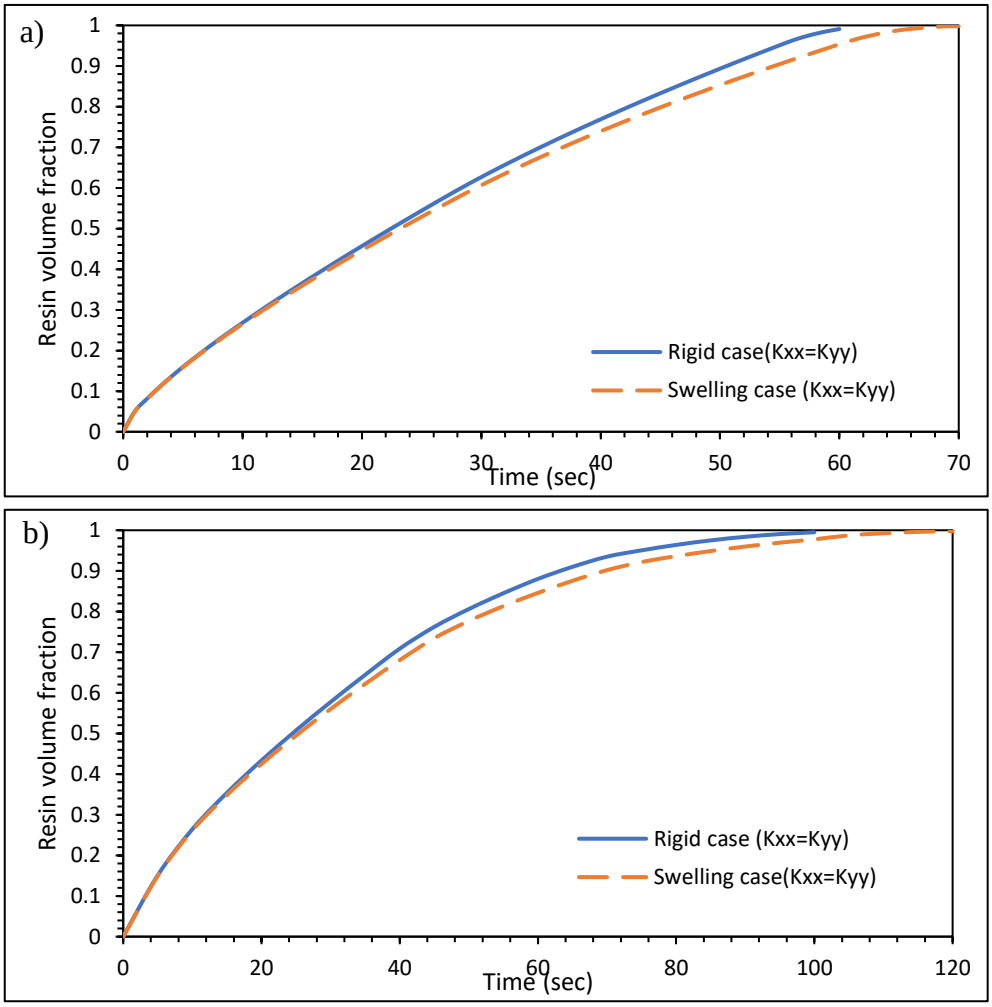


Figure 6-10 Plots of rein volume fraction Vs time for isotropic porous media (a) Central injection case (b) Eccentric injection case

Also, the ratios of resin volume fraction in the swelling condition and the rigid condition are plotted against the time to describe the effect of swelling on flow front propagation. Figure 6.11 reveals that the ratio of volume fraction shows linear behaviour till 55 seconds and 40 seconds for central injection and eccentric injection cases respectively. For the case of central injection, the flow front takes more time to reach the outlet than the eccentric injection case. The same thing is reflected in the behaviour of the resin volume fraction ratio. One can see that the volume fraction ratio shows a linear behaviour for a longer time for the central injection case than for eccentric injection. This even behaviour cannot be seen in Figure 6.10, hence, the

results related to resin volume fraction ratio could be helpful while selecting the outlet design and conditions while designing the LCM process.

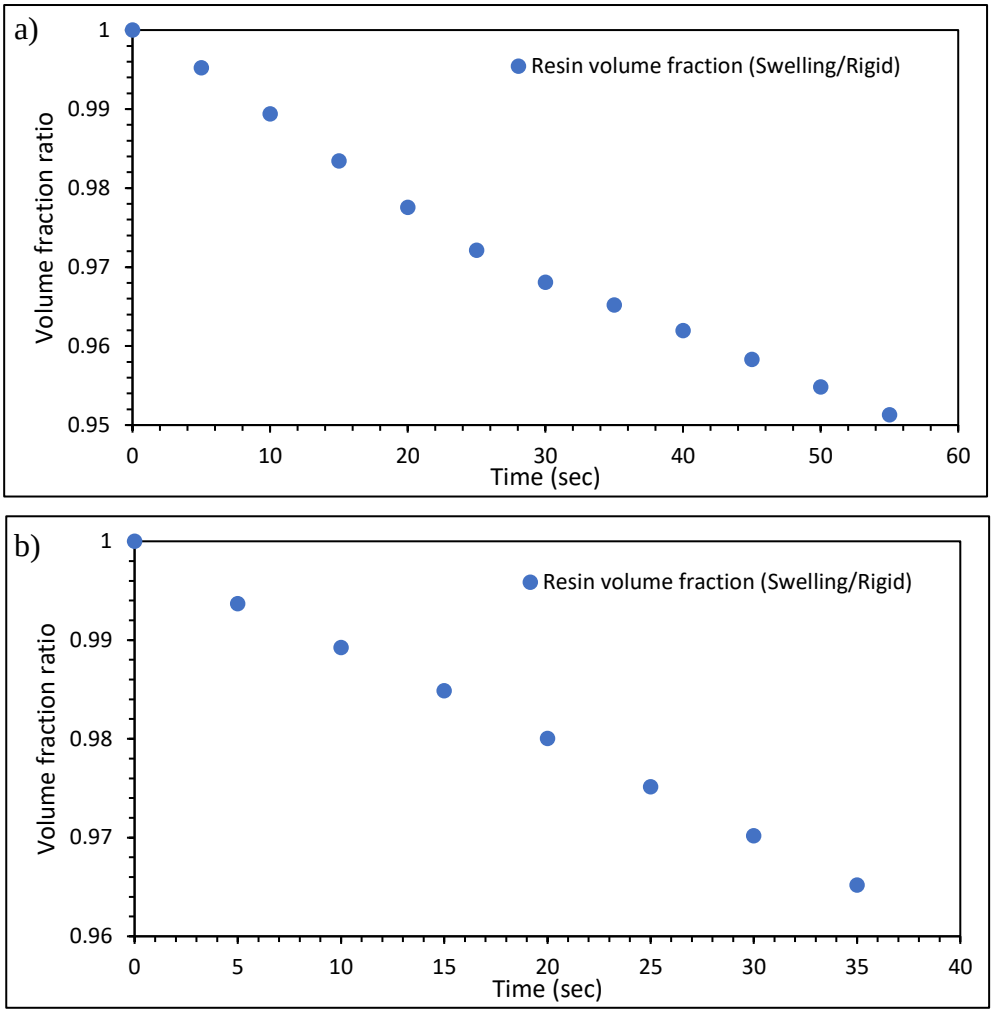


Figure 6-11 Plots of resin volume fraction ratio (Swelling/rigid) vs time for isotropic porous media (a) Central injection case (b) Eccentric injection case

### 6.4.2 Two-dimensional mould filling in an orthotropic porous media

For case study 2, An orthotropic porous medium was considered to evaluate the current approach to simulate the flow through orthotropic swelling porous media. For this case, the permeability in the *x*-direction was set ten times higher than in the *y*-direction (i.e., the resin will flow faster in the *x*-direction than the *y*-direction). Hence the initial permeability in the *y*-direction will be $6\times10^{-11}$ $m^2$. Besides, the remaining porous media properties and inputs are the same as that of the validation case. For this case as well the constant injection pressure condition is selected. The simulations are performed for the rigid and swelling conditions. The assumption of orthotropic porous media results in an increased overall resistance for the flow of resin than the isotropic case.

Figures 6.12 and 6.13 show the resin flow front locations for different times for both geometries to study the effect of distinct permeabilities on flow front advancement. For this case, the results are shown for 14 kPa injection pressure. As seen in Figures 6.12 and 6.13, the effect of the orthotropic porous media conditions can be seen on the flow front advancement. As a result, the flow pattern of the resin is elliptic in shape, as explained earlier the flow front advancement is dominant in the x-direction. Further, it can be seen that as compared to the isotropic porous media case, it takes a longer time for the resin flow front to reach the walls of the mould. Also, it is clearly evident that it will take more than 120 sec for the mould to get fully saturated by resin. This behaviour of the flow front advancement highlights the need for multiple injection ports when using the preform that is orthotropic in nature.

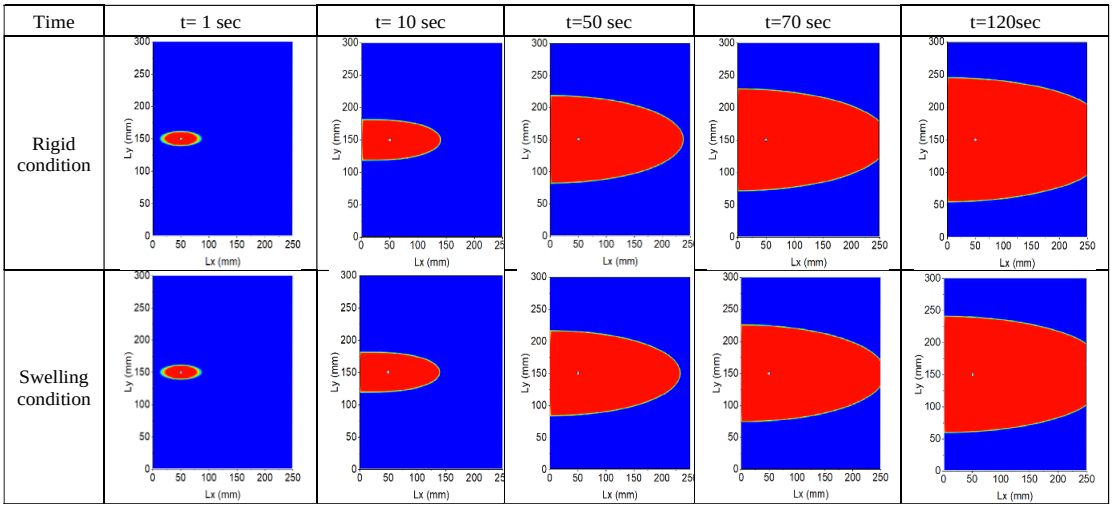


Figure 6-12 Transient contours of resin volume fraction for both rigid and swelling conditions for 14 kPa inlet pressure case (central injection case) (Orthotropic porous media)

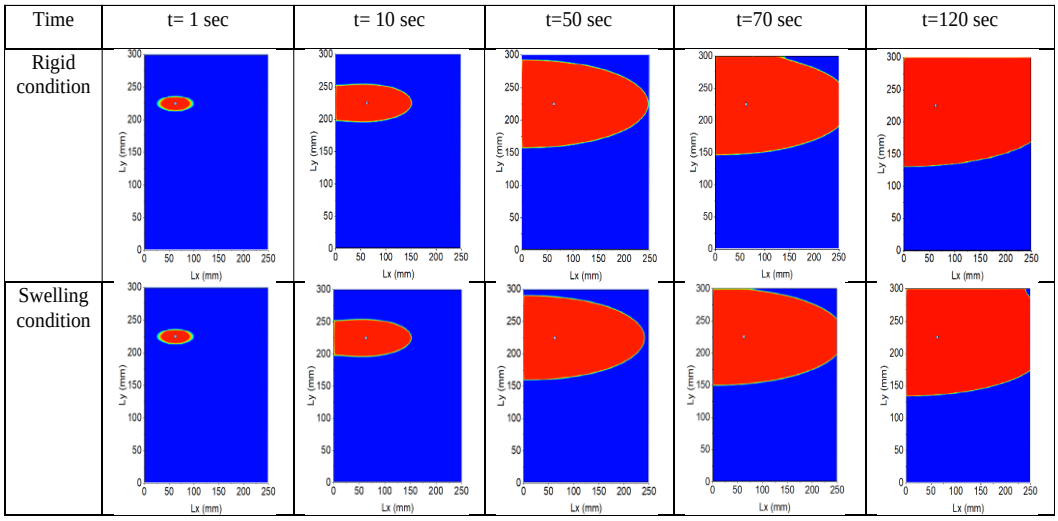


Figure 6-13 Transient contours of resin volume fraction for both rigid and swelling conditions for 14 kPa inlet pressure case (Eccentric injection case) (Orthotropic porous media).

Figure 6.14 compares the variation of the resin volume fraction with time for both arrangements. The effect of swelling can be clearly seen in the flow front advancement. From figure 6.14, it is observed that the flow front advancement becomes slow or negligible after 80 seconds for both arrangements. It is expected that, for larger domain sizes and longer simulation times, the swelling effect will become more dominant in both directions. In this case, as the porous media is assumed to be less permeable in the *y-direction*, the swelling effect will result in increased viscous resistance to flow in the *y-direction* than *x*, so the resulting flow may become closer to 1D in nature. Hence, it is clear that for orthotropic porous media the size, locations and number of injection ports play a vital role while designing the mould. Further, Figure 6.15 shows that the resin volume fraction in swelling porous media is about 6% less than that of rigid porous media, which is related to decreasing permeability due to swelling.

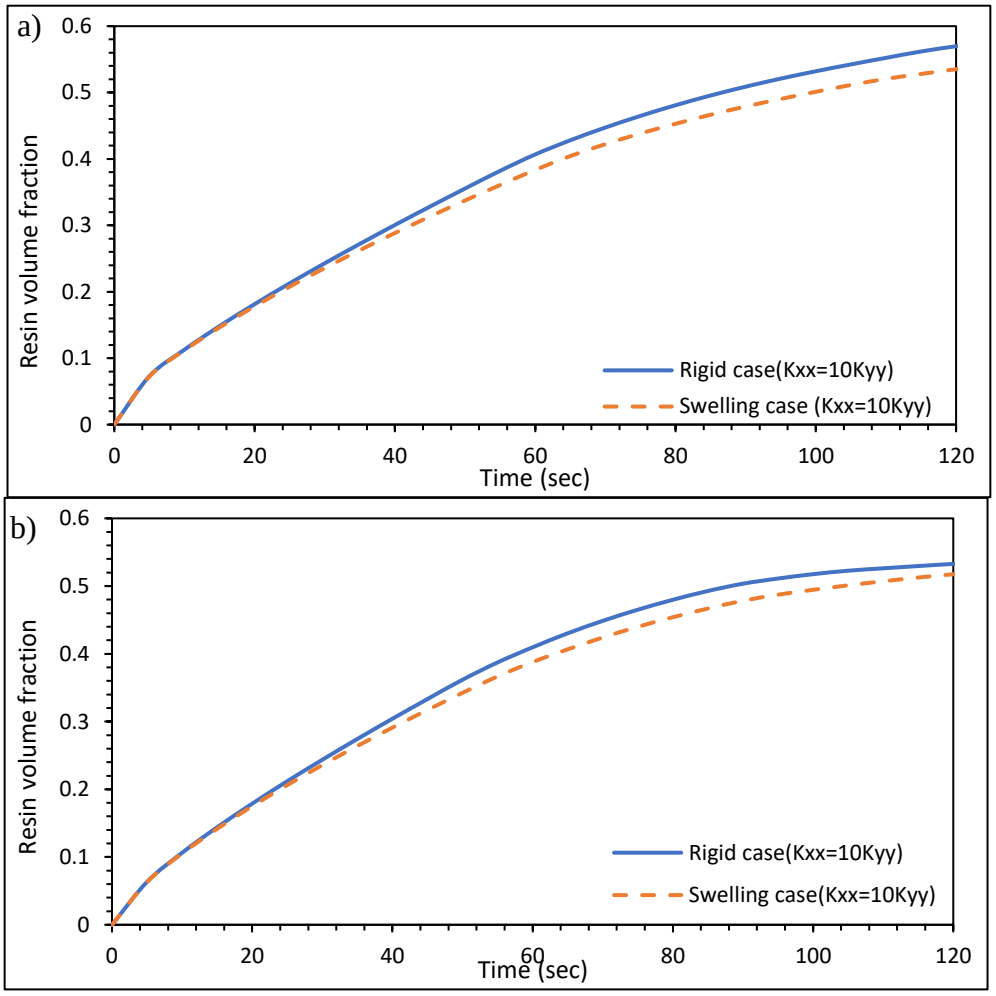


Figure 6-14 Plots of rein volume fraction Vs time for isotropic porous media (a) Central injection case (b) Eccentric injection case.

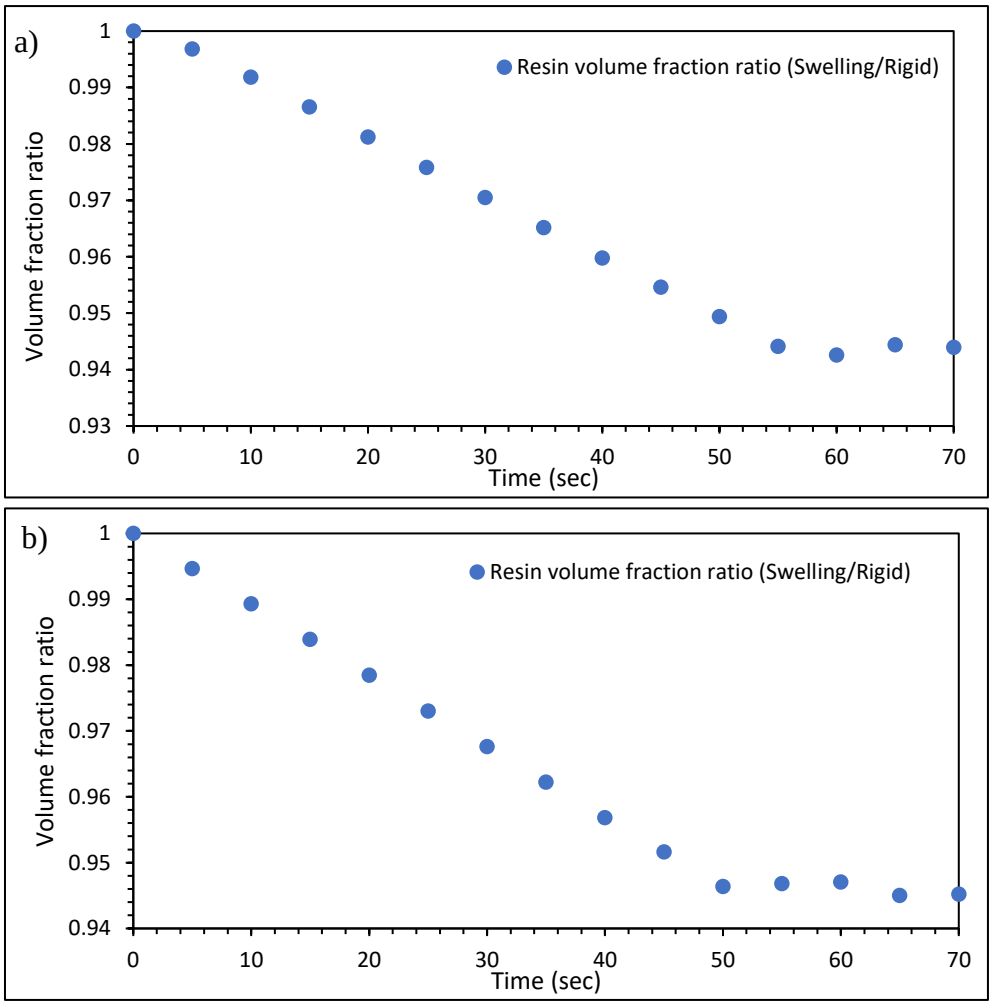


Figure 6-15 Plots of resin volume fraction ratio (Swelling/rigid) vs time for isotropic porous media (a) Central injection case (b) Eccentric injection case

## 6.5 Chapter Summary

The flow-through swelling porous media during the LCM mould-filling process is modelled using the volume of fluid method. A good agreement between CFD and experimental results is obtained for the 1-D rectilinear flow case. Also, the CFD predictions for inlet pressure changes for constant volume flow rate conditions showed good agreement with the experimental data. The 2-D transient results demonstrated the applicability of the present model to capture the sharp interface between air and resin under isotropic and orthotropic swelling porous media conditions. The results of this research showed that a computational model based on the finite volume and volume of fluid method can be used to model the flow through swelling porous media by measuring the change in the local permeability as a function of time.

The transient numerical results demonstrated the effect of swelling on the resin flow front advancement in isotropic and orthotropic porous media. The results showed that

the advancement of the flow front is considerably affected by the position of the inlet and by the size and location of the outlets. For the orthotropic case, it was observed that the flow front advancement becomes slower due to the swelling effect. It was also observed that the resin volume fraction in the rigid porous medium is about 6% higher than in the swelling porous medium. The finite volume method was found to be an efficient and flexible simulation method to model the flow in swelling porous media during the LCM mould-filling process. It is expected that these kinds of CFD simulations would help to design and optimize the LCM processes through flow front tracking, choosing the number of inlets and outlets, and prediction of mould filling time. There are also other industrial applications of this method such as modelling the flow in wipes and diapers which are swelling porous substances.

All commercial CFD packages can model the flow in rigid and non-swelling porous media only. The advantage of the proposed model is that any commercial solver based on the finite volume method can be easily adapted for flow simulation in swelling porous media. The majority of previous studies assume single-phase only while this method uses a multi-phase approach (volume of fluid method) to track the sharp interface between resin and air. It can help to track the smaller interface between air and resin (such as the formation of voids, bubbles, and defects in the process) for different geometries. In the current study, the flow is assumed to be in an isothermal condition, but this method can be extended to non-isothermal flow by using either local thermal equilibrium or non-equilibrium models. This method can easily be extended to 3D and can even be used with unstructured, or dynamic meshes.

# Chapter 7 Numerical simulation of liquid absorption into industrial porous wicks under rigid conditions

The performance of the absorbing porous media is an important factor in several practical applications such as hygiene industries, and industrial wicks. In the case of hygiene products, the primary goal is to absorb and retain a maximum amount of liquid. For other applications such as industrial wicks, different aspects of imbibition become important, such as rate of imbibition, wicking height, and volume/mass of liquid absorbed. Despite applications, in these types of products, the liquid flow is often driven by a strong capillary force. To evaluate the performance of such products the use of numerical simulations plays a vital role. Hence, Computational modelling of the liquid absorption process within rigid porous media would be helpful to design or modify these products. The modelling of capillary pressure effects is crucial in such simulations. Methods from literature based on the multiphase flow assumption such as Richard's equation-based approach and Eulerian approach require several fitting parameters to model such a flow scenario. If the values of these parameters are known correctly, the numerical predictions may not be accurate. This chapter demonstrates the application of a newly proposed approach for modelling liquid absorption within rigid porous media. The combination of the finite volume method and volume of fluid method is used for the first time to model liquid absorption in porous media. The proposed modelling approach uses fewer input parameters than previously used methods in literature which make it simple to implement. In this chapter, the wicking heights, predicted by computational fluid dynamics simulations, are in good agreement with the experimental and analytical data. The capability of the method to model the flow through absorbing porous media is explored by considering different flow cases. For the case where the flow front hits the walls of a porous domain, the results showed interesting patterns of the flow front under the action of gravity. It is observed that the nature of flow front propagation becomes 1D as time passes. Finally, the newly proposed cell zone condition to mimic the liquid hold-up showed promising results by allowing only air to pass through the porous domain.

## 7.1 Physical Description

This section provides the physical description of the different flow scenarios considered in this chapter. As a First step, the proposed modelling approach is

validated for 1D, 2D and 3D flow cases. For the 1D flow case, the experimental results are taken from Masoodi et al. (2007). The experimental setup consists of the 1D wicking flow setup as shown in Figure 7.1 (a).

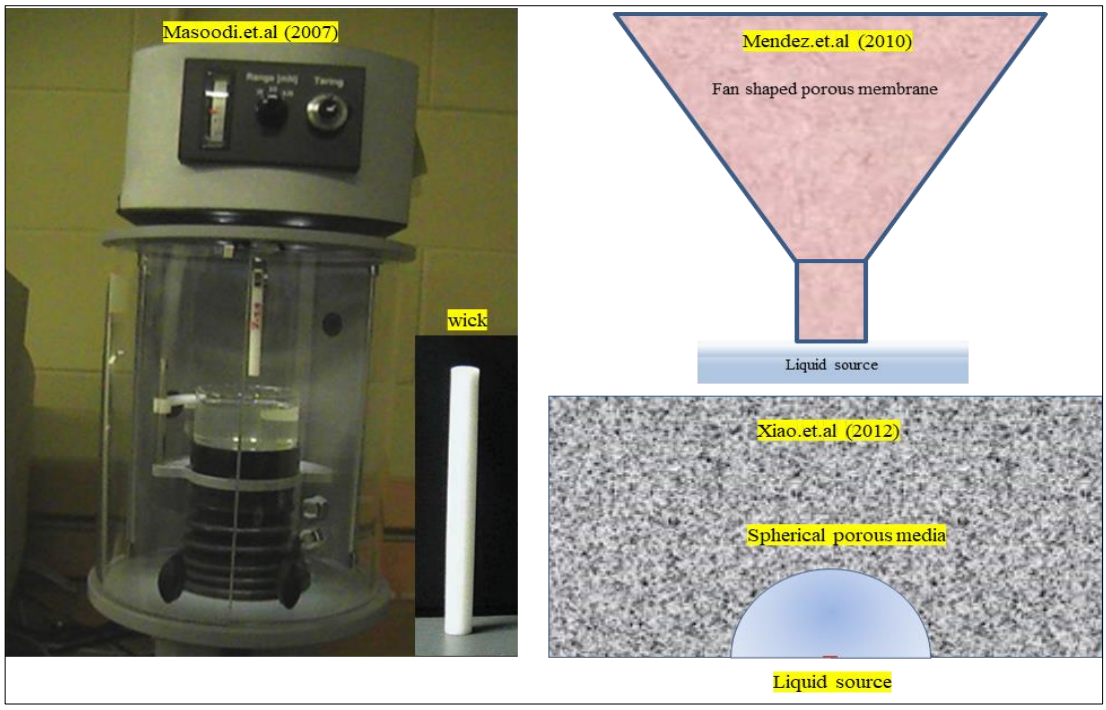


Figure 7-1 Schematic views of experiments for 1D,2D and 3D wicking case

For the experiments, a cylindrical polymer wick with a 7.2 mm diameter and 76 mm length is used. The experiments are then performed by using the alkane hydrocarbon liquid in form of hexadecane (HDEC) that has a density of 773 kg/m$^3$ and viscosity of 3.43 mPa.s. Finally, for the experiments, the Dynamics contact analyser is used to record the amount of mass absorbed in the wick. The values of porosity, permeability and capillary pressure are 0.4, $4.84\times10^{-10}$m$^2$ and 207.96 Pa respectively.

Further, for the 2D case, the experimental data from Mendez et al. (2010) is considered. For this case, the vertical wicking tests are performed to measure the rate of liquid absorption in a fan-shaped porous membrane of 90$^o$ angle as shown in Figure 7.1 (b). As the porous membrane has two different sections (rectangular and conical), the results for the flow front advancement are considered only for the conical section. For this study, the value of porosity, permeability and capillary pressure is 0.81, $6.83\times10^{-13}$ m$^2$ and 4196 Pa respectively.

Finally, for the 3D validation, the experimental data presented by Xiao et al. (2012b) is used. The experiments are conducted to measure the propagation of the flow front

with time. The porous media is developed by adding the soda-lime glass microspheres in a polycarbonate box. Further, a hole with a 0.64 mm diameter is drilled at the bottom as an inlet for the water. The measured values of porosity, permeability and capillary pressure are 0.36, $1.21\times10^{-11}m^2$ and 3480Pa. The schematic of the experiment is shown in Figure 7.1 (c).

## 7.2 Computational Description

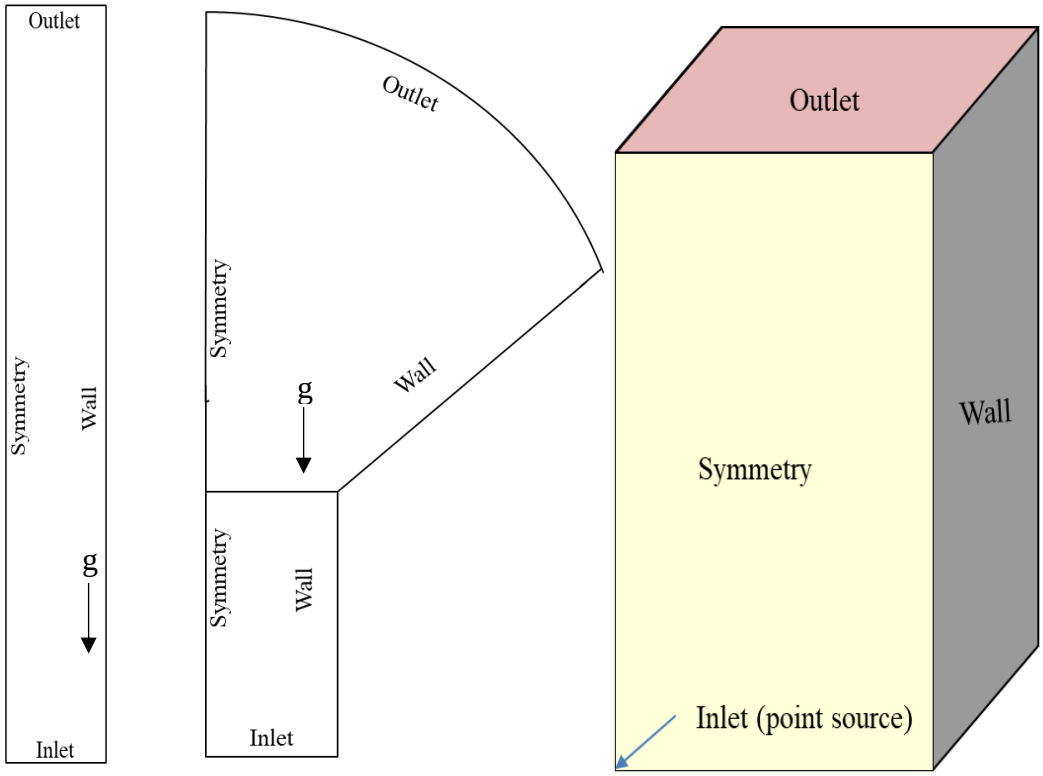


Figure 7-2 Details of boundary conditions for 1D,2D and 3D validation case

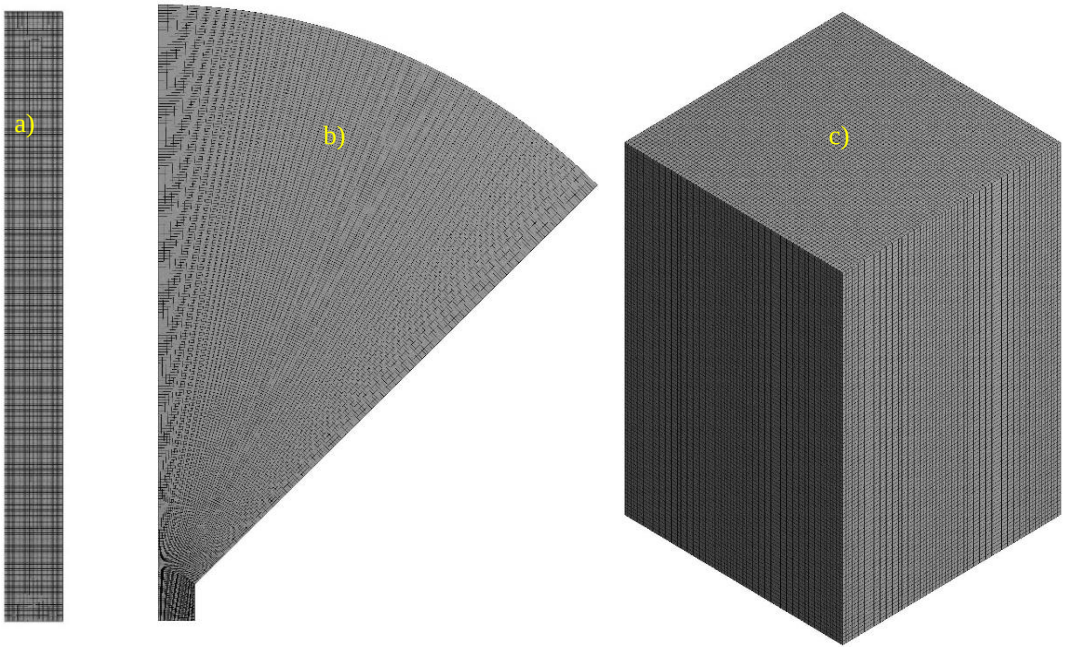


Figure 7-3 Representative computational mesh for the domain a) Details of mesh for 1D, 2D and 3D validation simulations.

Figure 7.2 shows the details of the boundary conditions defined for the 1D,2D and 3D validation simulations. The details of the mesh are shown in Figure 7.3. For 1D and 2D validation cases the quad mesh is used and for the 3D case hex type mesh is used for the simulation. The cell sizes of 0.1 mm, 1mm and 0.5 mm are used for 1D,2D and 3D simulation cases.

The porous media model with the volume of fluid method is used for simulating the flow for all cases. The properties/inputs of the porous media model are taken from each respected reference as mentioned in the previous subsection. The capillary pressure effects are added to the solver through user-defined functions based on the methodology as described in section 5.5.2. The defined capillary pressure is applied at the interface of the wetting and non-wetting phase at each timestep. This is done by applying the source terms in the momentum equation. The capillary pressure values of 207.16, 4196 and 3480 Pa are used for the 1D,2D and 3D simulations. For all cases, the air is taken as the non-wetting phase.

For the simulations discussed in this chapter, the following are the general boundary conditions defined at different boundaries.

**Inlet:** The atmospheric boundary conditions are defined at the inlet for all the simulations as the flow is mainly driven by the capillary forces.

**Outlet:** The pressure outlet boundary condition is defined at the outlets where flow exits the domain.

**Wall:** For walls, no-slip boundary conditions are defined for all flow cases

**Initial conditions:** To avoid errors in the simulations, the domain near the inlet is initialised with a small amount of wetting phase.

## 7.3 Validation

### 7.3.1 Validation of CFD approach for 1-D flow scenario

To validate the proposed numerical methodology in a 1D flow scenario the predictions from the CFD simulations are compared with the experimental data presented by Masoodi et.al. (2007) The computational domain and important boundary conditions are illustrated in Figure 7.2. The computational domain. The computational domain is a circular wick 76 mm in length and 7.2 in diameter. The bottom part of the wick was specified as an inlet, which is assumed to be in contact with the liquid reservoir at atmospheric conditions.

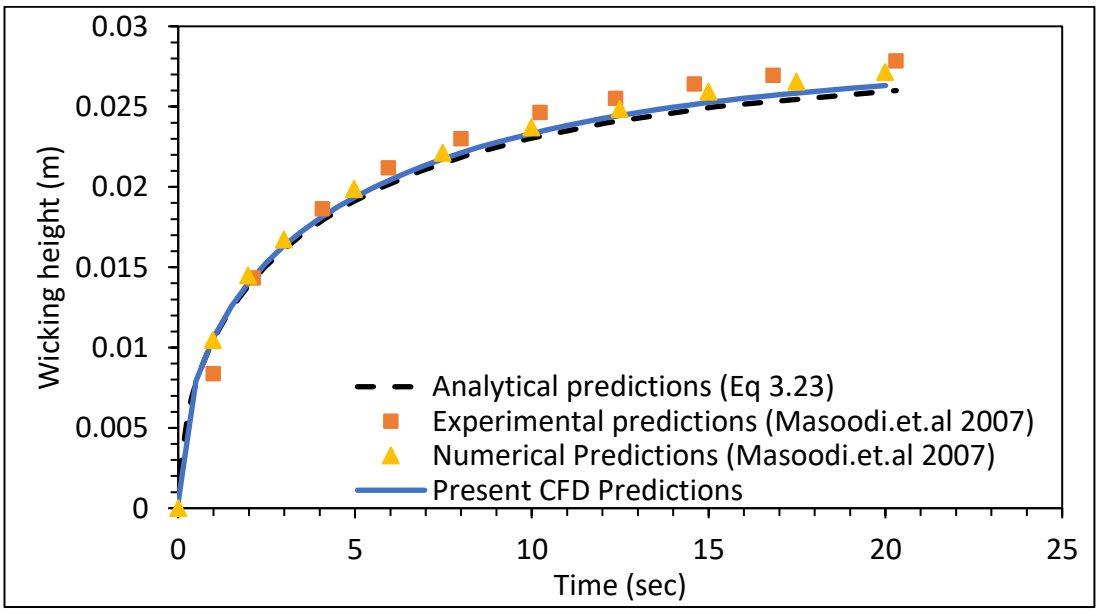


Figure 7-4 The comparison between experimental analytical (Masoodi et al., 2011) and CFD predictions for the wicking height for an upward wicking flow case

Figure 7.4 shows a comparison between the experimental data and CFD predictions for the wicking height in the case of upward-wicking flow conditions. It can be seen

that the CFD results are in good agreement with the experimental, analytical, and numerical predictions by Masoodi et al. (2011). The present CFD predictions show an average percentage error of 3.92%. compared to experimental data. In the case of wicking, the flow is mainly driven by the capillary force that pulls up the liquid against gravity. The liquid column that rises due to pulling created at the liquid-air interface gets balanced once the hydrostatic forces start to become dominant. As a result, the capillary forces acting upwards get balanced by the hydrostatic pressure developed within the liquid column. This effect is observable as the flow front advancement slows after 5 seconds.

To test the capability of the method, the developed model is also used to predict the liquid front advancement for downward flow where all the forces i.e., capillary, and gravitational are in the same direction. This flow scenario is called the liquid draining case. To do so, only the position of the inlet and outlet is reversed in the existing model of the upward-wicking case and simulations are done. As there is no such data available in literature where this type of flow condition is considered, the CFD results are validated against the analytical predictions by Eq 3.20**.** As mentioned in the analytical modelling section, the existing equation developed by Masoodi and Pillai (2012a) for the upward-wicking flow case is modified such that the effect of gravity on flow front advancement will be opposite to that of the upward-wicking case. As shown in Figure 5**,** the analytical and CFD predictions are in excellent agreement. As a result, it can be seen that the liquid movement is faster in this case as it takes 14 seconds to reach the depth of 0.07 m. This demonstrated the capability of the method to model the flow in the liquid-draining case. However, these results need to be validated against the experimental data. Hence such efforts need to be taken in future.

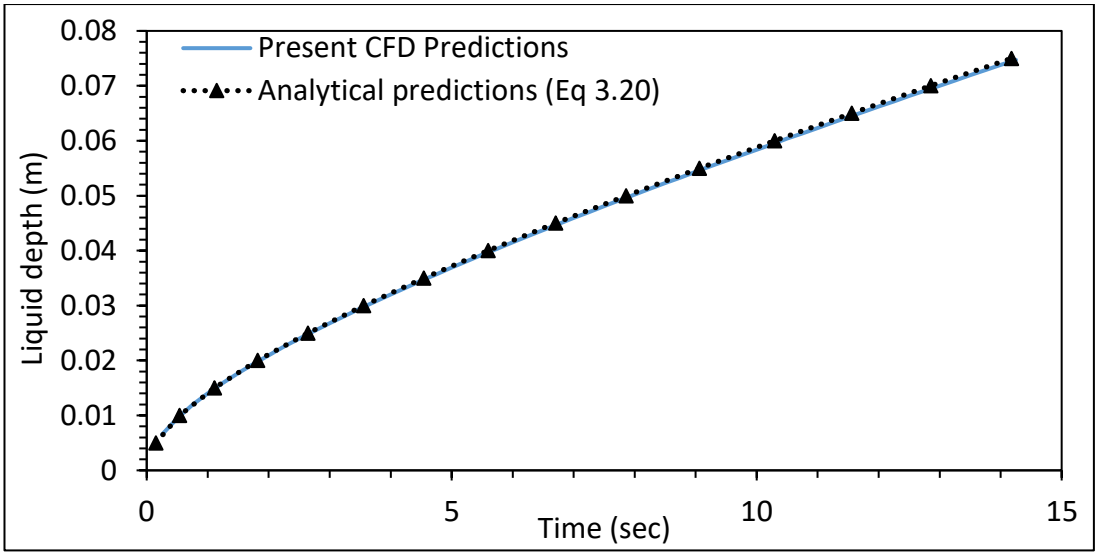


Figure 7-5 Comparison between CFD predictions and predictions from newly proposed analytical for a draining flow case

### 7.3.2 Validation of CFD approach for 2-D flow scenario (Imbibition in the annular porous membrane)

For a 2-D flow scenario, liquid absorption into a porous membrane is considered. In recent years, interest in the medical utility of paper substrates has resulted in the development of two-dimensional lateral flow assays and three-dimensional microfluidics. These lateral flow devices are used in medical applications that are fabricated to meet the need of users in poor areas. To validate the CFD approach, the obtained CFD simulation results are compared with the experimental and analytical data from Mendez et al. (Mendez et al., 2010) The computational domain and important boundary conditions are illustrated in Figure 7.2 (b). The computational domain is a fan-shaped porous membrane with a fan angle of $90^{\circ}$. The domain consists of two parts, a) a small rectangular section and b) an Angular section. For this case, the rectangular section is initialised with full saturation of liquid at the start of the simulation as we are interested in the flow front propagation in the angular section.

Figure 7.6 shows a comparison between CFD and experimental data for flow front locations in an annular porous zone. As seen in Figure 7.6 the CFD predictions are in excellent agreement with experimental data from Mendez et al (2010). As seen for the 1D wicking flow case, the effect of gravity is not seen in both CFD predictions or experimental data. The main reason for this could be the higher value of capillary pressure (4196 Pa).

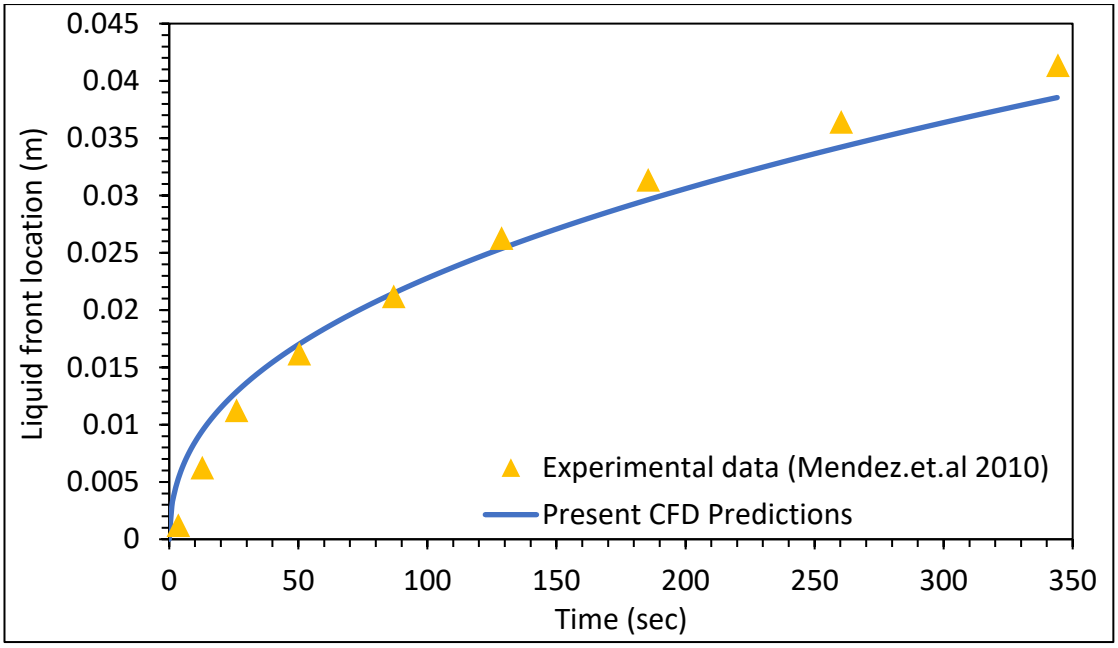


Figure 7-6 Comparison between CFD and experimental (Mendez et al., 2010) predictions for flow front displacement versus time for imbibition in a porous membrane of an annular sector shape

Further, Figure 7.7 shows the transient contours of variation of the liquid flow front, pressure, and velocity with time. It can be clearly observed that the pressure contours show the value of capillary pressure precisely at the interface which is consistent with liquid volume fraction contours. Further, the velocity contours are clipped in the range for better visualization, as result, a sharp line is present at the interface of the liquid-air interface. If observed clearly, the sharp line in velocity refers to the applied capillary pressure. As explained in Chapter 5, in a volume of the fluid method the momentum equation is solved at the mixture level. Hence, the velocity below the line is purely related to the absorbed liquid and the velocity beyond the line is purely related to the air being displaced as a result of wicking.

| Time | Volume fraction | Pressure | Velocity |
|---|---|---|---|
| 50 sec | 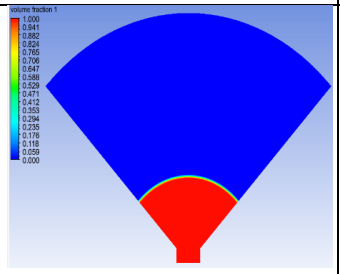 | 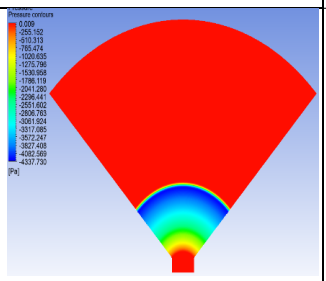 | 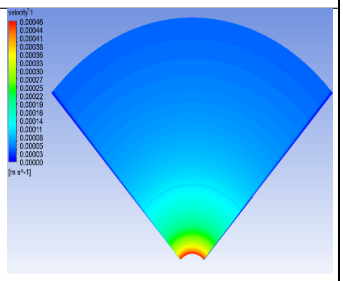 |
| 100 sec | 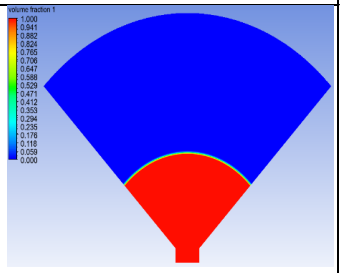 | 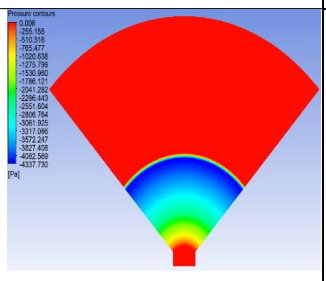 | 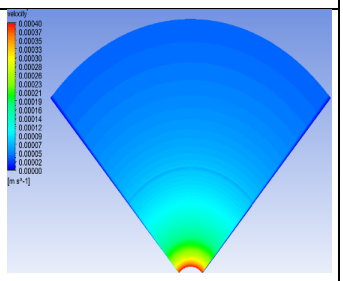 |
| 150 sec | 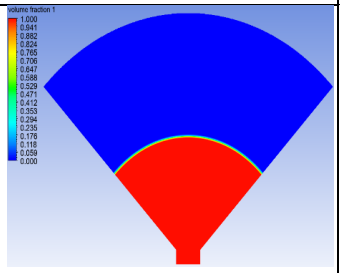 | 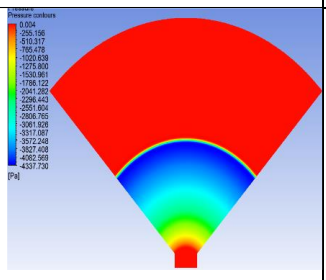 | 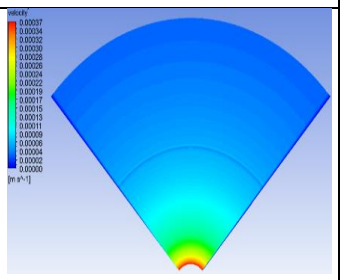 |
| 200 sec | 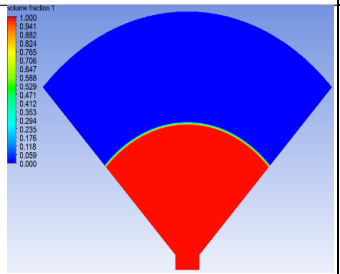 | 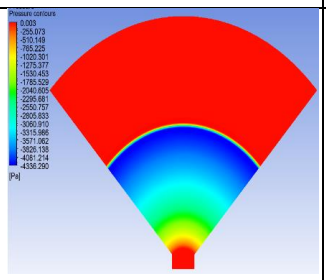 | 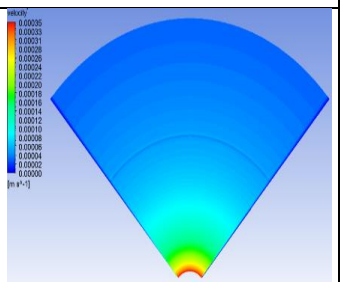 |

Figure 7-7 Transient contours of liquid volume fraction, pressure, and velocity for liquid imbibition in an annular section

### 7.3.3 Validation of CFD approach for 3-D flow (Imbibition from a point source in a semi-infinite porous domain)

Finally, the proposed methodology is validated for the 3D flow scenario. The liquid absorption in semi-infinite porous media is considered. For this case, the corrected version analytical model presented by Xiao et al. (2012a) is considered. For the validation, the predictions from the CFD model are compared with predictions from the analytical model The details of the boundary conditions are presented in Figure 7.2 (c).

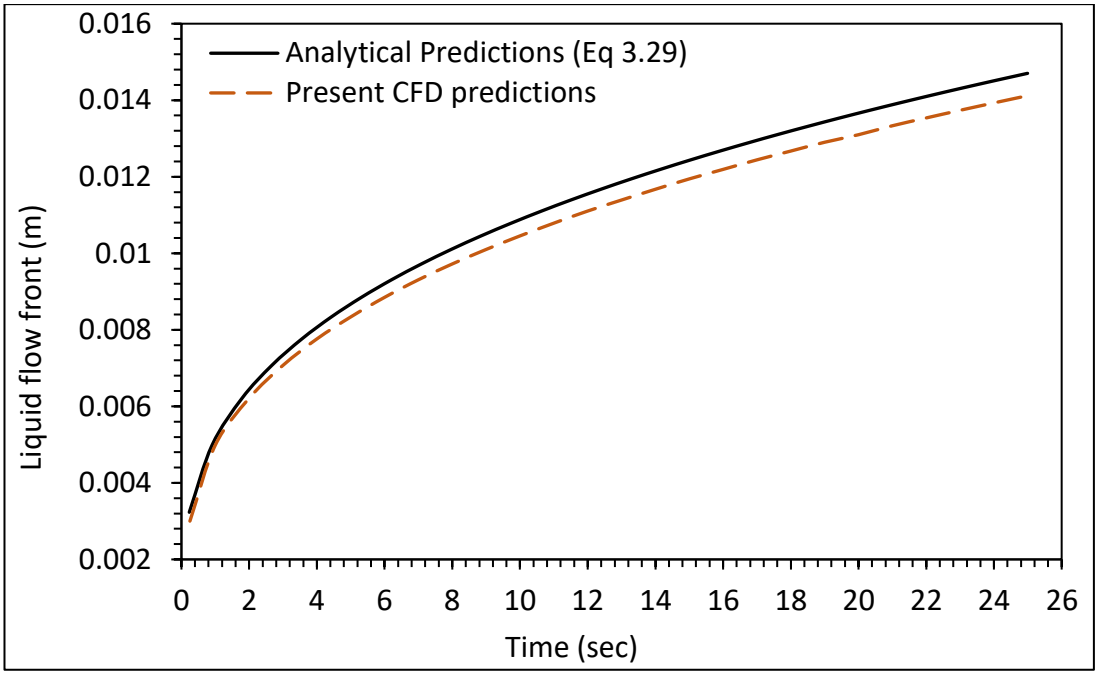


Figure 7-8 Comparison between the CFD and analytical predictions from Eq 3.2 for flow front displacement versus time for imbibition in a 3-D porous domain

Figure 7.8 shows a comparison between CFD predictions and analytical predictions for flow front advancement. For the present study, the porous media is assumed to be isotropic in nature, which results in equal flow front advancement in radial and lateral directions. Hence it is represented by a single set of results. The CFD predictions are in good agreement with analytical predictions by Equation 3.29. In this case, as well, the effect of gravity is not seen on the flow front advancement as the capillary pressure is higher, but it is expected that for the higher values of the wicking heights the effect of gravity would start to become dominant. The corresponding contours are shown in Figures 7.9 and 7.10.

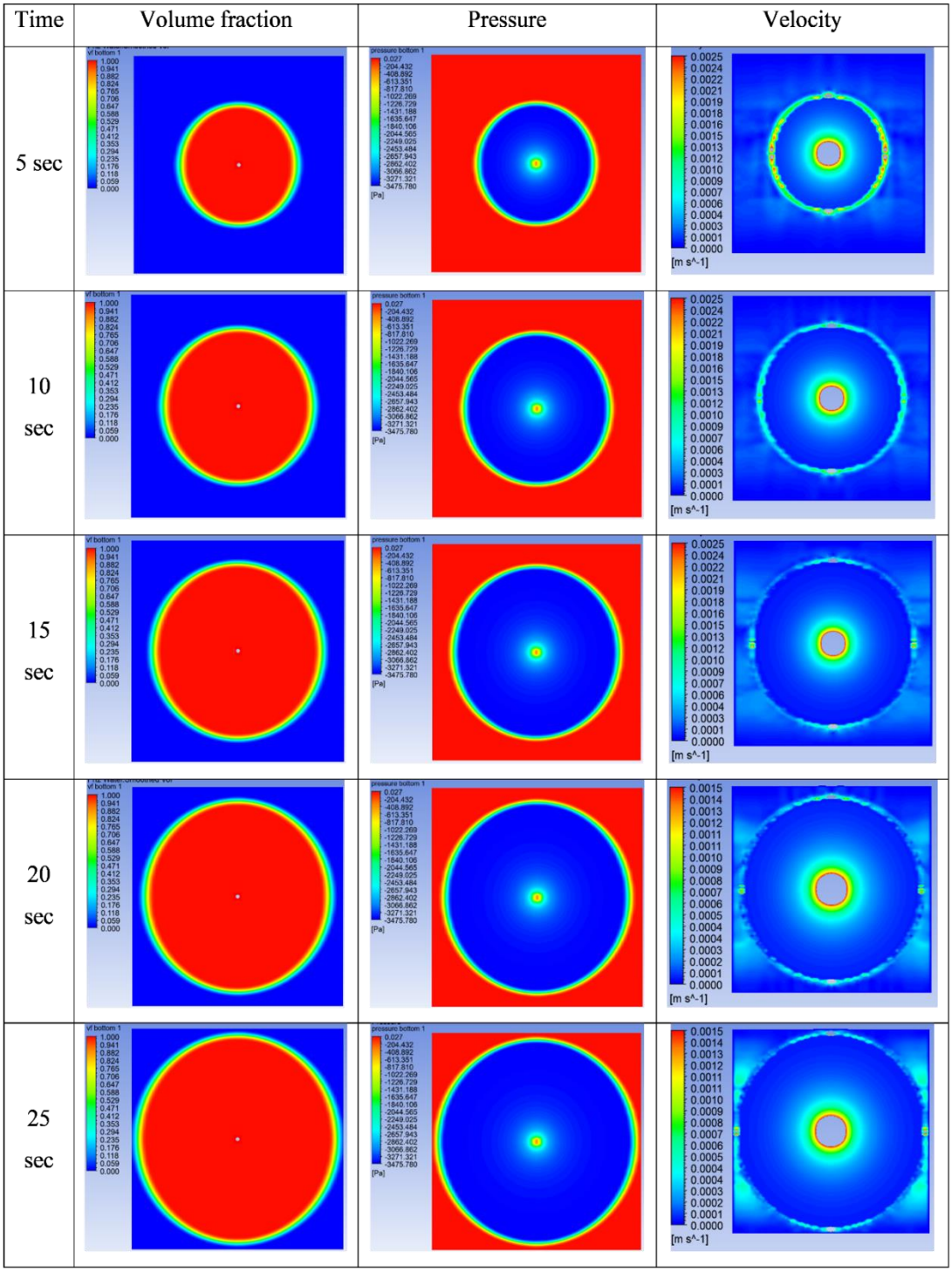


Figure 7-9 Transient contours of liquid volume fraction, pressure, and velocity on a ZX plane.

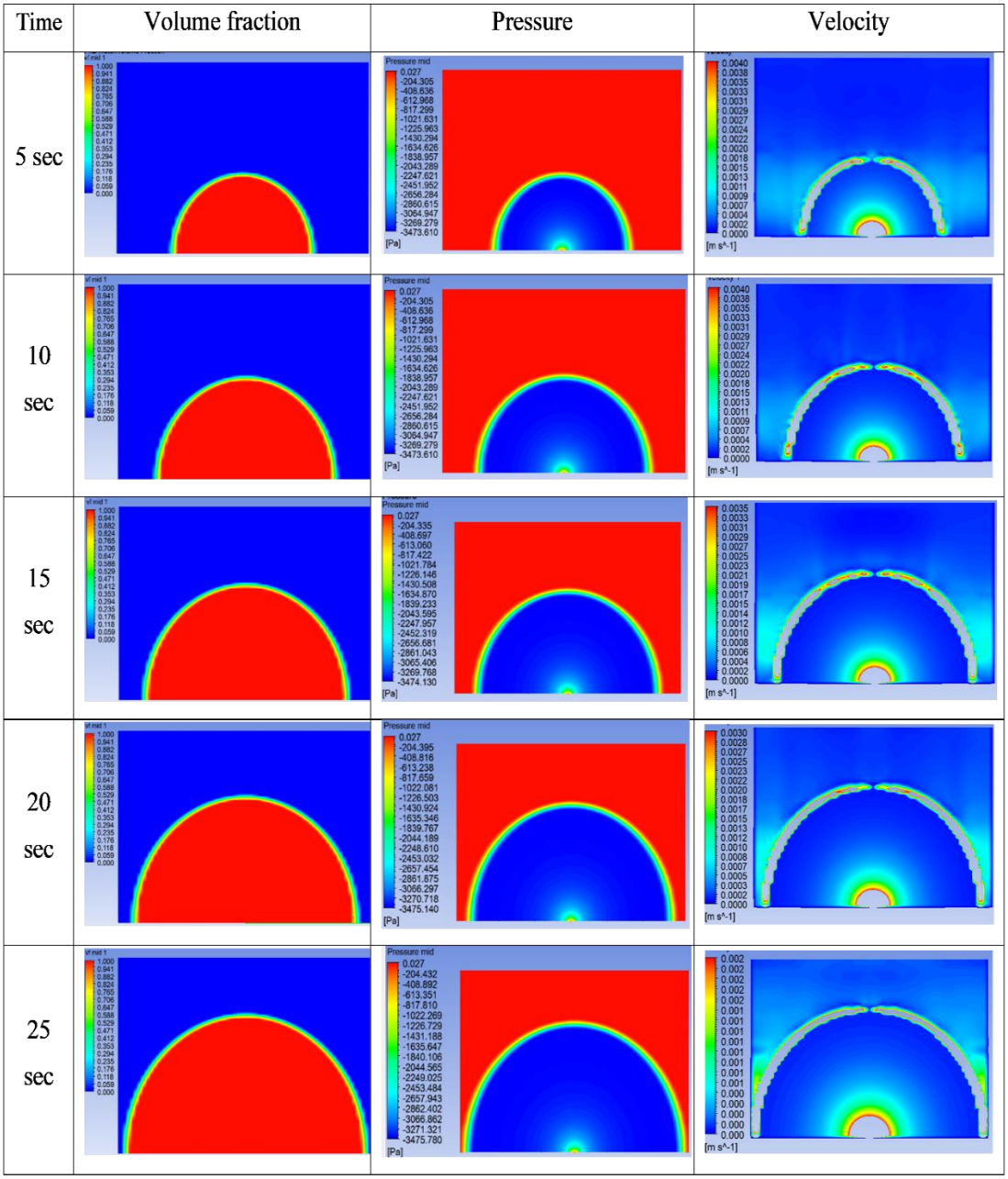


Figure 7-10 Transient contours of liquid volume fraction, pressure, and velocity on an XY and YZ plane

## 7.4 Case studies

To explore the ability of the proposed modelling approach, two different scenarios are studied here. The first scenario focuses on the behaviour of the liquid flow front when it hits the walls of a porous domain (i.e., during the experiments, the porous samples are usually held in a container). The second scenario is different and focuses on the newly proposed cell-zone condition that mimics the liquid hold-up within the porous domain, which is usually found in real-world applications (e.g., diapers, and paper napkins). To do so, another porous zone with higher viscous resistance to the wetting

phase is modelled (Figure 7.11). Hence, the outcomes from these case studies would help engineers design and optimise products that use absorbing porous materials by examining the pressure and velocity field at different locations within the porous domain. As cited in the literature, the analytical method is valid until the flow front reaches the walls of a porous domain. These case studies show the details of flow front behaviour that an analytical method fails to describe

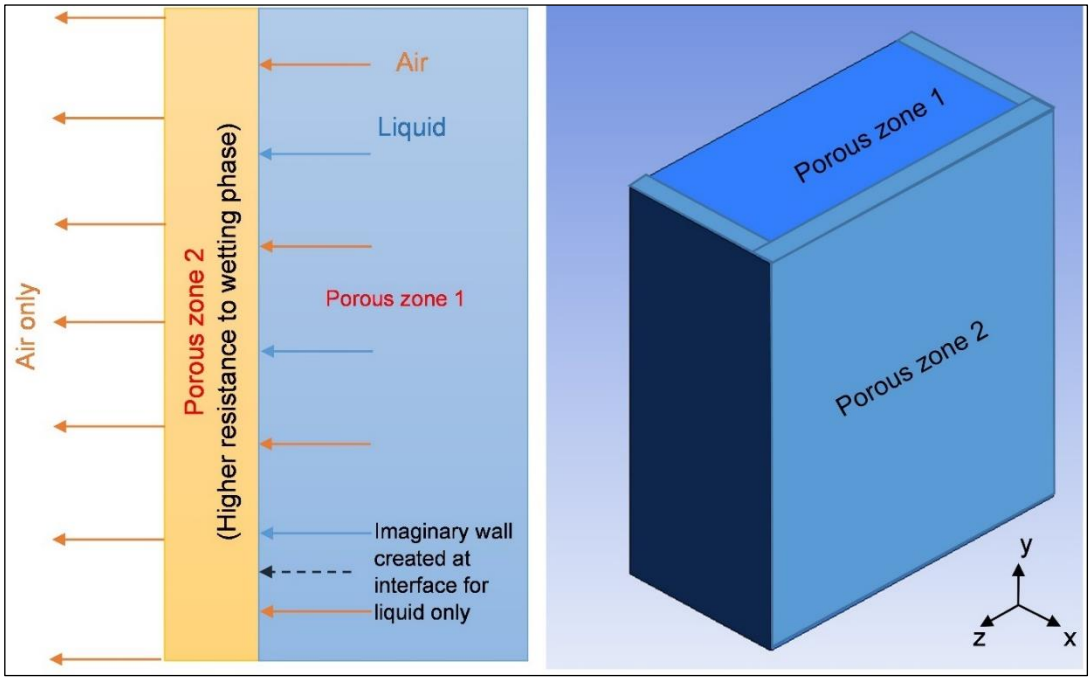


Figure 7-11 a) Details of newly proposed cell-zone condition to mimic the condition of liquid holdup within a porous domain. b) Details of the co-ordinates used for all case studies

The primary porous zone is the main domain in which liquid absorption due to capillary forces takes place. The secondary porous zone is so defined that it only allows air to pass through it while blocking the flow of liquid. This cell-zone condition act as a wall to the wetting phase (liquid), whereas for air it acts similar to the primary porous zone. This was simply done by defining the higher resistance for the wetting phase (liquid) in a secondary porous zone. For the present case, the permeability ratio $\left({k_{pz1}}/{k_{pz2}}\right)$ was taken as 10. We considered two cases with different values of capillary pressure along with the new type of cell-zone condition. The shape of the flow front for all case studies is represented by radius in orthogonal directions *(x and z-direction)* and height *(y-direction*) as shown in Figure 7.11 (b).

### 7.4.1 Case one: When the flow front reaches the wall.

To check the applicability of the model, the proposed methodology is expanded for the advanced flow conditions. The flow described by analytical models is valid until the flow front reaches the walls. Once the flow front reaches the wall, the analytical models fail to describe the flow. Hence, to explore this phenomenon, the CFD simulations are performed for the smaller domain size than the 3D validation case. For this case, the input data and boundary conditions for the model are taken the same as for the 3D validation case.

Figure 7.12 shows the variation of the flow front in the *x*, *y*, and *z*-direction. As shown in Figure 7.12, the flow front advancement in the *x* and *z* directions becomes almost constant when the flow front hits the walls around 20 sec of simulation time. On the other hand, the flow front continues to advance in the *y*-direction. From the trend of the graph, it can be seen that the flow front advancement in the *y*-direction is not affected by the termination of flow front advancements in other directions. The reason could be the higher value of capillary pressure.

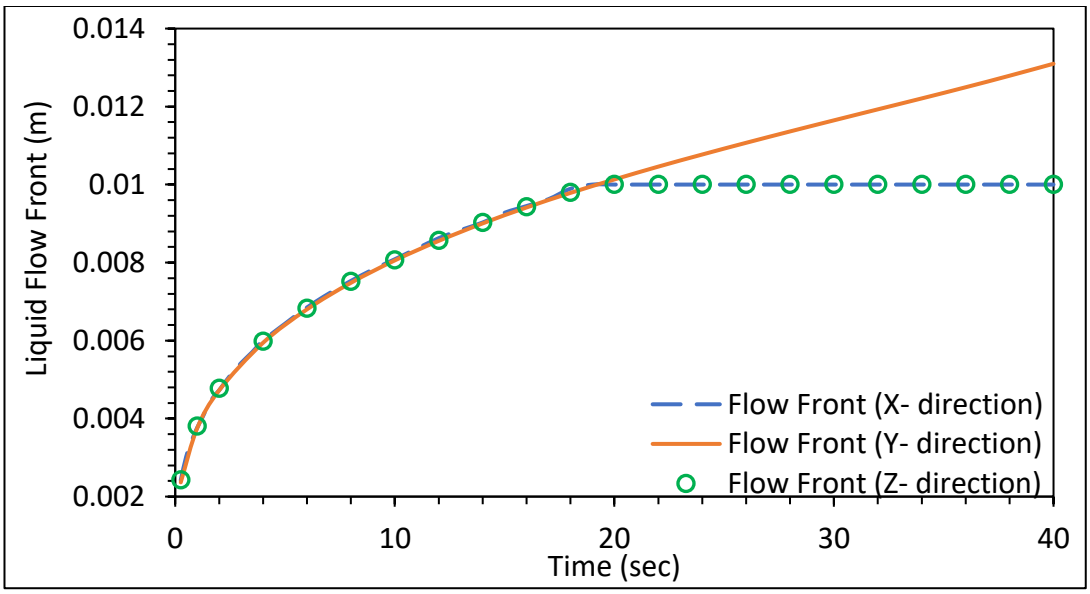


Figure 7-12 Variation of flow front locations in x, y, and z directions with time

Figure 7.13 shows the transient contours of the volume fraction, pressure, and iso-surfaces. By observing the volume fraction contours and iso-surfaces, it can be seen that the shape of the interface starts to change from a purely hemispherical nature when the flow front hits the walls. It is expected that for longer times, the nature of the flow front would start to become 1-D. The blue-painted sphere-like area shows the position

of the interface, and the volume-rendered red region shows the air volume fraction within the domain

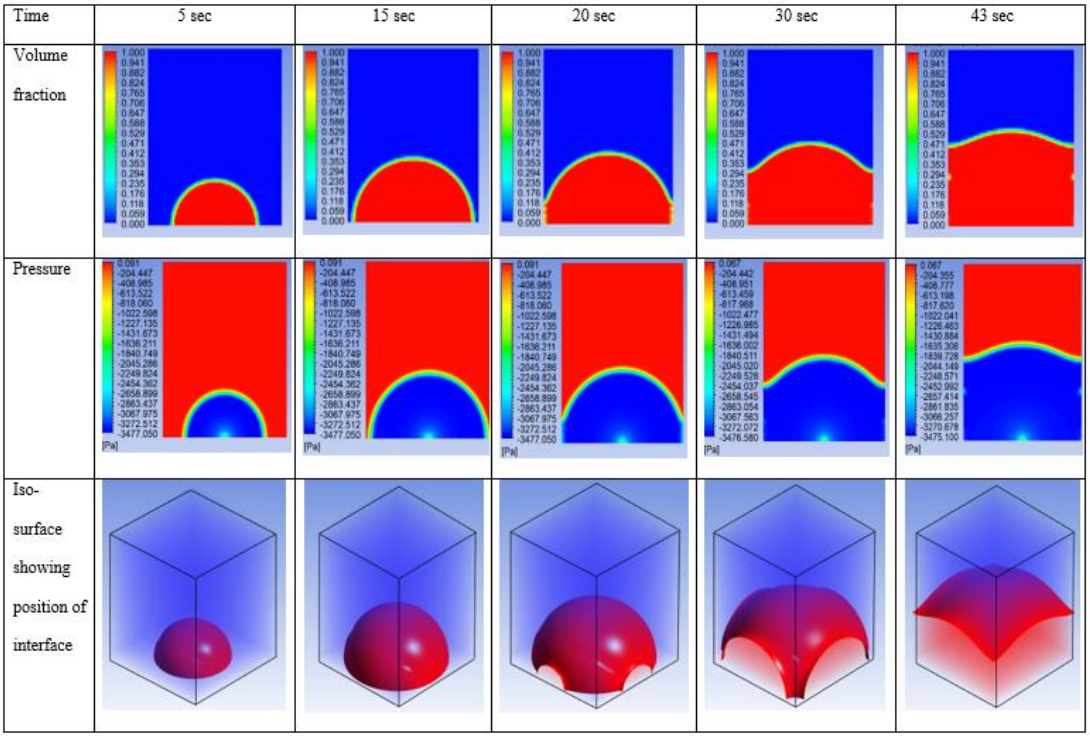


Figure 7-13 Transient contours showing the variation of volume fraction, and pressure within the porous domain for case 1

### 7.4.2 Case two: Newly proposed wall boundary condition with gravitational effects

As discussed in the previous sections, a new approach to model liquid retention in the porous media is proposed. To develop the model, the inputs (porosity, permeability) from the 3D validation case are used. For the secondary porous zone, the permeability for the wetting phase (liquid) is set to be 10 times lower than the primary porous zone. Two different values of capillary pressure (400Pa and 1000Pa) are used for the study.

Figure 7.14 shows the evolution of flow front locations in the *x*, *y* and *z*-direction for two values of capillary pressure. For both cases, the effect of gravity can be clearly seen in the flow front propagation in the *y*-direction, whose trend is similar to the 1-D validated case of upward wicking. Further, it is seen that the flow front advancement in the other two directions (*x* and *y*) stops after the flow front hits the interface of the porous zones, which demonstrates the capability of the proposed cell-zone condition.

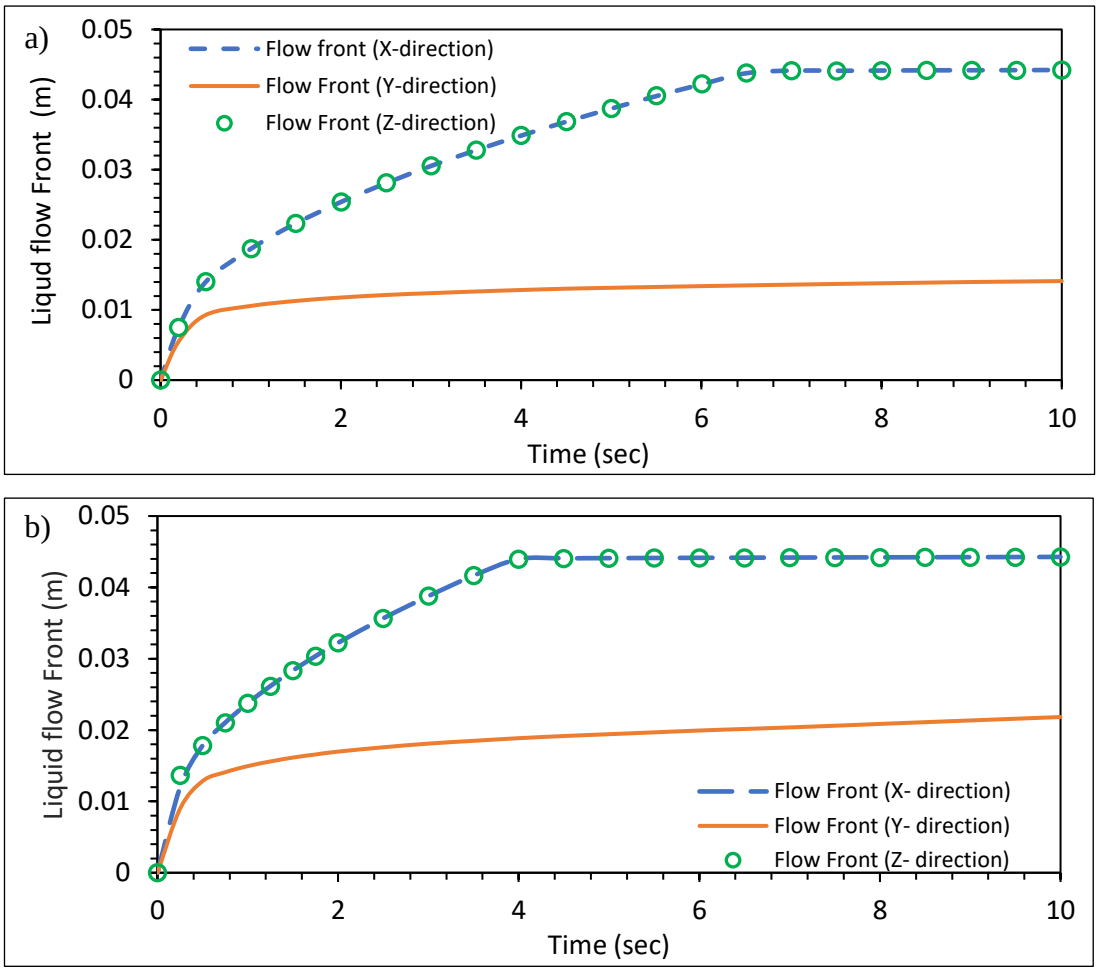


Figure 7-14 Variation of the liquid front in x, y, and z directions for case 2 a) Capillary Pressure = 400Pa and b) Capillary Pressure = 1000Pa.

For the capillary pressure values of 400 Pa and 1000 Pa, the flow front hits the interface around 6 sec and 4 sec, respectively. Also, it can be seen that the wicking height of the liquid is hardly affected by the value of capillary pressure, as the wicking height in the case of 1000 Pa capillary pressure did not vary significantly compared to the 400 Pa case. This can be related to the size of the porous domain. As the capillary force lifts the weight of the rising liquid column against gravity, it is expected that the wicking height would be higher for the same capillary pressure for the smaller sizes of the porous domain. To test this idea, the domain size is halved for the 400 Pa capillary pressure case and found the difference in the wicking height of the liquid was. Figure 7.15 clearly shows the effect of the porous domain size on the wicking height of the liquid. Further, Figures 7.16 and 7.17 show the transient contours of the liquid volume fraction, pressure, and iso-surfaces showing the position of the interface.

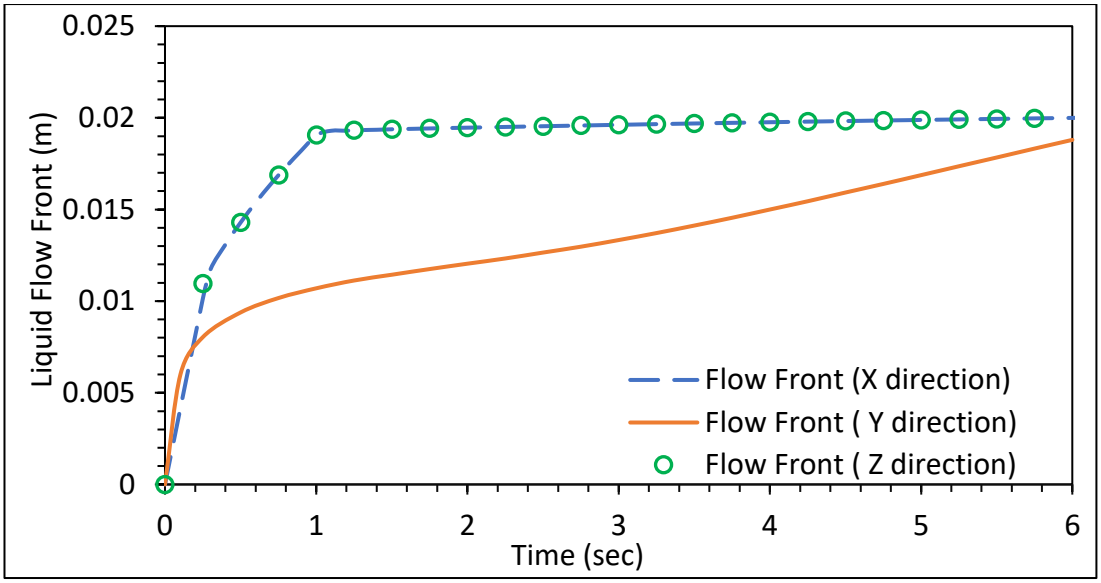


Figure 7-15 Variation of the liquid front in the x, y, and z-direction for the half domain in case of 400Pa capillary pressure.

From volume fraction and pressure contours, it can be seen that the capillary pressure is being applied at the interface which demonstrates the capability of the method model such a flow condition. Finally, the effect of the newly proposed boundary condition to mimic the liquid hold-up can be seen from the iso-surfaces. It is clearly seen that the liquid front climbs on the imaginary wall created due to the difference in permeabilities of the two porous zones. The changes in the shape of the interface can be clearly observed from the contours. For both cases, the changes in the shape of the interface can be seen in Figure 7.16 and Figure 7.17. Hence, this type of result related to the flow front location (liquid volume fraction contours), and pressure could be helpful while designing and optimising the sanitary products according to performance constraints.

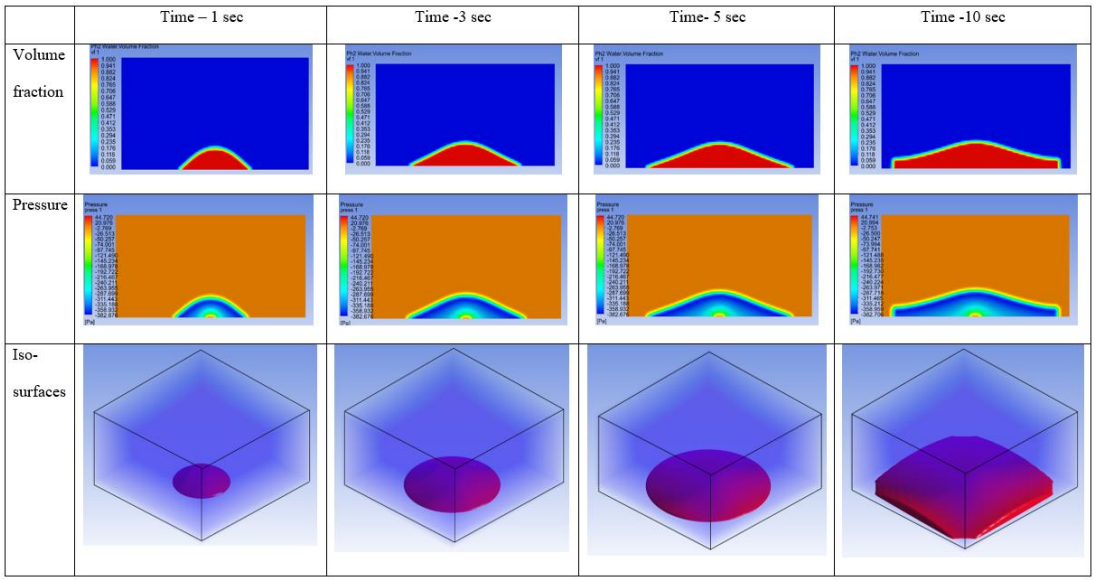


Figure 7-16 Transient contours of the liquid volume fraction, pressure, and Iso-surfaces for the 400Pa capillary pressure case.

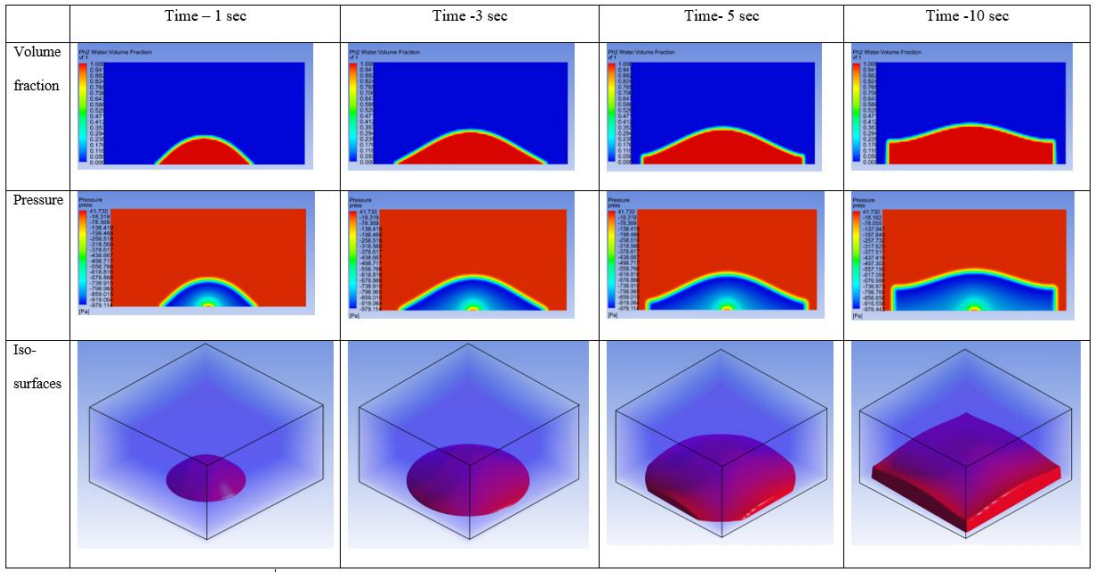


Figure 7-17 Transient contours of the liquid volume fraction, pressure, and Iso-surfaces for the 1000Pa capillary pressure case

## 7.5 Chapter Summary

The majority of the methods for modelling liquid absorption are based on the single-phase assumption within the porous domain. When a multiphase approach is assumed, the resulting model needs a lot of fitting parameters related to relative permeability, relative viscosity, and the relation between liquid saturation and capillary pressure. The multiphase approach suggested in this study is easier to implement than other methods available in the literature.

In this chapter, the liquid absorption in rigid porous media is modelled using the Volume of Fluid method. This is the first time that such a method in combination with the Finite Volume Method has been used to model such a flow scenario. A good agreement between the CFD, experimental data, and analytical data is obtained for all the developed models. Furthermore, the proposed analytical models for the liquid draining case and for the case where the flow front is assumed to be hemispherical (3D imbibition), are validated against the CFD predictions. A new approach to model the liquid holdup within porous media is proposed in this Chapter. The 3D transient results showed the ability of the model to track the interface during the liquid absorption process. The results also showed that a numerical model based on the combination of the Finite Volume Method and Volume of Fluid (FVM-VOF) can be used to model the liquid absorption process when the basic parameters, such as permeability, porosity, and capillary pressure, are known for any porous medium.

The results demonstrated the ability of the model to capture the interface when the propagating liquid front hit the walls. The shape of the interface slowly starts to become 1D in nature when the gravitational effects are neglected. Further, the model captured the interface when gravitational effects are considered. The effect of hydrostatic pressure was clearly seen in the flow front advancement. The newly proposed approach to mimic the liquid hold-up within porous media demonstrated its applicability. The results demonstrating the position of the interface clearly showed the liquid retention within the porous domain. Further, the results showed that the size of the porous domain has a considerable effect on the wicking height of the liquid.

The combination of the Finite Volume Method and Volume of Fluid method (FVM-VOF) provided an efficient approach to model the liquid absorption within rigid porous media. It is expected that this approach can serve as an alternative to the other

multiphase methods, such as Eulerian models or models based on the Richards equation, for analysing the flow front locations and pressure distribution within the porous media. The CFD analysis of the flow front locations using simulations would help to design and optimize sanitary and personal hygiene products, such as diapers, paper napkins and wipes, and tampons. The results showed that the method is capable of modelling and tracking the liquid-air interface under different working conditions. For our current scenario, the flow was assumed to be isothermal in nature, but this method can be further extended to model the non-isothermal effects within porous media, such as heat pipe modelling where heat is being transferred within the wick (porous region). Finally, the use of the FVM adds flexibility to model the flow within complex geometries. This method can be applied where the relationship between the capillary pressure and the liquid saturation is not known. Future work could extend this method further to applications where the swelling effects of porous media need to be considered.

# Chapter 8 Numerical simulation of flow through diapers under swelling conditions

This chapter presents the framework to model the flow through absorbing porous media under swelling conditions. Previously in Chapter 7, a novel framework based on the combination of the Finite Volume Method and Volume of Fluid Method is proposed to model the flow through absorbing porous media under rigid conditions. The results from the model showed a promising correlation with the experimental and analytical predictions for the wicking height and radius. However, the framework did not include the swelling porous media conditions. The swelling effect considerably affects the porosity and permeability of the porous medium causing errors in the flow front location predictions. In this chapter, the framework is extended by including the swelling effects. The local permeability in this case is defined as the function of time. To derive the expression for the permeability change, different analytical models from the literature are used. The CFD simulations are performed by considering the different permeability reduction functions developed from analytical models. It is found that the CFD predictions based on permeability reduction predicted by the Chen et.al model compared well with the experimental data. This comparative study showed the applicability of available analytical models to predict permeability changes. Further, the validated methodology is extended to model the flow through diaper-like geometry. The dimensions of the geometry are taken from the actual product. The results demonstrated the capability of the method to model the flow on the curved faces. The effect of gravity is clearly seen in the flow front propagation on the top and bottom faces of the domain.

## 8.1 Physical description

This section provides the physical description of the flow scenario considered in this chapter. The proposed modelling approach is validated against the experimental data obtained from the water absorption test (Chapter 4). The experiments included the analysis of the liquid absorption behaviour under the constant pressure head. The dimensions of the sample are 144mm × 144 mm × 25mm. During the experiments, the flow front advancement is recorded on the top as well as on the bottom face of the sample., the sample is made by stacking the different layers of cotton material and sewing it together as shown in Figure 8.1. Since the hand-sewing method is used to

stack the fabric pieces together, it can be observed from Figure 8.1 that the top face of the sample is not uniform. As a result, the samples are compressed at the edges on the top face as seen in Figure 8.1. The modelling of such a cell zone condition is challenging. On the other hand, it is observed that when the sample is placed inside the holder, its bottom face remains flat due to the weight of absorbed water. Hence, in this chapter, major attention is given to the flow front propagation on the bottom face of the sample for the validation of the proposed framework. The other details of the experiment are mentioned in Chapter 4. The values of porosity, permeability and capillary pressure are 0.88, 3.91 $\times 10^{-11} m^2$ and 1418Pa. Finally, as explained in Chapter 4, the predictions from the different analytical models for permeability reduction as a function of time are used to include the swelling effects.

Figure 8-1 The side view of the prepared sample shows the uneven shape on the top face.

For the case studies, the validated framework is extended to the real work application of diapers. For case study 1, the flow is modelled inside a diaper-like geometry. The details of the Pampers baby diapers are considered to make the realistic model. The details of the actual and simplified geometry of the diaper are shown in Figure 8.2. For this case, the single absorbent core is considered. The properties of porous media are taken the same as that of the validation case.

Finally, for case study 2, multiple porous layers with different permeabilities are assumed. The details of the geometry are shown in Figure 8.3. For this case, the CFD models are developed for two different scenarios. For the first scenario, the permeability of the top and bottom layers is taken as 3.91 $\times 10^{-11} m^2$ with porosity as 0.88. Further, the middle layer is assumed to swell upon the liquid absorption with an initial permeability of 1.98 $\times 10^{-10} m^2$. The value of capillary pressure is taken as 800Pa for all layers.

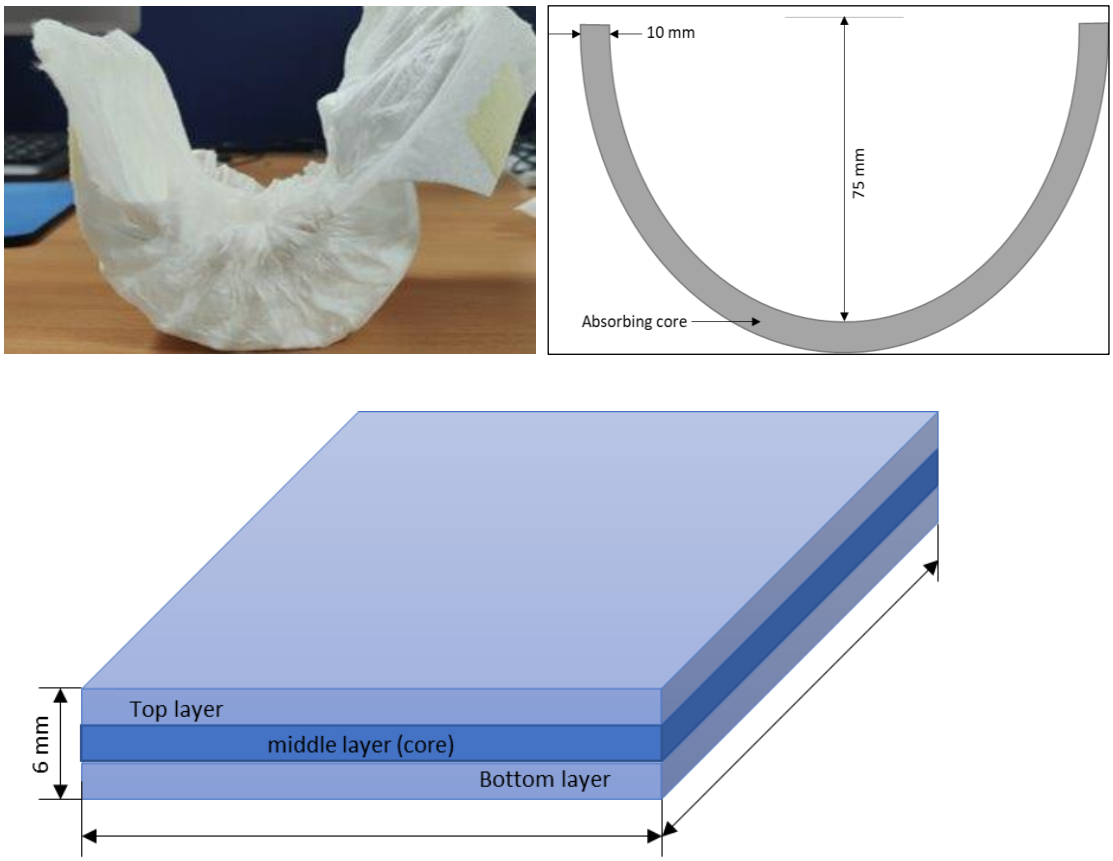


Figure 8-2 Details of the different geometries selected for the case studies a) Actual baby diaper b) simplified geometry of diaper c) The porous zone with multiple layers

## 8.2 Computational description

The details of the boundary conditions and mesh are shown in Figure 8.3 and Figure 8.4. The porous media model with the volume of fluid method is used for simulating the flow for all cases. The properties/inputs of the porous media model are taken from each respected reference as mentioned in the previous subsection. The swelling and capillary pressure effects are added to the solver by user-defined functions as described in 5.5.1 and 5.5.2 respectively. For the case of swelling effects, the functions based on the predictions from theoretical models from the literature are developed and adapted for the simulations. Finally, the defined capillary pressure is applied at the interface of the wetting and non-wetting phase at each timestep. For all cases, the air is taken as the nonwetting phase.

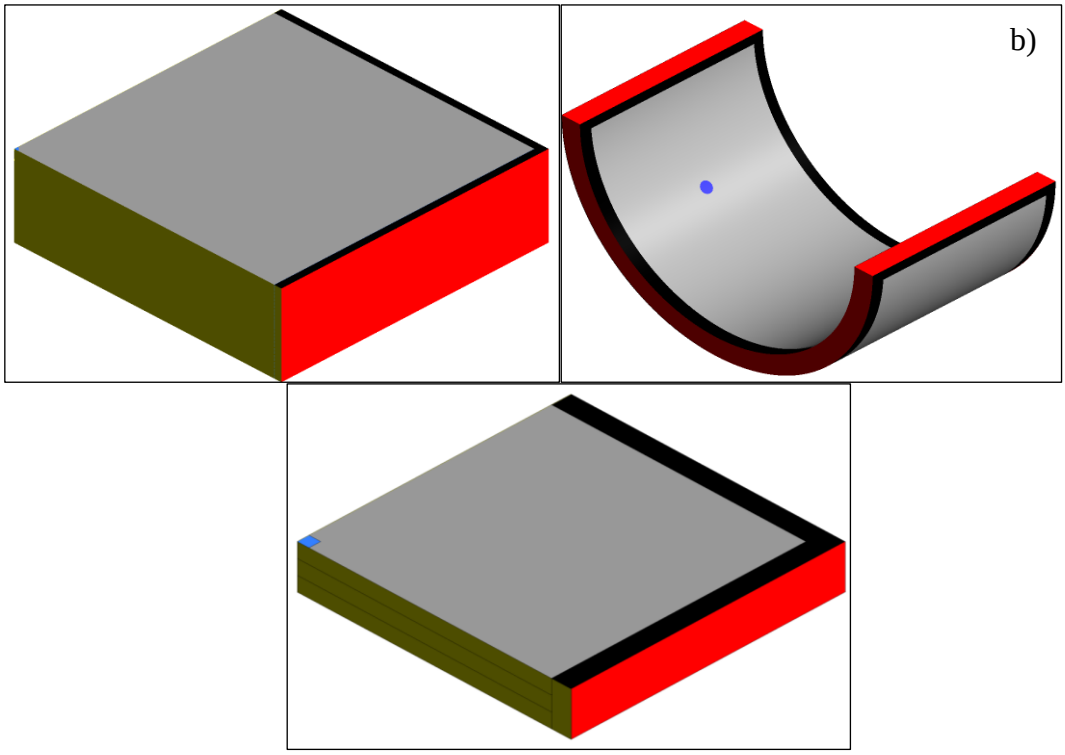


Figure 8-3 Details of boundary conditions for a) Validation case b) Case study one c) Case study two. Following are the colour codes: Blue- Inlet, Red- Outlet, Yellow -Symmetry, Gray and Black-walls of porous zone 1 and porous zone 2

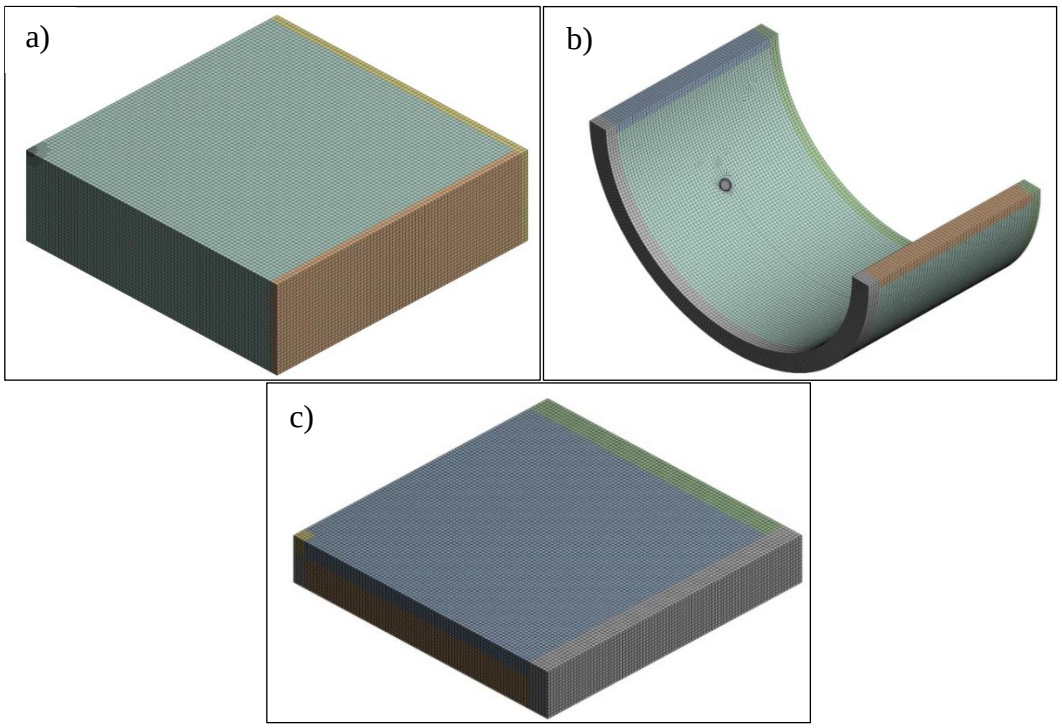


Figure 8-4 Details of mesh for a) Validation case b) Case study one c) Case study two

For the simulations discussed in this chapter, the following are the general boundary conditions defined at different boundaries.

**Inlet:** The pressure inlet is used for all cases studied in this chapter. For the validation, the CFD model, 5179 Pa and 12753 Pa are taken as the inlet pressure. Further, for case study one, the 50Pa is defined at the inlet which gives a mass flow rate of 0.0023kg/sec. Finally, for case study two, 10P is selected as inlet pressure which gives a mass flow rate of 0.00033kg/sec. The values of the mass flow rate are selected as stated by (Olsen et al., 2009).

**Outlet:** The pressure outlet boundary condition is defined at the outlets where flow exits the domain.

**Wall:** The Top and bottom faces of all computational domains are specified as walls whereas the side faces are made permeable to the non-wetting phase (air) only. The details of the arrangement are described in Chapter 6.

## 8.3 Validation

The proposed modelling framework in this chapter is validated against the experimental data presented in Chapter 4. The constant pressure head of 52 cm and 130 cm are applied at the inlet and for the outlet atmospheric pressure conditions are specified.

Figure 8.5 and Figure 8.6 shows the comparison between the experimental data and CFD predictions for the flow front advancement of water on the bottom face of the sample. The CFD predictions are in excellent agreement with experimental data for both values of pressure head (52 cm and 130 cm). The CFD predictions show an average percentage error of 2.63% and 7.78% for 52 cm and 130 cm pressure head values respectively. Also, Figure 8.6 shows the comparison between the CFD predictions based on different permeability reduction models and experimental data for the case of a 130 cm water head. Figure 8.6 shows that CFD predictions from the Terzaghi (1925) and Chen (1995) based permeability models are in excellent agreement with experimental data. Whereas the predictions from the Devis (1952) and Gebart (1992) permeability model show a considerable difference.

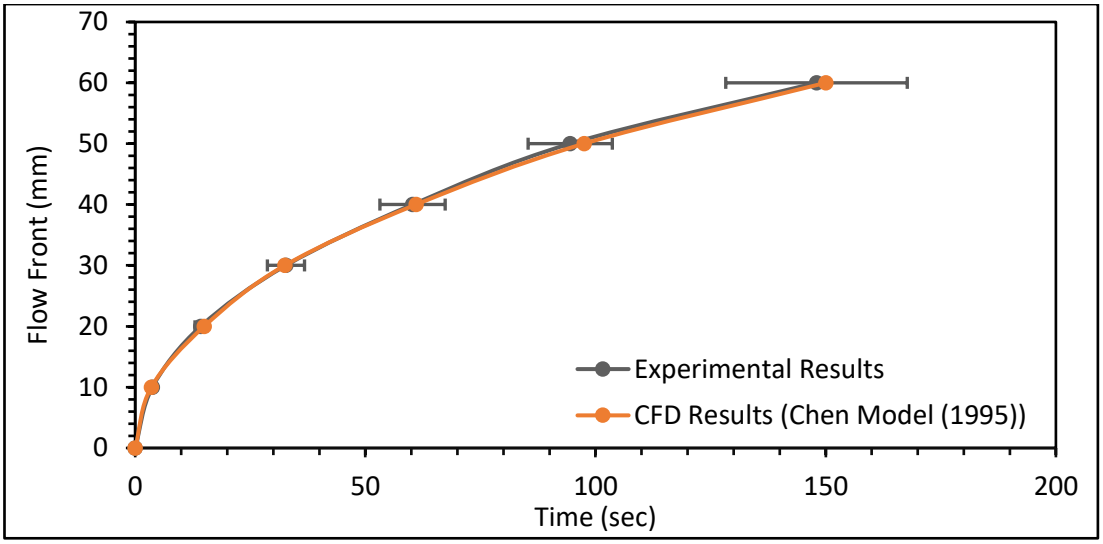


Figure 8-5 Comparision between the experimental and CFD predictions for the 0.52 m water head case

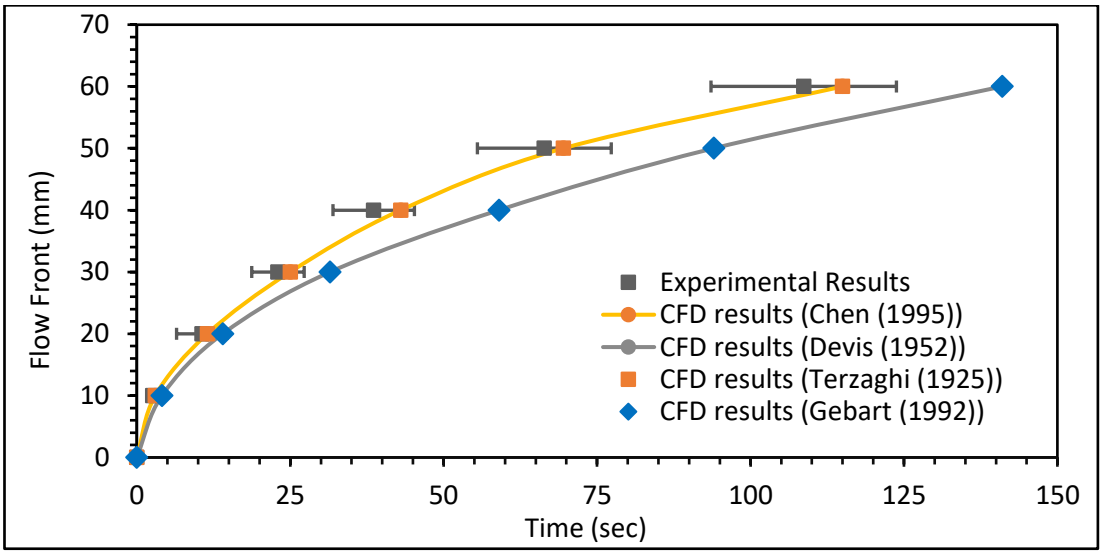


Figure 8-6 Comparision between the experimental and CFD predictions for the 1.32 m water head case

Based on these results, the predictions for the permeability under fully swollen conditions from the theoretical models presented in Chapter 4 can be compared. The table below shows the comparisons between the theoretically predicted permeability and the measured permeability. The experimentally estimated value of permeability under fully swollen conditions is 2.403 $\times 10^{-11} m^2$. Further, Figure 8.7 compares the CFD flow front locations (shown in red colour) and the experimental flow front locations. The results are shown for the case of 0.52 m water head. Note that, all the results shown here are extracted for the bottom face of the sample.

Table 8.1 The predictions from the different analytical models cited in Masoodi and Pillai (2010) for the permeability reduction with time

| Model and year | Predicted K | Percentage Error |
|---|---|---|
| Blake (1922), Kozeny (1927), Carman (1937) | $1.57\times10^{-11}m^2$ | 34% |
| Zunkar (1920) | $1.97\times10^{-11}m^2$ | 18% |
| Terzaghi (1925) | $2.54\times10^{-11}m^2$ | 6% |
| Fehling (1939) | $1.40\times10^{-11}m^2$ | 42% |
| Rose (1945) | $1.38\times10^{-11}m^2$ | 42% |
| Rumpf (1971) | $1.18\times10^{-12}m^2$ | 51% |
| Bruschke and Advani (1993) | $7.04\times10^{-12}m^2$ | 71% |
| Gebart (1992) | $2.00\times10^{-11}m^2$ | 17% |
| Devis (1952) | $2.09\times10^{-11}m^2$ | 13% |
| Chen (1955) | $2.45\times10^{-11}m^2$ | 4% |

| Time | CFD Flow Front locations (h = 0.52 m) | Experimental Flow Front locations (h = 0.52 m) |
|---|---|---|
| 0 sec | 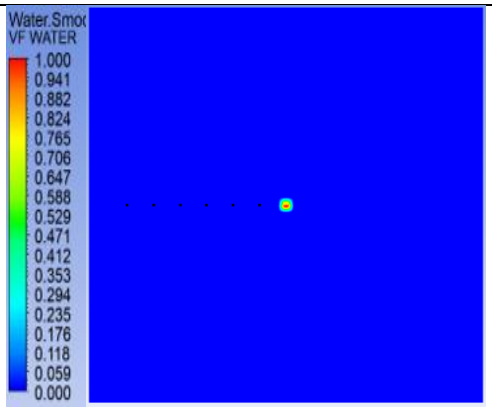  | 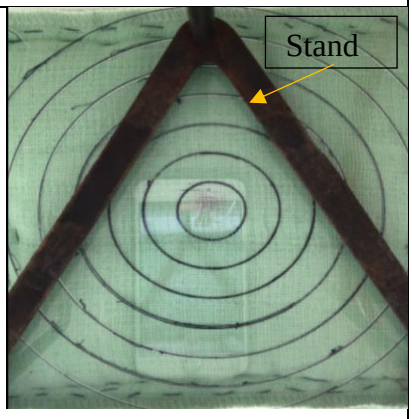  |
| 3.5 sec | 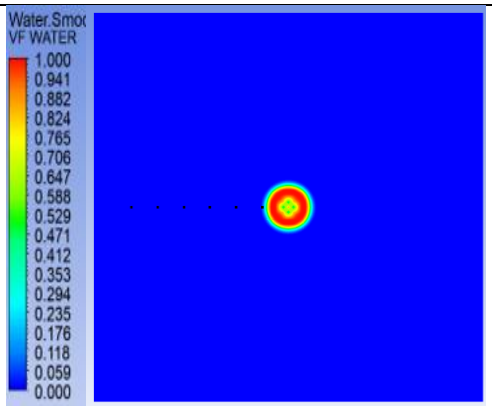  | 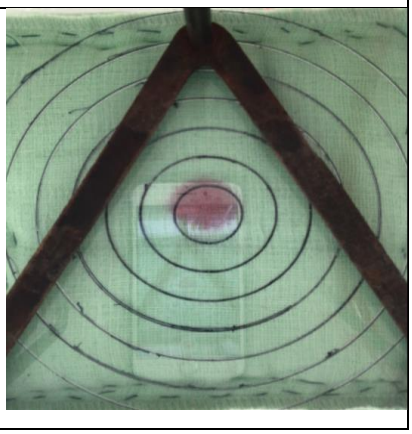 |

| | | |
|---|---|---|
| 15 sec | 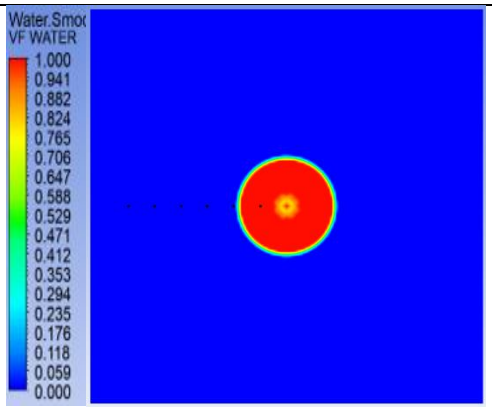 | 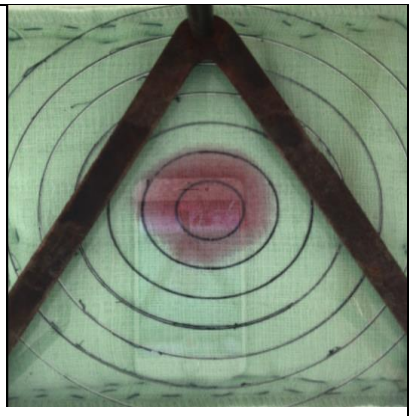 |
| 32.5 sec | 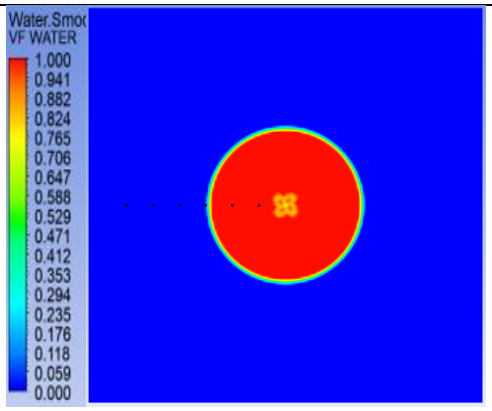 | 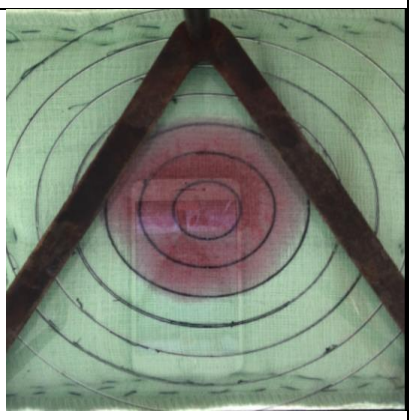 |
| 61 sec | 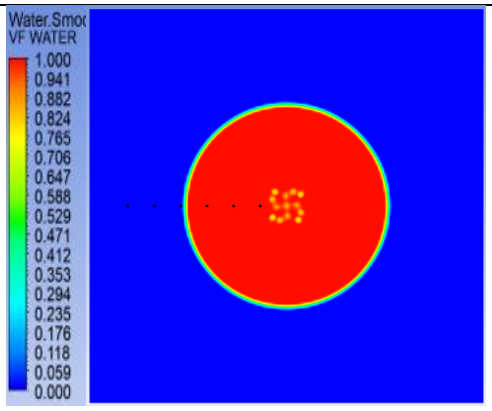 | 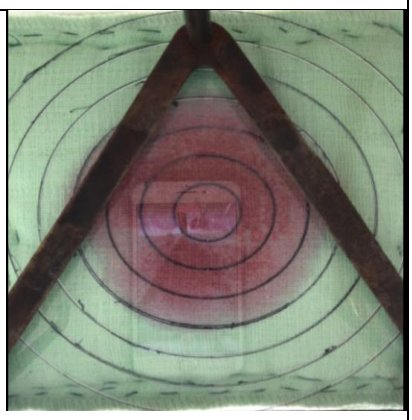 |
| 97.5.sec | 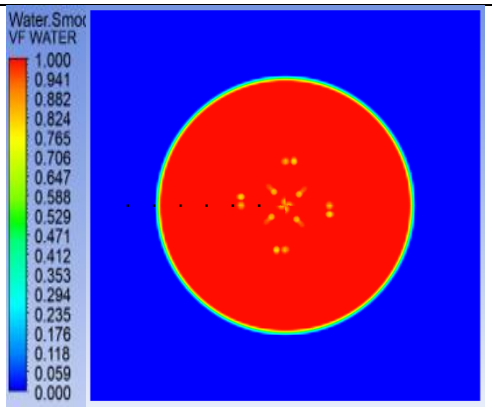 | 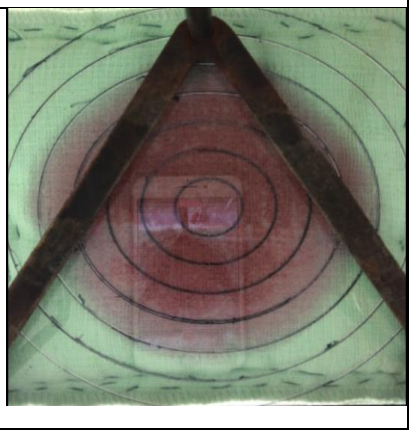 |

| | | |
|---|---|---|
| 150 sec | 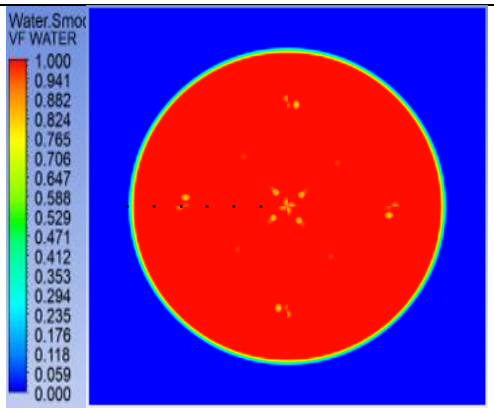 | 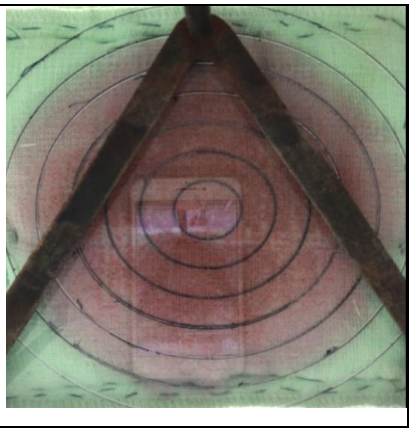 |

Figure 8-7 Comparison between CFD flow front predictions and experimentally obtained flow front locations for 0.52 m case (The black V shape is the stand used in experiments).

## 8.4 Case studies

The validated numerical methodology is further extended to model the flow through real-world applications. Two different cases are considered in this study, the first case considers the flow through a simple diaper with a single absorbing layer. For this case, the geometrical details are taken from the pampers baby diaper. The second case study considers the diaper with multiple porous layers with different permeabilities is considered. All input data related to the porous media such as porosity, permeability and capillary pressure is taken from the experiments presented in Chapter 4.

### 8.4.1 Case study one: Simulation of the flow-through diaper under swelling conditions

To explore the ability of the proposed numerical framework, the validated model is extended to model the flow through the diaper. For this case, only a single absorbing layer is considered. It is assumed that the diaper is made up of cotton material. The mass flow rate of 0.0023 kg/sec is selected for this case (Olsen et al., 2009). The position of the inlet is so selected that the resulting flow would be similar to the actual flow scenario through diapers. The flow-through actual diaper is a combination of the wicking and draining case (along and against gravity).

Figure 8.8 shows the variation of the liquid volume fraction on the top and bottom faces of the diaper. It can be seen that the flow front propagation is becoming dominant on the bottom face as time progresses. This is the effect of gravity as highlighted in chapter 4. Figure 8.9 shows the transient contours of the volume fraction of liquid. The effect of the capillary forces and gravity forces can be seen in the flow front propagation. As a result, the liquid front propagates at different rates in the vertical

and downward directions. The liquid front propagates dominantly in a downward direction because of the combined effect of the capillary forces and gravitational forces. The same behaviour is observed on both faces. Further, different shapes of the flow front can be observed during the forced imbibition process. Initially, the nature of flow is 3D until the liquid front reaches the bottom face of the diaper in the initial stages. The flow becomes 1D in nature as time passes. Finally, the variation of the relative volume fraction is plotted against the time to study the effect of the capillary and gravitational forces on the relative liquid front propagation

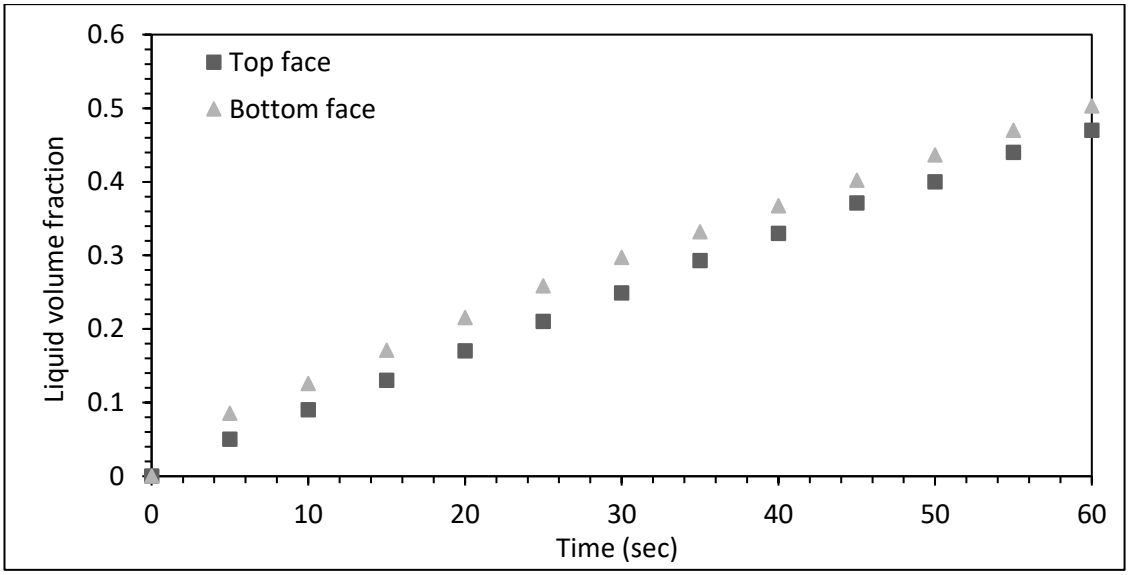


Figure 8-8 The evolution of the volume fraction on the top and bottom face of the diaper

| Time | Volume Fraction (Top face) | Volume Fraction (bottom face) |
|---|---|---|
| 5 sec | 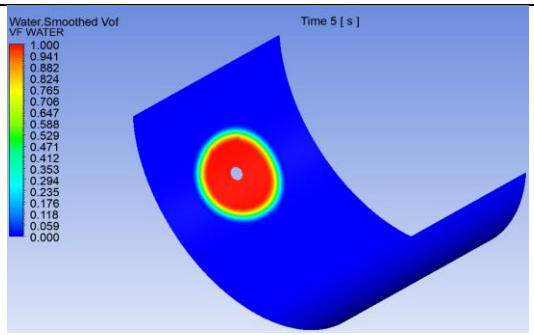 | 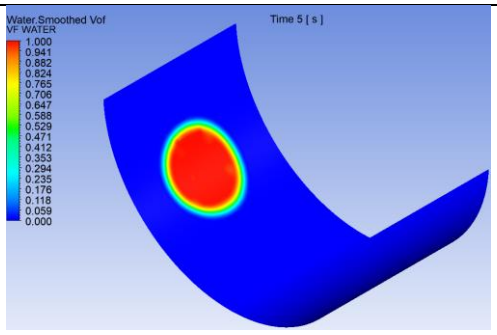 |

| | | |
|---|---|---|
| 10 sec | 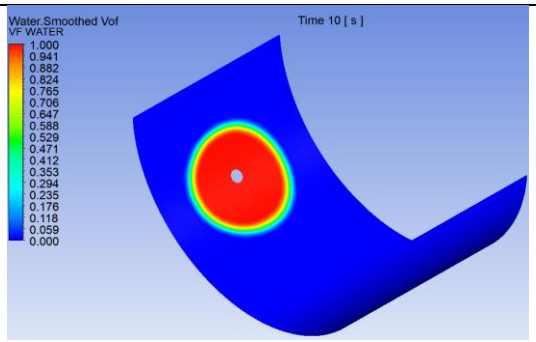 | 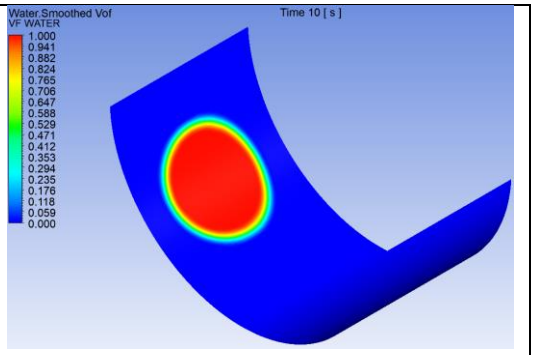 |
| 20 sec | 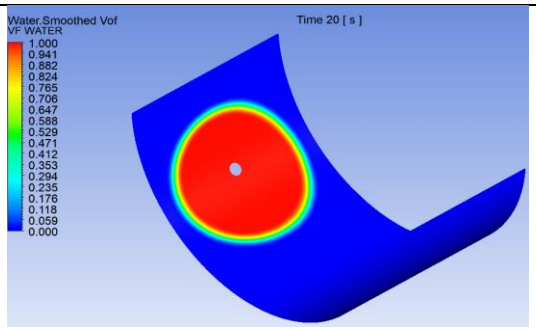 | 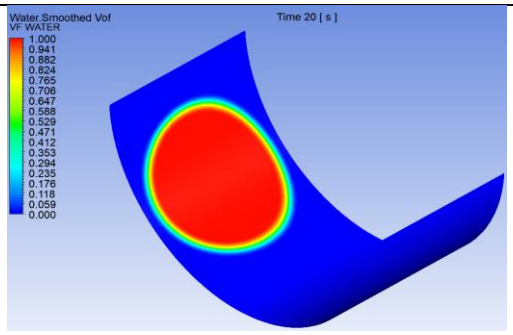 |
| 30 sec | 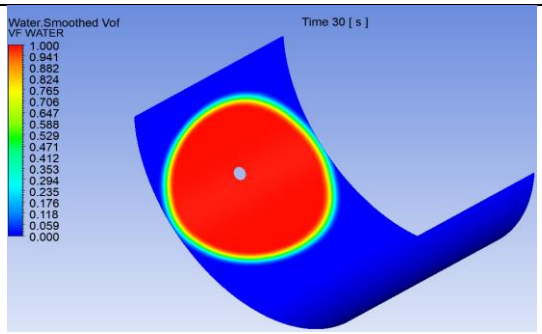 | 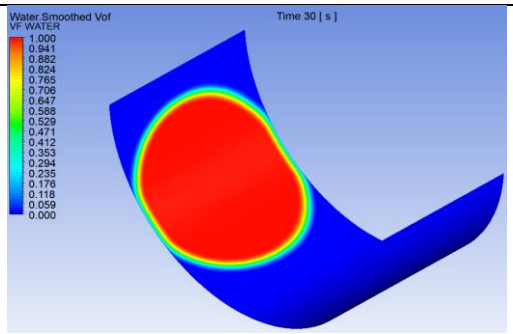 |
| 40 sec | 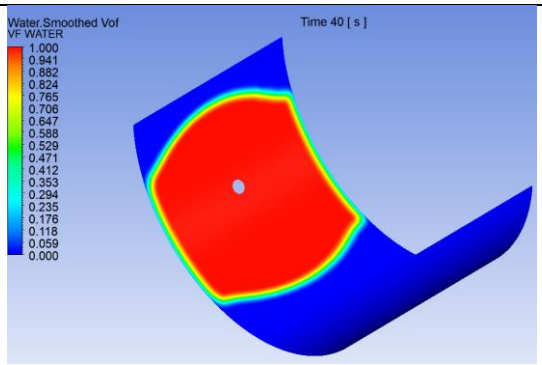 | 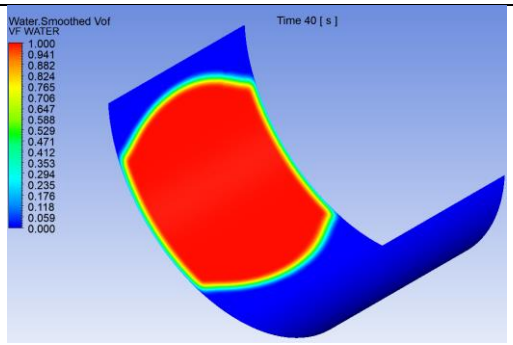 |
| 50 sec | 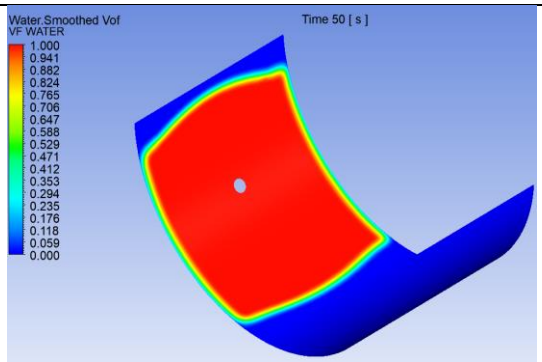 | 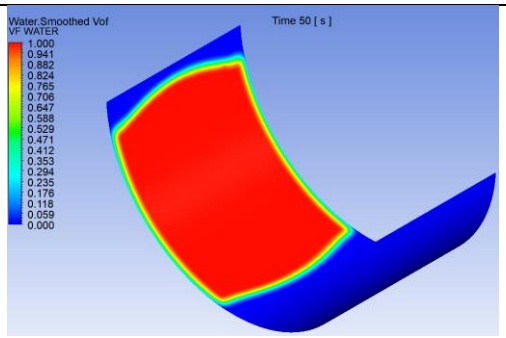 |

Figure 8-9 Transient contours for the liquid volume fraction on the top and bottom faces of the diaper

Figure 8.10 shows the variation of the relative volume fraction with tine. It shows that liquid spreads faster on the bottom face of the diaper in the initial stages of the imbibition till 10 seconds which becomes slower till 45 seconds. After that, it is observed that the changes in relative volume fraction become constant which means the liquid front propagates at the same rate on both faces. The reason behind this can be explained by the volume fraction results shown in Figure 8.9, as explained earlier the variation of the liquid front becomes 1D in nature. The volume fraction contours at 50 seconds and 60 seconds for both faces clearly show negligible differences. This set of results would be useful for designing and optimising the hygiene products such as a diaper, sanitary napkins etc. The details of the interface between the wetting phase (liquid) and the non-wetting phase (air).

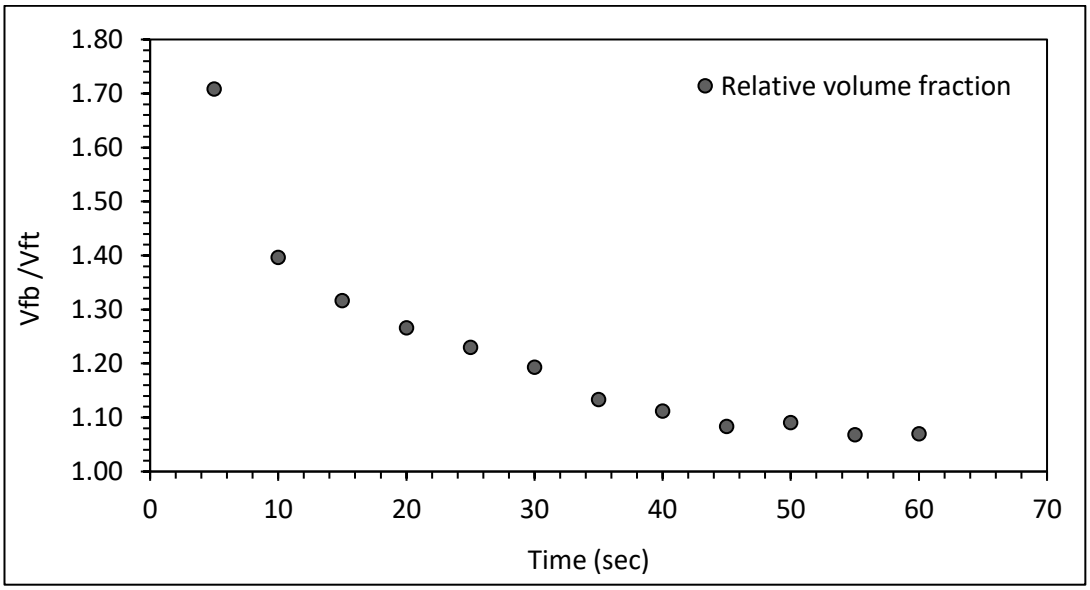


Figure 8-10 Variation of the changes in the relative volume fraction with time

### 8.4.2 Case study two: Simulation of the flow-through multi-layered porous media

For case study two, the flow through multiple porous layers is considered. The geometry is composed of three layers of porous material as shown in Figure 8.2. The top and the bottom layer has the same permeability. The middle layer of the domain is called as core and is assumed to be in swelling conditions. In this case, two different scenarios are considered. In the first scenario, the permeabilities of all layers are taken the same and for the second scenario, the core is made five times more permeable than the top and bottom layers. Note that in this case study, all properties related to porous media are taken from the experimental study. The table below shows the details of permeability values used for each layer.

Table 8.2 Details of the permeabilities for each layer considered for this case study

| | Top layer (Rigid permeability) | The middle layer (Swelling) (Initial permeability) | Bottom layer (Rigid permeability) |
|---|---|---|---|
| Case 1 | $3.91 \times 10^{-11} m^2$ | $3.91 \times 10^{-11} m^2$ | $3.91 \times 10^{-11} m^2$ |
| Case 2 | $3.91 \times 10^{-11} m^2$ | $1.98 \times 10^{-10} m^2$ | $3.91 \times 10^{-11} m^2$ |

Figure 8.11 and 8.12 shows the evolution of the liquid front location on the top face of each layer for both cases. The liquid front advancement on the bottom layer is seen as more dominant than the other two layers for both cases which is the result of the combined effect of inflow force, capillary forces and gravitational forces which should not cause any surprise.

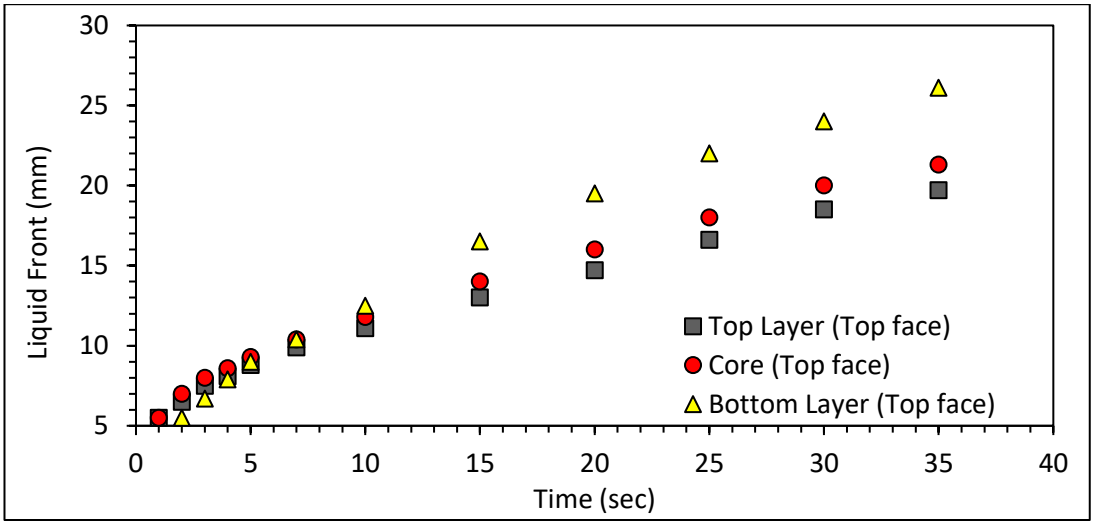


Figure 8-11 Comparison between the evolution of liquid front locations on the top face of each layer (Case 1)

.

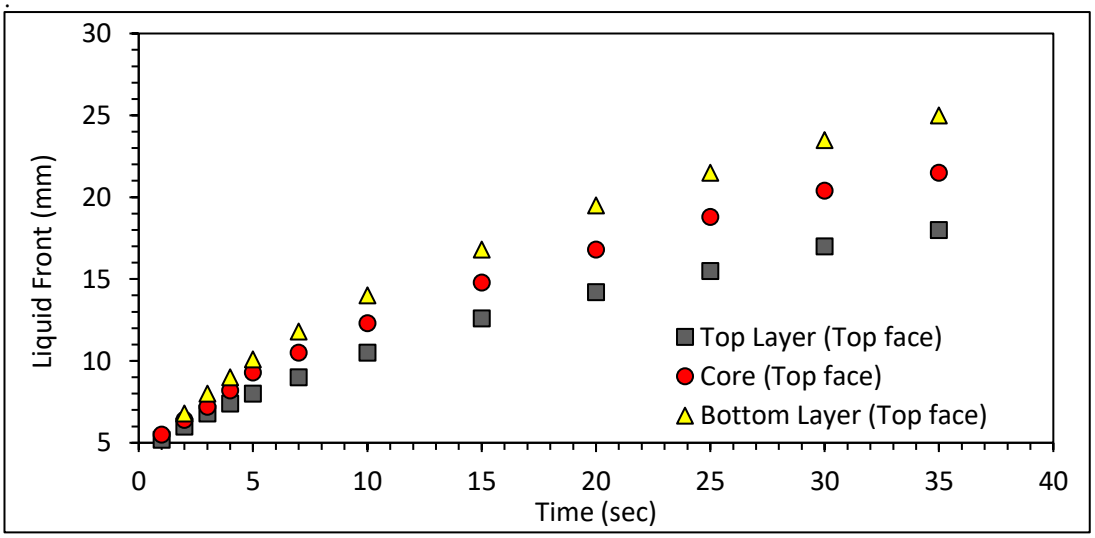


Figure 8-12 Comparison between the evolution of liquid front locations on the top face of each layer (Case 2)

Also, if observed clearly the changing in core permeability did not affect considerably on the flow front propagation on the top and bottom layers, the only difference is the time when the liquid front reaches the bottom layer which can be ignored. However, a significant difference can be seen in the flow front propagation on the top face of the core which is the result of the difference in the permeability. Figure 8.13 and 8.14 shows the relative changes in the liquid front locations on the core layer with top and bottom layers. It shows that for case 1, where the initial permeability of all layers is the same. The relative changes in liquid front locations between the core and top layers are not significant. Further, for case 2 where the core is assumed to be five-time more permeable than other layers, the results show about a 10-11% difference in the liquid front locations. Finally, relative changes in liquid front locations between the core and bottom layer show that initially, the liquid front propagation on the core layer is dominant which decreases sharply as time passes which means the liquid front propagation on the bottom layer becomes dominant.

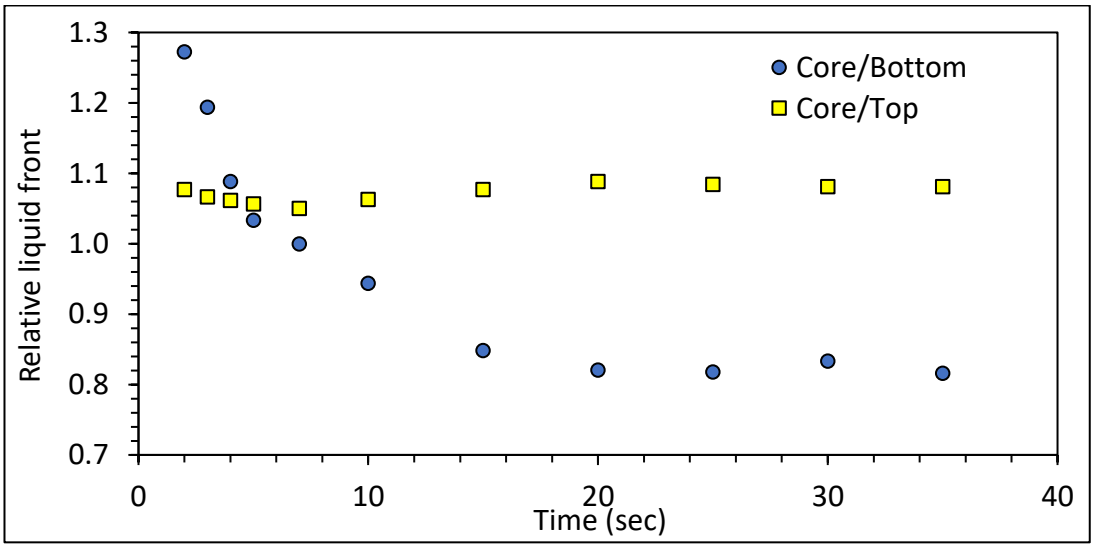


Figure 8-13 Relative changes in the liquid front locations for case 1 (Core initial permeability = $3.91\times10^{-11}m^2$)

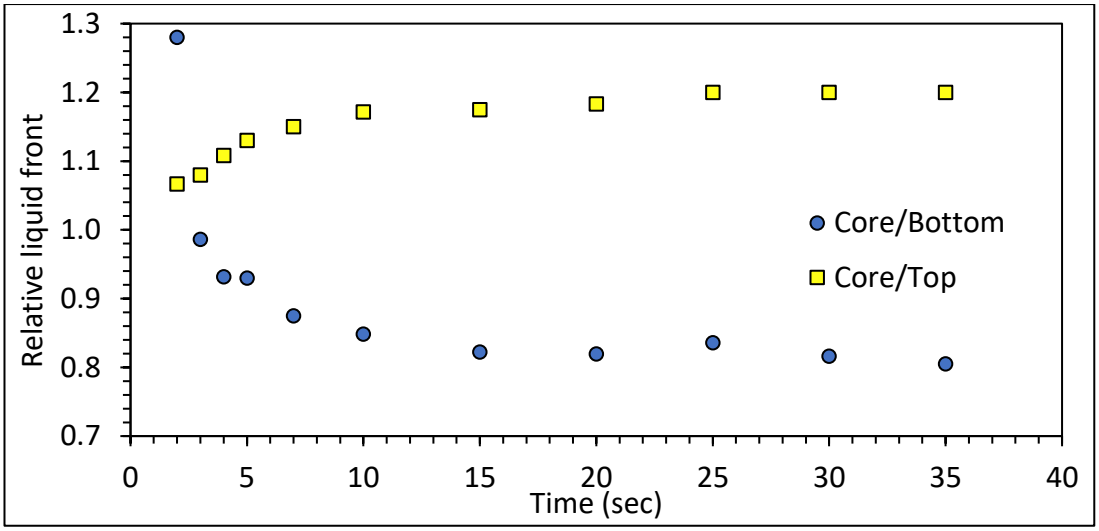


Figure 8-14 Relative changes in the liquid front locations for case 1 (Core initial permeability = $1.98\times10^{-10}m^2$)

Finally, Figure 8.15 and 8.16 shows the transient contours of liquid front locations on the top and side faces of each layer. The wetting phase liquid is represented by red colour whereas the non-wetting phase air is represented by blue colour. Note that Figure 8.15 shows liquid front locations only for Case 2. From figure 8.16 it is observed that the changes in the permeability can considerably affect the flow front propagation on the side faces of all layers. It can be observed that flow front propagation on the side face of the core for case 1 is slower than in case 2. For case 1 initially the shape of the liquid front appears like a rectangle which can be seen for the time range of 4 sec to 10 sec. The reason behind this can be related to the same initial permeability. However, for case 2 the shape of the liquid front changes rapidly as time passes. The liquid front propagation on the core part is seen as dominant initially which is seen from the contours shown for 1 sec to 4 sec. however, as time passes, swelling effects become dominant and liquid front propagation slows down. As mentioned earlier, the changes in the permeability of the core do not affect much the liquid front propagation of the top as seen in Figure 8.15. Hence, these types of results related to the liquid front evolution could be useful for designing hygiene and sanitary products which are made up of the different porous layers.

| Time (sec) | Top layer | Middle layer (Core) | Bottom layer |
|---|---|---|---|
| 1 sec | 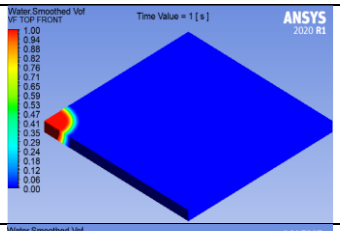 | 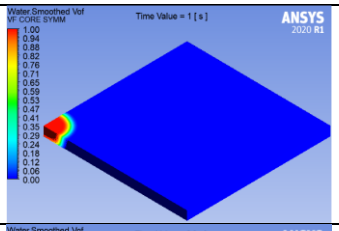 | 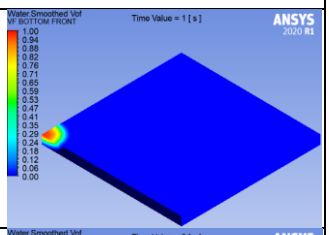 |
| 2 sec | 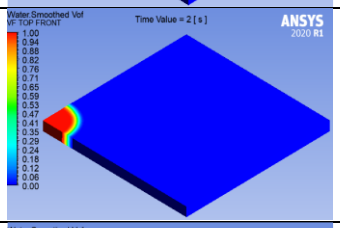 | 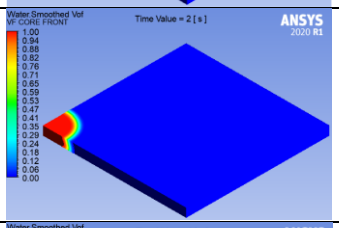 | 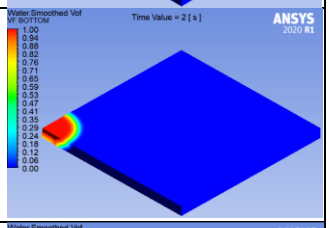 |
| 4 sec | 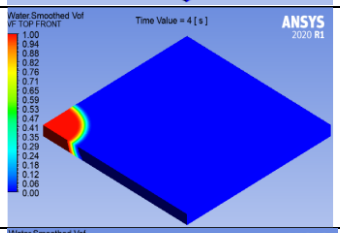 | 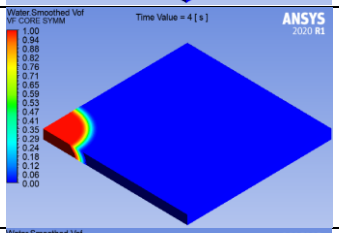 | 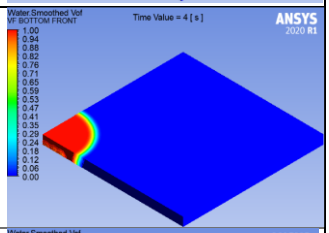 |
| 6 sec | 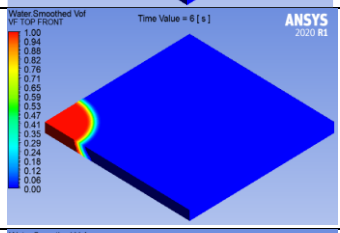 | 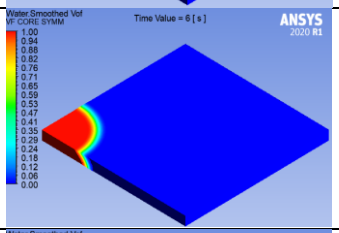 | 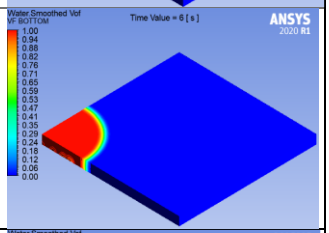 |
| 10 sec | 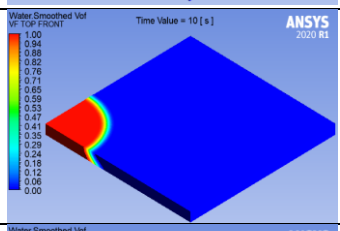 | 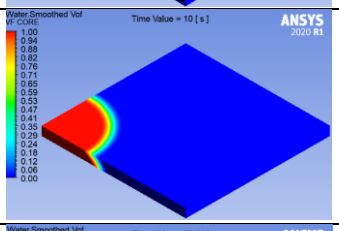 | 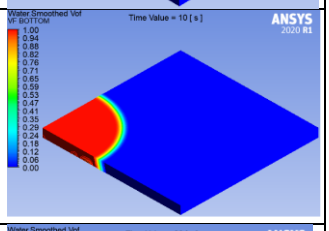 |
| 20 sec | 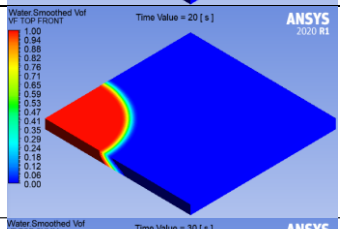 | 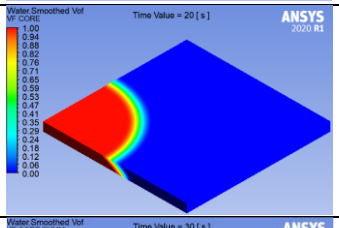 | 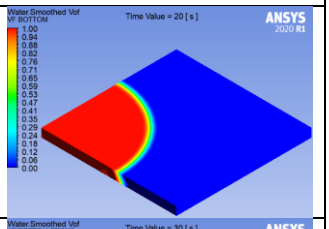 |
| 30 sec | 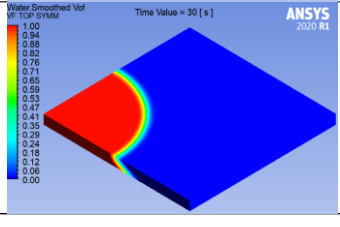 | 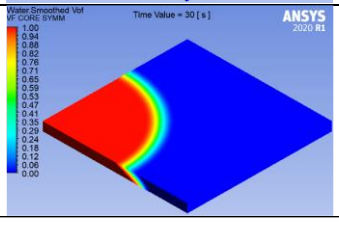 | 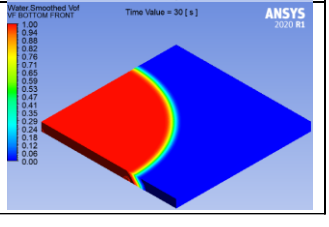 |

Figure 8-15 The transient contours of the liquid volume fraction on the top faces of each layer (Top, middle and bottom)

| Time | Case 1<br>Core initial Permeability<br>$K_o = 3.91 \times 10^{-11} m^2$ | Case 2<br>Core initial Permeability<br>$K_o = 1.98 \times 10^{-10} m^2$ |
|---|---|---|
| 1 sec |  | 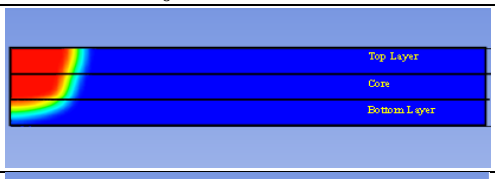 |
| 2 sec | 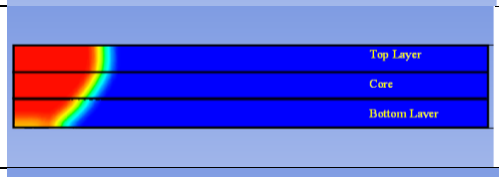 | 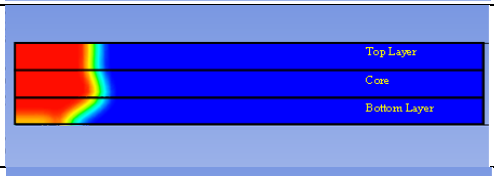 |
| 4 sec | 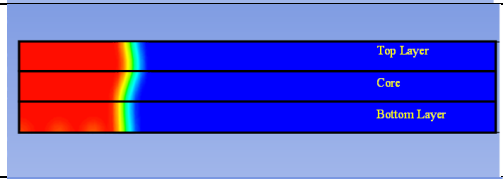 | 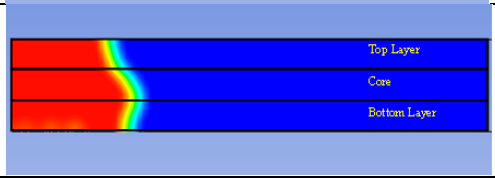 |
| 6 sec | 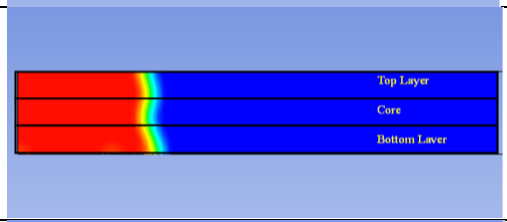 | 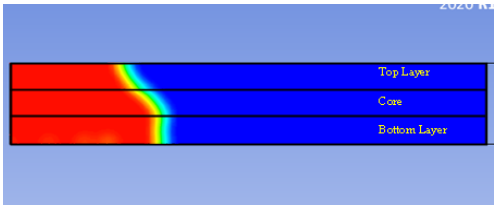 |
| 10 sec | 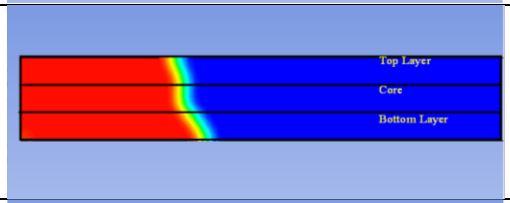 | 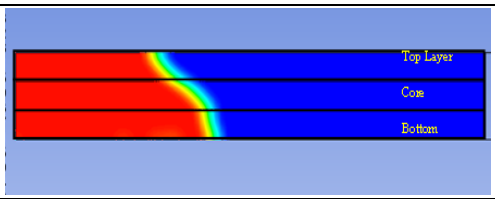 |
| 20 sec | 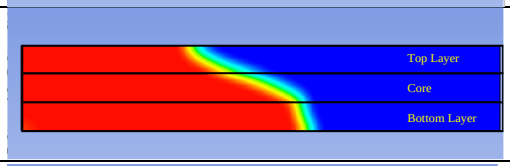 | 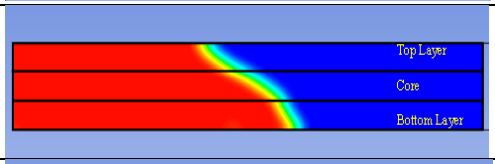 |
| 30 sec | 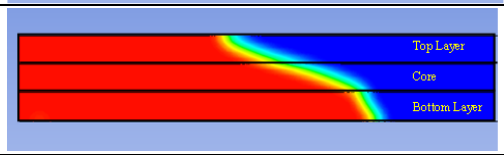 | 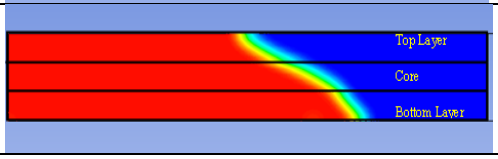 |

Figure 8-16 Liquid front propagation on the side faces of each layer (Top, middle and bottom)

## 8.5 Chapter Summary

In this chapter, the liquid absorption within swelling porous media is modelled using the novel combination of the Finite Volume Method and Volume of fluid method. This is the first time this combination is used to model such a flow scenario. A good agreement between the experimental data and CFD predictions is obtained for the developed model. Further, as a part of the validation activity, the predictions for liquid front locations from different CFD models based on different permeability reduction models are compared against the experimental data. The modelling framework is then extended to capture the liquid imbibition process in diaper-like geometry and porous media made up of multiple layers with variable permeability values. The models showed promising results demonstrating the capability of the Finite Volume Method and volume fluid method (FVM-VOF) to model the flow through absorbing porous media under swelling conditions with lesser input parameters. If the basic parameters, such as permeability, porosity, and capillary pressure, are known for any porous medium this method allows an efficient way to model such a flow scenario.

The results demonstrated the ability of the proposed method to track the liquid-air interface on the curved faces. The flow of liquid on the curved faces is the combination of wicking and draining flow through porous media where gravitational forces play a significant role. Case study one focused on the modelling of this flow scenario. The computational model is developed for the diaper-like geometry whose dimensions are taken from the actual diaper product (pampers). In this case study, only a single absorbing layer is considered, and the liquid holdup is modelled by the special wall boundary condition proposed in chapter 7. The results showed interesting patterns of the liquid front at different time values due to the combined effect of capillary and gravitational forces. Initially, the shape of the liquid front appeared like an asymmetric circle (2D) which becomes rectangular (1D) as time passes. The effect of gravity is clearly seen in the liquid front propagation. Finally, the modelling approach is extended to model the flow through multiple porous media with different permeabilities. For case study two the flow through porous media made up of three different layers is modelled. The top and bottom layers are assumed to be in rigid conditions with the same permeability whereas the middle part is assumed to be in swelling conditions. The computational models are developed for two different core permeabilities. The results revealed that changing the permeability of the core does

not affect much the liquid front propagation on the top faces of each bottom and top layer. However, the liquid propagation on the side faces of each layer showed significant differences. The proposed combination of the FVM-VOF has proven the efficient approach to model the flow through absorbing porous media with lesser input parameters than other methods cited in the literature

# Chapter 9 Overall Conclusions and Future works

## 9.1 General conclusions

The broad objective of this research is to advance understanding in the field of modelling of imbibition (natural or forced) in porous media. A novel methodological framework based on the combination of the Finite Volume Method (FVM) and Volume of Fluid Method (VOF) is proposed to model different flow scenarios within porous media. The computational models are presented for the following conditions: a) flow through a porous medium under swelling conditions b) flow through an absorbing porous medium under rigid conditions and c) flow through an absorbing porous medium under swelling conditions. The following are the main conclusions deducted from the present study:

i. The study identified the current gaps in the current approaches available to model the flow through porous media under swelling and absorbing conditions. For the case of swelling porous media, the available modelling approaches are based on the Finite Element-Control Volume method (FE-CV) with single-phase flow assumptions. The flow through absorbing porous media is modelled using the different approaches that are based on either single-phase flow assumptions or multiphase flow assumptions. In the case of the multiphase flow approach, the resulting model requires a lot of fitting parameters. To model the swelling effects and capillary pressure effects, the Finite Volume Method and Volume of Fluid method are rarely used. Further, the literature showed that there is insufficient experimental data available related to the cotton fabric under swelling conditions and highlighted the gaps in the modelling of flow through absorbing porous media under swelling conditions. Overall, this study identified the current gaps in the field of flow through swelling porous media.

ii. To overcome the gaps highlighted by literature, Firstly, the study proposed a novel combination of the Finite volume method and the Volume of Fluid method (FVM-VOF) to model the flow through swelling porous media. The computational models are developed using ANSYS Fluent solver for the Liquid composite Moulding process. The predictions from the developed CFD model for liquid front locations and inlet pressure changes compared well with

available experimental data with an average error of 2.27%. The proposed framework is further extended to model the 2D flow scenario through swelling porous media under isotropic and orthotropic conditions. The results showed that for the central injection point and eccentric injection point the total mould fill times for rigid conditions are lesser by 14% and 16 % than swelling conditions respectively. Further, the results for the orthotropic porous media revealed the need for multiple injection ports to fill the mould with resin as the flow front advancement in the y direction became negligible as time passed further. The proposed method allowed us to model and track the liquid-air interface at different time values. The results demonstrated the effect of positions of the inlet and permeability on the total mould filling time. All commercial CFD packages are capable of modelling the flow in rigid and non-swelling porous media only. The advantage of the proposed model is that any commercial solver based on the finite volume method can be easily adapted for flow simulation in swelling porous media. The majority of previous studies assume the flow to be single-phase, while this method uses a multi-phase approach (volume of fluid method) to track the sharp interface between resin and air. It can help to track the smaller interface between air and resin (such as the formation of voids, bubbles, and defects in the process) for different geometries.

iii. The liquid absorption and retention are modelled using the FVM-VOF method. The Analytical model for the 1D liquid draining case is proposed and in the case of 3D liquid imbibition, the analytical model proposed by Xiao et al. (2012a) is corrected and validated in this study. The predictions from developed 1D,2D and 3D CFD models were validated against the experimental data with average errors of 3.92%, 7.62% and 4.7% respectively. The validation study highlighted that the flow through absorbing porous media can be modelled efficiently with fewer input parameters such as porosity, permeability, and capillary pressure. The proposed approach is further extended to study the different cases of flow. The first case study highlighted the limitation of traditional analytical methods. The results demonstrated the ability of the model to capture the interface when the propagating liquid front hit the walls. The shape of the interface slowly starts to become 1D in nature when the gravitational effects are neglected. Finally, a novel cell zone

condition is proposed to mimic the liquid holdup within porous media. The results showed the effect of the size of the porous domain on wicking height. This makes the proposed approach a substitute for other multiphase models based on Richard's approach and the Eulerian multiphase approach. The proposed approach can be easily extended to model the flow through hygiene products such as diapers, paper napkins and wipes, and tampons. The major advantage of this method is the modelling of capillary pressure effects, if the value of capillary pressure, permeability and porosity are known for given porous media then using this approach one can easily model the wicking flow.

iv. The study investigated the swelling behaviour of cotton fabrics experimentally. The changes in the fibre diameter, porosity and permeability are measured experimentally in this study. The cotton fibres showed a total of 11% swelling upon absorption by water. To measure the porosity in swelling conditions, a novel method is proposed in this study. The porosity of a sample was found to be reduced by 12% as a result of swelling. The porosity reduction was also predicted analytically by using the available analytical models. The analytical model overpredicted the changes in porosity. The available analytical model is corrected by proposing new correction factors that account for inter-fibre interactions. For the case of permeability, the results showed a 60.34% reduction in the permeability of the sample due to the swelling effect. Finally, the water absorption tests are performed for two different liquid heights (0.52 m and 1.32 m). The results demonstrated the effects of gravity on the flow front advancement on the upper and lower face of the prepared sample. It was found that the flow front advancement on the lower face found to be dominant than the upper face.

v. Finally, the study investigated the flow through absorbing porous media under swelling conditions. The developed computational models are validated against the data obtained from water absorption experiments with averaged percentage errors of 2.63% and 7.78%. The study compared the predictions from the CFD models developed using different theoretical permeability models. The validated numerical approach is further extended to model the flow through single-layered and multi-layered diapers. For the case of the single-layered diaper, the results showed interesting patterns of liquid fronts demonstrating the combined effects of capillary forces and gravitational

forces. It was found that initially, liquid front propagation is faster on the bottom face of the diaper than the top face which reduces and becomes almost the same as time passes. For the case of the multi-layered diaper, the results demonstrated the effects of changes in core permeability on flow front propagation on the top and bottom face. The results showed about a 10-11% changes difference in liquid front locations of the top face of the core Hence, the results demonstrated the ability of the method to model the flow on the curved plane where the resulting flow is the combination of wicking and draining flow.

vi. In summary, the novel combination of the Finite volume and Volume of Fluid Method is proposed to model flow through swelling porous media. This is the first time when such a modelling approach is used to include swelling and capillary pressure effects within porous media. The assumption of a multiphase flow system would help to understand and analyse the interactions between liquid and air accurately in isothermal working conditions. The method allows us to track the liquid-air interface, pressure and velocity distributions efficiently. The proposed modelling approach is easy to implement and requires lesser fitting parameters to accurately model the different flow scenarios within porous media. Finally, this method can be applied to any commercial software based on the Finite volume method to model the capillary pressure and swelling effects.

## 9.2 Future works

Based on the obtained results from the present study following are the several recommendations suggested for further research,

a) The proposed methodology in the case of modelling flow through swelling porous media for Liquid composite moulding (LCM) applications assumed the isothermal flow conditions. The future study should consider the non-isothermal conditions to explore the further features of the proposed methodology. Such as extending the modelling approach to model the heat transfer during the mould-filling process. The application of temperature would have effects on the physical properties of resin such as density, and viscosity. Especially with viscosity, as temperature increases the viscosity of

resin decreases which makes resin flow faster within mould Investigation of swelling effects under such non-isothermal conditions would be interesting.

b) The proposed modelling approach for the capillary-driven flow should be extended for the case where more than two fluids are present. For the present case, the multiphase flow of gas-liquid is considered. Hence, the modelling framework should be further extended for different flow scenarios where multiple liquids are present such as oil recovery applications where gas, oil and water co-exist within pores at the same time. This will help to check the capability of the proposed approach to model liquid-liquid and liquid-gas interactions.

c) The proposed modelling approach for the capillary pressure effects is based on the assumption of negligible effects of liquid evaporation on liquid absorption within porous wicks. However, this is not the case for different liquids, some liquids tend to evaporate under ambient working conditions Hence, future works should consider an extension of the present method to include liquid evaporation effects. The best example is the fragrance dispersion applications where the rate of evaporation of the absorbed fragrant liquid is an important factor.

d) In the present study, the numerical models are developed only for single-layered porous media. Some applications such as baby diapers, tissue papers, and sanitary napkins may include multiple porous layers with variable properties Hence, the proposed modelling framework should be extended to model the flow through multi-layered porous media with variable permeability, porosity, and capillary pressures of each layer.

e) A comparative study of computational cost should be conducted between the proposed modelling approach and other available multiphase approaches cited in the literature for previously mentioned different flow scenarios. For example, a comparative study of liquid absorption modelling using the proposed approach (FVM-VOF), Eulerian method and Richard's approach. The outcome of this study would be helpful while the selection of the best approach according to the previously mentioned flow scenarios.

# References


ABOUKHEDR, M. 2019. *Two-Phase Flow Simulation in Porous Media Geometries Reconstructed from micro CT Data : Application to Fluid Transport at Low Capillary Numbers.* Doctoral, City University of London.

ADVANI, S. G. 2018. 2.2 Role of Process Models in Composites Manufacturing. *In:* BEAUMONT, P. W. R. & ZWEBEN, C. H. (eds.) *Comprehensive Composite Materials II.* Oxford: Elsevier.

AHMED, T. 2019. Chapter 5 - Relative Permeability Concepts. *In:* AHMED, T. (ed.) *Reservoir Engineering Handbook (Fifth Edition).* Gulf Professional Publishing.

ALEKSENDRIC, D. & CARLONE, P. Soft computing techniques. SOCO 2015, 2015.

ASHARI, A., BUCHER, T., TAFRESHI, H. V., TAHIR, M. & RAHMAN, M. 2010. Modeling fluid spread in thin fibrous sheets: Effects of fiber orientation. *International journal of heat and mass transfer,* 53**,** 1750-1758.

ASHARI, A. & TAFRESHI, H. V. 2009. General capillary pressure and relative permeability expressions for through-plane fluid transport in thin fibrous sheets. *Colloids and Surfaces A: Physicochemical and Engineering Aspects,* 346**,** 114-122.

AZHAR, M. & SANYAL, J. Numerical Study of Water Flooding Simulations Using ANSYS Fluent. Proceedings of the 4th World Congress on Momentum, Heat and Mass Transfer, 2019. 1-8.

BAKER, R. O., YARRANTON, H. W. & JENSEN, J. L. 2015. 2 - Rock and Fluid Properties. *In:* BAKER, R. O., YARRANTON, H. W. & JENSEN, J. L. (eds.) *Practical Reservoir Engineering and Characterization.* Boston: Gulf Professional Publishing.

BARBOUR, S. L. & KRAHN, J. 2004. Numerical modelling–prediction or process. *Geotechnical News,* 22**,** 44-52.

BEAR, J. 2013. *Dynamics of fluids in porous media*, Courier Corporation.

BELL, J. M. & CAMERON, F. K. 2002. The Flow of Liquids through Capillary Spaces. *The Journal of Physical Chemistry,* 10**,** 658-674.

BEYHAGHI, S., GEOFFROY, S., PRAT, M. & PILLAI, K. M. 2014. Wicking and evaporation of liquids in porous wicks: A simple analytical approach to optimization of wick design. *AIChE Journal,* 60**,** 1930-1940.

BICKERTON, S., GOVIGNON, Q. & KELLY, P. 2013. 7 - Resin infusion/liquid composite moulding (LCM) of advanced fibre-reinforced polymer (FRP). *In:* BAI, J. (ed.) *Advanced Fibre-Reinforced Polymer (FRP) Composites for Structural Applications.* Woodhead Publishing.

BIJELJIC, B. 2000. *Flow and mass transfer in fibrous and granular porous media.* PhD, Imperial College London (University of London).

BOYARD, N. 2016. *Heat Transfer in Polymer Composite Materials: Forming Processes*, John Wiley & Sons.

BRUSCHKE, M. V. & ADVANI, S. G. 1994. A numerical approach to model non-isothermal viscous flow through fibrous media with free surfaces. *International Journal for Numerical Methods in Fluids,* 19**,** 575-603.

CHANG, C.-Y. & HOURNG, L.-W. 1998. Numerical simulation for the transverse impregnation in resin transfer molding. *Journal of reinforced plastics and composites,* 17**,** 165-182.

CHATTERJEE, P. K. & GUPTA, B. S. 2002. *Absorbent technology*, Elsevier.

CHATTOPADHYAY, K. & GUTHRIE, R. I. 2014. Single Phase, Two Phase, and Multiphase Flows, and Methods to Model these Flows. *Treatise on Process Metallurgy.* Elsevier.

COULTER, J. P. & GUCERI, S. I. 1988. Resin Impregnation During the Manufacturing of Composite Materials Subject to Prescribed Injection Rate. *Journal of Reinforced Plastics and Composites,* 7**,** 200-219.

CUISSINAT, C. & NAVARD, P. Swelling and Dissolution of Cellulose Part 1: Free Floating Cotton and Wood Fibres in N-Methylmorpholine-N-oxide–Water Mixtures. Macromolecular Symposia, 2006. Wiley Online Library, 1-18.

DHALIWAL, J. S. 2019. Natural fibers: applications. *Generation, development and modifications of natural fibers,* 2**,** 1-23.

DIERSCH, H.-J. G., CLAUSNITZER, V., MYRNYY, V., ROSATI, R., SCHMIDT, M., BERUDA, H., EHRNSPERGER, B. J. & VIRGILIO, R. 2011. Modeling unsaturated flow in absorbent swelling porous media: Part 2. numerical simulation. *Transport in porous media,* 86**,** 753-776.

DULLIEN, F. A. L. & BRENNER, H. 2012. *Porous Media: Fluid Transport and Pore Structure,* Elsevier Science.

F. ZARANDI, M. A. & PILLAI, K. M. 2021. Investigating liquid fronts during spontaneous imbibition of liquids in industrial wicks. Part I: Experimental studies. *AIChE Journal,* 67**,** e17324.

FLUENT 2020. ANSYS Fluent Theory Guide 2020 R1. ANSYS.

FRANCUCCI, G., RODRÍGUEZ, E. S. & MORÁN, J. 2014. Novel approach for mold filling simulation of the processing of natural fiber reinforced composites by resin transfer molding. *Journal of Composite Materials,* 48**,** 191-200.

FRANCUCCI, G., RODRÍGUEZ, E. S. & VÁZQUEZ, A. 2010. Study of saturated and unsaturated permeability in natural fiber fabrics. *Composites Part A: Applied Science and Manufacturing,* 41**,** 16-21.

GEBART, B. R. 1992. Permeability of unidirectional reinforcements for RTM. *Journal of composite materials,* 26**,** 1100-1133.

HU, H. H. 2012. Computational fluid dynamics. *Fluid mechanics.* Elsevier.

HUANG, J. & QIAN, X. 2007. A new test method for measuring the water vapour permeability of fabrics. *Measurement Science and Technology,* 18**,** 3043.

HUANG, J. & QIAN, X. 2008. Comparison of test methods for measuring water vapor permeability of fabrics. *Textile Research Journal,* 78**,** 342-352.

HUSSEIN, M. M., AL-SARKHI, A., BADR, H. M. & HABIB, M. A. 2019. CFD modeling of liquid film reversal of two-phase flow in vertical pipes. *Journal of Petroleum Exploration and Production Technology,* 9**,** 3039-3070.

JAVADI, A., PILLAI, K. & SABO, R. An experimental estimation of liquid absorption coefficient for cellulose nano-fiber films. 11th international conference on flow processes in composite materials (FPCM11), Auckland, 2012. 9-12.

JEONG, S.-M., HSIEH, L.-H. C., HUANG, C.-Y. & SEAN, W.-Y. 2017. Direct numerical simulation of CO2 hydrate dissociation in pore-scale flow by applying CFD method. *International Journal of Heat and Mass Transfer,* 107**,** 300-306.

KISSA, E. 1996. Wetting and wicking. *Textile Research Journal,* 66**,** 660-668.

LI, H., VASQUEZ, S. A. & AZHAR, M. Modeling of Multiphase Flows in Porous Media With Applications to Reservoir and Well Performance Analysis. ASME 2016 Fluids Engineering Division Summer Meeting collocated with the ASME 2016 Heat Transfer Summer Conference and the ASME 2016 14th International Conference on Nanochannels, Microchannels, and Minichannels, 2016a. V01BT21A003.

LI, H., VASQUEZ, S. A. & AZHAR, M. Modeling of multiphase flows in porous media with applications to reservoir and well performance analysis. Fluids Engineering Division Summer Meeting, 2016b. American Society of Mechanical Engineers, V01BT21A003.

LIU, P. & CHEN, G.-F. 2014. *Porous materials: processing and applications*, Elsevier.

LIU, Z. & WU, H. 2016. Pore-scale modeling of immiscible two-phase flow in complex porous media. *Applied Thermal Engineering,* 93**,** 1394-1402.
LUCAS, R. 1918. Rate of capillary ascension of liquids. *Kolloid Z,* 23**,** 15-22.
MASOODI, R. & PILLAI, K. 2012a. A general formula for capillary suction-pressure in porous media. *Journal of Porous Media,* 15.
MASOODI, R. & PILLAI, K. M. 2010. Darcy's law-based model for wicking in paper-like swelling porous media. *AIChE journal,* 56**,** 2257-2267.
MASOODI, R. & PILLAI, K. M. 2012b. A study on moisture absorption and swelling in bio-based jute-epoxy composites. *Journal of Reinforced Plastics and Composites,* 31**,** 285-294.
MASOODI, R., PILLAI, K. M., GRAHL, N. & TAN, H. 2012a. Numerical simulation of LCM mold-filling during the manufacture of natural fiber composites. *Journal of Reinforced Plastics and Composites,* 31**,** 363-378.
MASOODI, R., PILLAI, K. M. & VARANASI, P. P. 2007. Darcy's law-based models for liquid absorption in polymer wicks. *AIChE journal,* 53**,** 2769-2782.
MASOODI, R., PILLAI, K. M. & VARANASI, P. P. Role of hydraulic and capillary radii in improving the effectiveness of capillary model in wicking. Fluids Engineering Division Summer Meeting, 2008. 251-259.
MASOODI, R., PILLAI, K. M. & VARANASI, P. P. 2010. Effect of externally applied liquid pressure on wicking in paper wipes. *Journal of Engineered Fibers and Fabrics,* 5**,** 155892501000500307.
MASOODI, R., TAN, H. & PILLAI, K. M. 2011. Darcy's law–based numerical simulation for modeling 3D liquid absorption into porous wicks. *AIChE journal,* 57**,** 1132-1143.
MASOODI, R., TAN, H. & PILLAI, K. M. 2012b. Numerical simulation of liquid absorption in paper-like swelling porous media. *AIChE Journal,* 58**,** 2536-2544.
MASOODI, R., TAN, H. & PILLAI, K. M. 2012c. Numerical simulation of liquid absorption in paper-like swelling porous media. *AIChE journal,* 58**,** 2536-2544.
MELCIU, I. & PASCOVICI, M. Imbibition of liquids in fibrous porous media. IOP Conference Series: Materials Science and Engineering, 2016. IOP Publishing, 012041.
MENDEZ, S., FENTON, E. M., GALLEGOS, G. R., PETSEV, D. N., SIBBETT, S. S., STONE, H. A., ZHANG, Y. & LÓPEZ, G. P. 2010. Imbibition in porous membranes of complex shape: quasi-stationary flow in thin rectangular segments. *Langmuir,* 26**,** 1380-1385.
MIRNYY, V., CLAUSNITZER, V., DIERSCH, H., ROSATI, R., SCHMIDT, M. & BERUDA, H. 2012. Wicking in absorbent swelling porous materials. *Traditional and Modern Modeling Approaches, Wicking in Porous Materials***,** 161-200.
MOLINS, S., TREBOTICH, D., STEEFEL, C. I. & SHEN, C. 2012. An investigation of the effect of pore scale flow on average geochemical reaction rates using direct numerical simulation. *Water Resources Research,* 48.
MOORE, A. T., SCOTT, L. W., DEGRUY, I. V. & ROLLINS, M. L. 1950. The swelling of cotton in water: A microscopical study. *Textile Research Journal,* 20**,** 620-630.
O'DELL, J. L. Natural fibers in resin transfer molded composites. Fourth international conference on woodfiber-plastic composites, 1997. 280-285.
OĞULATA, R. T. & MAVRUZ, S. 2010. Investigation of porosity and air permeability values of plain knitted fabrics.
OLSEN, L. H., GROTHE, I., RAWASHDEH, Y. F. & JØRGENSEN, T. M. 2009. Urinary flow patterns of healthy newborn males. *The Journal of urology,* 181**,** 1857-1861.
PACHEPSKY, Y., TIMLIN, D. & RAWLS, W. 2003. Generalized Richards' equation to simulate water transport in unsaturated soils. *Journal of Hydrology,* 272**,** 3-13.

PATANAIK, A. & ANANDJIWALA, R. 2009. Some studies on water permeability of nonwoven fabrics. *Textile Research Journal,* 79**,** 147-153.

PATARI, S. & MAHAPATRA, P. S. 2020. Liquid Wicking in a Paper Strip: An Experimental and Numerical Study. *ACS Omega,* 5**,** 22931-22939.

PILLAI, K. M. 2002. Governing equations for unsaturated flow through woven fiber mats. Part 1. Isothermal flows. *Composites Part A: Applied Science and Manufacturing,* 33**,** 1007-1019.

PILLAI, K. M. 2004. Modeling the unsaturated flow in liquid composite molding processes: a review and some thoughts. *Journal of Composite materials,* 38**,** 2097-2118.

PINILLA, A., ASUAJE, M., HURTADO, C., HOYOS, A., RAMIREZ, L., PADRÓN, A. & RATKOVICH, N. 2021. 3D CFD simulation of a horizontal well at pore scale for heavy oil fields. *Journal of Petroleum Science and Engineering,* 196**,** 107632.

POOYOO, N., KUMAR, S., CHAROENSUK, J. & SUKSANGPANOMRUNG, A. 2014. Numerical simulation of cylindrical heat pipe considering non-Darcian transport for liquid flow inside wick and mass flow rate at liquid–vapor interface. *International journal of heat and mass transfer,* 70**,** 965-978.

PORTO, J. D. S., LETZOW, M., SANTOS, E. D. D., AMICO, S. C., SOUZA, J. A. & ISOLDI, L. A. 2012. Computational modeling of RTM and LRTM processes applied to complex geometries.

RANJAN, R., MURTHY, J. Y., GARIMELLA, S. V. & VADAKKAN, U. 2011. A numerical model for transport in flat heat pipes considering wick microstructure effects. *International Journal of Heat and Mass Transfer,* 54**,** 153-168.

RANJAN, R., PATEL, A., GARIMELLA, S. V. & MURTHY, J. Y. 2012. Wicking and thermal characteristics of micropillared structures for use in passive heat spreaders. *International Journal of Heat and Mass Transfer,* 55**,** 586-596.

RAOOF, A., NICK, H. M., HASSANIZADEH, S. M. & SPIERS, C. J. 2013. PoreFlow: A complex pore-network model for simulation of reactive transport in variably saturated porous media. *Computers & Geosciences,* 61**,** 160-174.

REMADEVI, R., GORDON, S., WANG, X. & RAJKHOWA, R. 2017. Investigation of the swelling of cotton fibers using aqueous glycine solutions. *Textile research journal,* 87**,** 2204-2213.

RODRÍGUEZ, E. S., FRANCUCCI, G. & VÁZQUEZ, A. Study of saturated and unsaturated permeability in natural fiber fabrics. The 9th International Conference on Flow Processes in Composite Materials, Montreal, QC, Canada, 2008.

ROWELL, R., O'DELL, J., BASAK, R., SARKAR, M., SANANDI, A. R., CAULFIELD, D. F. & JACOBSON, R. E. Applications of jute in resin transfer molding. In: Proceedings, International seminar on jute and allied fibres: changing global scenario; Calcutta, India. Calcutta, India: Ijira Associaiton, 1997. 89-96.

ROY, T. & PILLAI, K. M. 2005. Characterization of dual-scale fiber mats for unsaturated flow in liquid composite molding. *Polymer composites,* 26**,** 756-769.

SAAD, A., ECHCHELH, A., HATTABI, M. & EL GANAOUI, M. 2018. An Optimized Control Volume/Finite Element Method (CV/FEM) for Non-Isothermal Liquid Composite Molding (LCM) Process. *In:* DRISS, Z., NECIB, B. & ZHANG, H.-C. (eds.) *Thermo-Mechanics Applications and Engineering Technology.* Cham: Springer International Publishing.

SANTAGATA, T., SOLIMENE, R., APREA, G. & SALATINO, P. 2020. Modelling and experimental characterization of unsaturated flow in absorbent and swelling porous media. *Chemical Engineering Science***,** 115765.

SHAMS, M. 2018. Modelling two-phase flow at the micro-scale using a volume-of-fluid method.

SHIH, C. H. & LEE, L. J. 1998. Effect of fiber architecture on permeability in liquid composite molding. *Polymer Composites,* 19**,** 626-639.
SHOJAEI, A., GHAFFARIAN, S. R. & KARIMIAN, S. M.-H. 2003. Numerical analysis of controlled injection strategies in resin transfer molding. *Journal of composite materials,* 37**,** 1011-1035.
SIMACEK, P., ADVANI, S. & BINETRUY, C. 2004. Liquid injection molding simulation (LIMS) a comprehensive tool to design, optimize and control the filling process in liquid composite molding. *JEC–Composites,* 8**,** 58-61.
SRINIVASAN, V., SALAZAR, A. J. & SAITO, K. 2011. Modeling the disintegration of modulated liquid jets using volume-of-fluid (VOF) methodology. *Applied mathematical modelling,* 35**,** 3710-3730.
SZEKELY, J., NEUMANN, A. & CHUANG, Y. 1971. The rate of capillary penetration and the applicability of the Washburn equation. *Journal of Colloid and Interface Science,* 35**,** 273-278.
TAN, H. & PILLAI, K. M. 2010. Numerical simulation of reactive flow in liquid composite molding using flux-corrected transport (FCT) based finite element/control volume (FE/CV) method. *International Journal of Heat and Mass Transfer,* 53**,** 2256-2271.
TANG, K.-P. M., KAN, C.-W. & FAN, J.-T. 2017. Comparison of test methods for measuring water absorption and transport test methods of fabrics. *Measurement,* 97**,** 126-137.
TROCHU, F., GAUVIN, R. & GAO, D. M. 1993. Numerical analysis of the resin transfer molding process by the finite element method. *Advances in Polymer Technology: Journal of the Polymer Processing Institute,* 12**,** 329-342.
UM, M. K. & LEE, W. I. 1991. A study on the mold filling process in resin transfer molding. *Polymer Engineering & Science,* 31**,** 765-771.
WEIN, F., CHEN, N., IQBAL, N., STINGL, M. & AVILA, M. 2019. Topology optimization of unsaturated flows in multi-material porous media: Application to a simple diaper model. *Communications in Nonlinear Science and Numerical Simulation,* 78**,** 104871.
XIAO, J., STONE, H. A. & ATTINGER, D. 2012a. Source-like solution for radial imbibition into a homogeneous semi-infinite porous medium. *Langmuir,* 28**,** 4208-4212.
XIAO, X., ZENG, X., BANDARA, P. & LONG, A. 2012b. Experimental study of dynamic air permeability for woven fabrics. *Textile Research Journal,* 82**,** 920-930.
YANG, B., JIN, T., LI, J. & BI, F. 2015. Three-Dimensional Numerical Simulation of Mold Filling Process in Compression Resin Transfer Molding. *Applied Composite Materials,* 22**,** 209-230.
YANG, B., TANG, Q., WANG, S., JIN, T. & BI, F. 2016. Three-dimensional numerical simulation of the filling stage in resin infusion process. *Journal of Composite Materials,* 50.
YOO, Y. E. & LEE, W. I. 1996. Numerical simulation of the resin transfer mold filling process using the boundary element method. *Polymer Composites,* 17**,** 368-374.
ZADE, A. & KUPPUSAMY, R. R. P. 2019. Mould fill time sensitivity analysis using isothermal mould filling simulations for applications in liquid composite moulding processes. *Materials Today: Proceedings*.
ZARANDI, M. A. & PILLAI, K. M. 2018. Spontaneous imbibition of liquid in glass fiber wicks, Part II: Validation of a diffuse-front model. *AIChE Journal,* 64**,** 306-315.
ZARANDI, M. A. F. 2019. *Experimental, Theoretical and Numerical Evaluation of Wicking Models for Liquid Imbibition in Dry Porous Wicks.* The University of Wisconsin-Milwaukee.
ZARANDI, M. A. F. & PILLAI, K. M. 2021. Investigating liquid-fronts during spontaneous imbibition of liquids in industrial wicks. Part I: Experimental studies. *AIChE Journal***,** e17324.

ZARANDI, M. A. F., PILLAI, K. M. & KIMMEL, A. S. 2018. Spontaneous imbibition of liquids in glass-fiber wicks. Part I: Usefulness of a sharp-front approach. *AIChE Journal,* 64**,** 294-305.